Development towards Sensitive Point-of-Care Tests for HIV and COVID-19

Qin Wang

A dissertation

submitted in partial fulfillment of the

requirements for the degree of

Doctor of Philosophy

University of Washington

2023

Reading Committee:

Barry R. Lutz, Chair

Paul Yager

Xiaohu Gao

Program Authorized to Offer Degree:
Bioengineering

University of Washington

Abstract

Development towards Sensitive Point-of-Care Tests for HIV and COVID-19

Qin Wang

Chair of the Supervisory Committee:
Barry R. Lutz
Bioengineering

Human immunodeficiency virus (HIV), with approximately 39 million people living with HIV globally, persists as one of the foremost challenges to global health. Sensitive HIV testing is needed for both early diagnosis and routine viral load monitoring in patients receiving antiretroviral therapy (ART). However, the most sensitive testing approach, rt-qPCR, is limited to centralized laboratories. A sensitive point-of-care HIV test using fingerstick samples could expand testing coverage, especially in low-resource settings. In the thesis, I explored two independent approaches aiming towards a simple yet sensitive HIV test. The first approach targets the reverse transcription activity of the reverse transcriptase (RT) enzyme encapsulated inside HIV. Specifically, engineered nucleic acid substrates are added for HIV RT to generate complementary DNA (cDNA), followed by amplification and detection mediated by LAMP or CRISPR-Cas

systems. In addition to HIV detection, the phenotypic HIV RT activity assay holds potential for HIV drug resistance screening and could be adapted for other pathogen-derived enzyme targets. The second approach directly adds fingerstick plasma into large-volume RT-LAMP for extraction-free HIV RNA detection. The results highlight the feasibility of scaling up LAMP reaction volumes, providing a fresh perspective on isothermal amplification.

In response to the COVID-19 pandemic started in 2019, we have additionally targeted improving the sensitivity of rapid antigen tests that are widely adopted for point-of-care COVID-19 diagnosis. While saliva offers a sample volume of up to 5mL, most antigen tests can only accommodate 50-100μL samples, leading to an inevitable sensitivity loss. We have developed a simple streptavidin-biotin-based agglutination system that could enrich analytes from larger sample volumes to improve assay sensitivity. Besides COVID-19, we anticipate the simple agglutination system could be employed for other targets to facilitate processing larger sample volumes with enhanced sensitivity.

TABLE OF CONTENTS

LIST OF FIGURES

LIST OF TABLES

ACKNOWLEDGEMENT

I would like to first acknowledge my advisor, Dr. Barry Lutz. Thank you for all your insightful questions and valuable advice as an adviser, all your encouragement, support, training as a mentor, and the shared moments of laughter and solace as a friend. I would like to thank my committee, Dr. Paul Yager, Dr. Xiaohu Gao, Dr. James Mullins, and Dr. Patrick Stayton. I feel truly fortunate to get to know you through classes, collaborations, meetings, and coffees, and grateful to have your support throughout the thesis. I would like to thank Dr. James Lai, whom I have worked with from the first day of graduate school through different projects. Thank you for all your mentorship and support, all the brisket and happy hours. Thank you all for inspiring me to continue the research path.

I would like to thank everyone from the Lutz Lab. Nuttada, thank you for being the best panda buddy and a life model; Ian, thank you for sharing the journey throughout graduate school and all the moral support getting through a windowless office; Garima, thank you for organizing the lab and offering help whenever needed; Shane, Enos, Wookyeom, thank you for all the engaging conversations. Thank everyone in the Lutz Lab, past and present, for your help and support.

I would like to thank all my friends, whether you are my roommates, tennis partners, outdoor buddies, hot pot buddies, or drinking buddies. I would also like to thank my cat, Little Orange, for being my cuddle buddy and home supervisor. Graduate school is not easy, and graduate school in a different country may be even harder. But thank you all for making Seattle feel like a home to me now.

Finally, I would like to thank my family: My dad and mom, my brother, and my grandma. Thank you for your unconditional trust and love, and for being my forever support.

Chapter 1. Introduction

1.1 POC Tests in HIV

1.1.1 **Need for sensitive POC HIV tests**

Human immunodeficiency virus (HIV) persists as one of the foremost challenges to global health. As of 2022, approximately 39 million people worldwide are living with HIV, with 0.63 million deaths from HIV-related causes and 1.3 million acquired new cases within 2022 [1]. With neither vaccines nor cures currently available, people living with HIV rely on life-long antiretroviral therapy (ART) to suppress HIV viral load and prevent disease progression. As a pathway to end the AIDS epidemic, the Joint United Nations Programme on HIV/AIDS (UNAIDS) launched the 95-95-95 target for HIV. The 95-95-95 initiative sets forth a call to action: by 2025, 95% of all people living with HIV should know their HIV status, 95% of all people with diagnosed HIV infection should receive sustained ART, and 95% of all people receiving ART should have viral suppression [2]. As of 2022, these percentages are 86%, 89%, and 93%, respectively, calling for continued efforts to bridge the remaining gap [1]. With approximately 69.5% of people living with HIV in the sub-Saharan Africa region with limited resources, technology developments aiming towards ending the AIDS epidemic should be tailored for low-resource settings to be effectively deployed [3].

Sensitive HIV testing holds a central position in the HIV management network [4]. The first “95 target” calls for early HIV diagnosis, the first step to trigger linkage to HIV care that can facilitate ART initiation and reduce further transmission. In addition, HIV viral load monitoring is required in patients receiving ART to assess treatment efficacy and determine regimen adjustments. The

current viral load threshold established by the WHO is set at 1000 RNA copies per milliliter of plasma, underscoring the need for a highly sensitive HIV test.

While sensitive HIV testing is needed for both early diagnosis and routine viral load monitoring, the most sensitive approach, reverse transcription-quantitative polymerase chain reaction (rt-qPCR), is limited to centralized laboratories due to the labor-intensive process and the requirement for high-end instrumentation. Bringing sensitive HIV tests to the point-of-care could expand the testing coverage, especially in low-resource settings [5]. Existing point-of-care HIV tests targeting HIV antibodies suffer from a minimum one-month window period of human immune response and subsequently delayed detection [6]. Tests detecting both HIV antigen (e.g., p24) and antibodies claim to shorten the window period to around two weeks (e.g., Alere Determine HIV-1/2 Ag/Ab Combo Test), but they are not applicable to viral load monitoring due to the limited analytical sensitivity and infant HIV diagnostics due to the presence of maternal HIV antibodies [7]. Various platforms have been developed aiming to bring the HIV nucleic acid amplification test (NAAT) to point-of-care settings, such as Alere q NAT [8], SAMBA Semi-Q [9,10], and Cepheid GeneXpert [11]. The platforms often integrate microfluidics with isothermal amplification or miniaturized PCR, simplifying testing workflows and automating user steps [12]. Compared to laboratory-based HIV NAAT, those platforms have made significant advancements in delivering rapid, user-friendly, and more cost-effective nucleic acid tests [13]. However, the developed HIV NAATs aiming for the point-of-care are not yet CLIA-waived and often require complex equipment and disposable cartridges that could add to overall test costs.

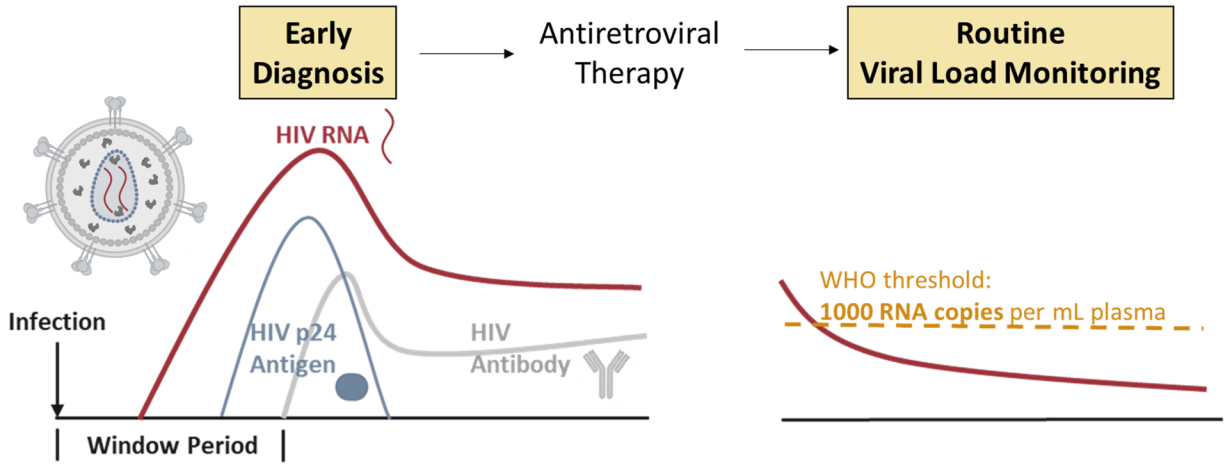

Figure 1.1. Need for sensitive POC HIV tests.

1.1.2 Development challenges for sensitive POC HIV tests

A standard NAAT starts with nucleic acid extraction where DNA/RNA targets are purified from crude samples, followed by nucleic acid amplification reactions where target sequences are replicated to detectable levels. Conventionally, polymerase chain reaction (PCR), the gold standard nucleic acid amplification method, has limited NAATs to centralized laboratories due to the need for specialized instrumentation with precise temperature cycling controls. The development of various isothermal amplification techniques has removed the barrier tied to thermal cycling and brought NAAT closer to the point of care [14]. For example, loop-mediated isothermal amplification (LAMP) only requires a constant temperature of around 65°C, which facilitates point-of-care products detecting SARS-CoV-2 RNA [15]. However, several challenges still need to be addressed for a highly sensitive point-of-care HIV test.

First, point-of-care tests use fingerstick blood samples, which can only provide small volumes of plasma (~20µL). The threshold of 1000 HIV RNA copies per milliliter of plasma translates to a limit of detection (LoD) target at 20 RNA copies from fingerstick plasma volumes (~20µL), a demanding requirement for test sensitivity. Second, sample preparation remains challenging at the

point of care. The plasma environment contains various NAAT inhibitors, such as albumin, IgG, and salts [16], which can impede the performance of the amplification assay. In addition, the highly abundant ribonucleases (RNase) in plasma could degrade RNA targets within seconds at the room temperature [17]. Standard nucleic acid extraction procedure involves multiple rounds of centrifugation, thus it is constrained to laboratory settings [18]. While various approaches have been demonstrated to streamline the extraction process for the point of care, such as paper membranes or microfluidics coupled with silica beads, magnetic beads, or sequence-specific probes [19–23], they typically adhere to a lyse-bind-wash-elute paradigm, which adds to the device complexity and testing costs. Last, the low abundance of HIV RNA targets in the sample demands a sensitive isothermal amplification assay, but the highly diverse genetic sequences among HIV subtypes pose significant challenges to the assay design. While multiple RT-LAMP assays have been reported with a sensitivity down to 10 copies of HIV RNA [24–27], the performance may vary drastically among different subtypes [28].

1.2 Development towards Sensitive POC HIV Tests: Method Introduction

In my thesis, I explored two independent approaches aiming towards a sensitive POC HIV test. In the first approach, instead of detecting HIV RNA, the assay targets the reverse transcription activity of the reverse transcriptase (RT) enzyme encapsulated inside the HIV virus. The second approach targets the HIV RNA but bypasses the nucleic acid extraction step through large-volume RT-LAMP to streamline the workflow.

1.2.1 **HIV reverse transcriptase activity assay**

1.2.1.1 HIV RT activity as a biomarker

As a retrovirus, the replication process of HIV relies on the essential role of encapsulated reverse transcriptase (RT), which generates complimentary DNA (cDNA) from its RNA genome. The reverse transcription activity of HIV RT presents an opportunity as an alternative biomarker, where engineered RNA is added as assay substrates for HIV RT to generate cDNA which will be subsequently amplified and detected (**Figure 1.2**). As a biomarker, the reverse transcription activity of HIV RT offers several potential advantages compared to HIV RNA. First, each HIV virion is reported to contain 50-100 copies of RT enzymes in contrast to only two copies of the RNA genome, providing more targets available for detection [29,30]. Second, as a protein, HIV RT is inert to RNases abundant in plasma and less prone to degradation than RNA. Third, as an enzyme, each HIV RT could generate multiple copies of cDNA, providing an additional front-end enhancement. Fourth, RT in different HIV subtypes should share the same activity since it is critical for HIV replication, making the assay inherently robust against diverse HIV subtypes. Lastly, the sequence of the added RNA substrates could be engineered to achieve high efficiency for HIV reverse transcription and subsequent cDNA amplification.

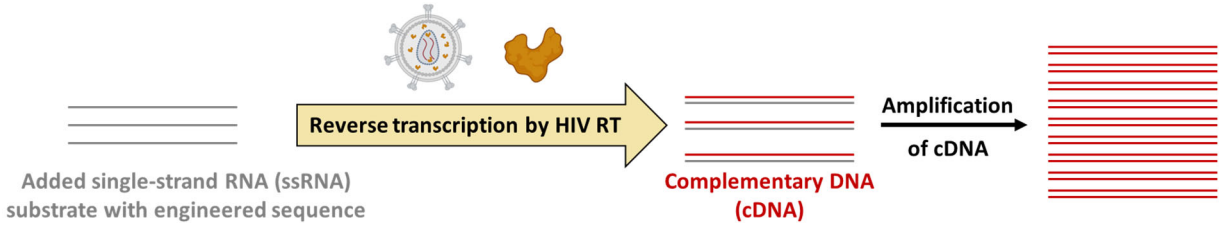

Figure 1.2. The reverse transcription activity of HIV RT as a biomarker.

1.2.1.2 Previous HIV RT activity assays

The earliest HIV RT activity assays date back to the 1980s [31], soon after HIV was identified and before PCR was invented. The early versions of HIV RT activity assays included radioactively labeled dNTP analogues in the reaction, such as ^{3}H-dTTP and ^{125}I-dUTP, to be incorporated into the cDNA product by HIV RT for detection, and a homopolymeric RNA strand (e.g., poly-A) was often used as the template [32,33]. With a limited sensitivity, the assays were mostly used for HIV RT characterization and studies. Thereafter, radiolabels were replaced with biotin- or digoxigenin-labeled dNTP analogues that were compatible with HIV RT, and the detection was achieved through streptavidin or anti-dig conjugated horseradish peroxidase (HRP) binding to the cDNA and subsequent colorimetric reactions catalyzed by HRP [34,35]. The signal amplification provided by HRP improved the assay sensitivity, and workflows built upon the assays were further applied to HIV viral load monitoring by quantifying the RT levels in patient samples [36]. However, the tests required extended incubation time for HIV RT to generate detectable levels of cDNA, thus limiting their clinical implementations.

PCR-based HIV RT activity assays were soon developed in the 1990s after PCR was invented. In those assays, namely, PERT (product-enhanced reverse transcriptase assay) developed by Pyra *et al.* and Amp-RT developed by Heneine *et al.*, PCR was used to amplify and detect the cDNA generated by HIV RT [37,38]. With the exponential amplification offered by PCR, the assays were extremely sensitive and could detect down to hundreds of HIV RT copies. The PERT assay was further validated on clinical samples with different subtypes for HIV viral load quantification and showed a good correlation with RNA-based assays [39]. Similarly, Amp-RT was tested for viral load monitoring in clinical samples and the results showed the levels of virion-associated RT varies among different patients [40,41]. As a phenotypic assay, Amp-RT was further explored for HIV

drug resistance screening by quantifying the inhibition of HIV RT activity in the presence of HIV RT inhibitors such as Nevirapine and Lamivudine ([42–45]). While the assays demonstrated exceptional sensitivity for HIV detection, ultracentrifugation was used for sample preparation and PCR was used for cDNA amplification, limiting the assays to use in centralized laboratories. In addition, the assays consisted of multiple separate steps including cDNA generation, RNA digestion, and PCR amplification, adding to the complication for point-of-care applications. Nevertheless, the assays have validated the feasibility of HIV RT activity as a biomarker and built the foundation for the work described in Chapter 2.

1.2.1.3 Method Overview

To address the limitations of previous HIV RT activity assays in the context of point-of-care HIV testing, Chapter 2 of the thesis aims to replace PCR with LAMP for cDNA amplification and detection, combined with direct immunocapture of HIV RT for sample preparation. In addition, we aim to combine the cDNA generation by HIV RT and subsequent LAMP amplification into one pot to simplify the workflow. Furthermore, we propose another version of HIV RT assay using CRISPR-Cas to detect the cDNA generated by HIV RT, combining the frond-end enhancement offered by HIV RT and the signal amplification offered by CRISPR-Cas. Since CRISPR-Cas provides quantitative detection, we aim to use the assay to characterize HIV RT activity for potential drug resistance screening. Moreover, owing to the inherent high programmability of CRISPR-Cas, we hypothesize the platform can be readily adapted for other enzyme targets for broader applications. The relevant work is described in **Chapter 2**.

1.2.2 **Large-volume RT-LAMP for extraction-free HIV RNA amplification**

1.2.2.1 Extraction-free amplification in LAMP

Extraction-free amplification refers to directly adding biological samples into nucleic acid amplification reactions for DNA/RNA detection. It eliminates the laborious nucleic acid extraction step and streamlines the testing workflow, matching the simplicity offered by LAMP. In addition, extraction-free amplification avoids potential target loss during nucleic acid extraction due to imperfect recovery efficiency, especially when targets are present in low abundance [23]. Therefore, various reports have employed extraction-free amplification in LAMP for point-of-care diagnostics [46].

To maintain the same performance as LAMP with purified DNA/RNA, extraction-free LAMP needs to address several concerns. First, pathogens need to be fully lysed to release genetic materials for detection. Reported extraction-free LAMP assays have achieved efficient lysis through the incorporation of digestive enzymes (e.g., proteinase K) [47], chemical agents (e.g., detergents) [48], or thermal treatment [49] as part of the sample pretreatment step or directly within the LAMP reaction. In addition, the elevated reaction temperature of LAMP (around 65°C) could further facilitate pathogen lysis. Priya *et al.* have reported similar RT-LAMP performance using intact ZIKV virus and extracted ZIKV RNA, suggesting efficient viral lysis under LAMP conditions. Second, the sample matrix could contain inhibitors that impede the amplification efficiency, such as albumin and IgG in plasma, hemoglobin in whole blood, mucin in saliva and nasal swabs, and urea in urine [16]. In addition, the inhibitors could interfere with the detection system used for LAMP, such as protein aggregates obscuring fluorescence readouts or turbidity measurements [50], hemoglobin quenching fluorescence [51], or sample matrix disrupting the pH conditions critical for endpoint colorimetric detections [52]. Sample dilution is often required to

minimize the sample inhibition and maintain the same amplification LoD. For example, Curtis *et al.* developed a method for HIV detection where whole blood was diluted 4-fold with lysis buffer and directly added into an RT-LAMP assay [24]. Similar strategies have been demonstrated with other human samples such as plasma [53], urine [54], nasal swabs [15], and saliva[55]. Lastly, the endogenous RNases in the specimen could degrade the RNA targets, causing a reduction in assay sensitivity. The issue is especially detrimental in HIV detection from plasma samples, due to the low copy number of HIV RNA targets present and the high abundance of RNases in plasma that could degrade RNA within seconds after lysis [17]. Bender *et al.* systematically evaluated additives that could inactivate RNase activity in serum [47]. The additives could be included in the sample pretreatment or the LAMP reaction to preserve RNA integrity. In addition, the RNA targets are protected inside the viruses until lysis, and the dilution may allow the reverse transcription to outpace the RNase degradation.

Despite the promises of extraction-free LAMP, the required sample dilution and the typical ~20μL LAMP reaction volumes limit the input sample quantity, leading to an inevitable sensitivity loss. Therefore, extraction-free LAMP may be suitable for applications where the sample matrix is less inhibitory and targets are present at high concentration levels, such as SARS-CoV-2 detection from nasal swabs [15]. For POC HIV tests that demand exceptional sensitivity and/or more disruptive inhibitory substances, the limitation on input sample volumes needs to be addressed.

1.2.2.2 Large-volume LAMP

Expanding the reaction volumes can facilitate the inclusion of the whole fingerstick plasma in LAMP and avoid sample loss. The small reaction volumes of nucleic acid amplification assays (usually 10-20μL) are likely associated with the historical constraints of PCR requiring fast heat transfer for rapid thermal cycling and high reagent costs limiting reaction volumes. However,

LAMP only requires a single reaction temperature of around 65°C, eliminating the volume limitation tied to thermal cycling. The high reagent cost is likely due to limited suppliers or proprietary materials, and it could be significantly reduced by switching to non-commercial or lower-cost reagents [56,57], opening the door to running LAMP at larger reaction volumes. Curtis *et al.* demonstrated RT-LAMP at 100µL reaction volumes with similar amplification LoD as standard volumes. Nevertheless, the potential of LAMP at even larger volumes remains unexplored.

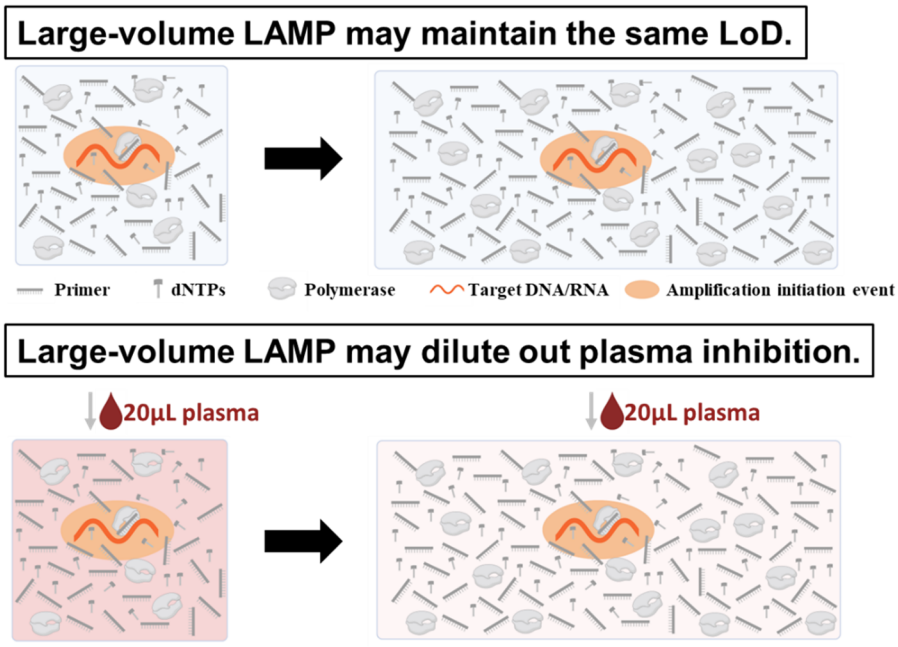

Figure 1.3. Illustration of the potential benefits of large-volume LAMP.

1.2.2.3 Method Overview

We propose running RT-LAMP at large reaction volumes to enable directly adding whole fingerstick plasma (around 20µL) into the assay for sensitive HIV detection. The relevant work is described in **Chapter 3**.

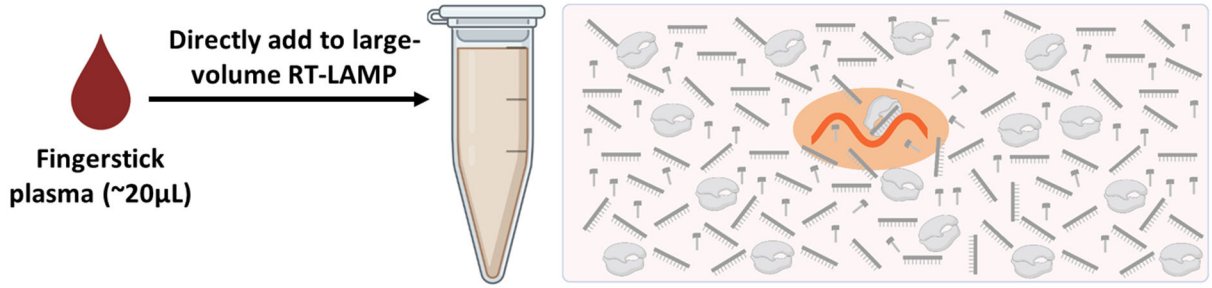

Figure 1.4. Illustration of the proposed method for extraction-free HIV detection from fingerstick plasma through large-volume RT-LAMP.

1.3 POC Tests in COVID-19

1.3.1 **Rapid COVID-19 antigen test**

The COVID-19 pandemic caused a profound global public health crisis. Since its outbreak in December 2019, the pandemic has tragically claimed over 6 million deaths globally according to the WHO [58]. Despite the development of effective vaccines, as of the date of writing, there continue to be more than 10,000 new daily cases around the world. Therefore, diagnosis remains critical in controlling the spread of infection. Massive point-of-care testing has proven to be a highly effective strategy for "flattening the curve" of infected cases [59], and rapid antigen tests are widely adopted for point-of-care or self-testing of COVID-19.

Most COVID-19 rapid antigen tests are in the format of lateral flow assays (LFA) and detect the SARS-CoV-2 nucleocapsid antigens in respiratory specimens such as nasal swabs and saliva [60]. While the rapid antigen tests are simple to run and offer a rapid turnaround time, they exhibit lower sensitivity compared to NAATs and are mostly recommended for symptomatic populations only [60]. The WHO target product profile (TPP) for COVID-19 point-of-care tests sets the acceptable limit of detection (LoD) at 1000 genome copies per µL. However, most rapid antigen tests fall short of meeting the threshold [61].

1.3.2 **Opportunities to increase test sensitivity by increasing sample volumes**

While nasal swab elution could provide a sample volume of around 0.5mL [62] and saliva could provide up to 5mL [63], most LFAs used in COVID-19 rapid antigen tests are designed to accommodate only 50-100μL of samples, leading to an inevitable sensitivity loss. Various techniques have been developed to concentrate target analytes from larger sample volumes, showcasing enhancements in assay sensitivity [64–67]. For example, Golden *et al*. reported concentrating the malaria antigen in plasma through the capture of stimuli-responsive polymer-antibody conjugates at porous membranes [68]. Since saliva has been reported to have similar viral concentrations of SARS-CoV-2 to nasal swab elution [69], we anticipate that concentrating SARS-CoV-2 antigens from large-volume saliva could improve the sensitivity of COVID-19 rapid antigen tests by loading more target analytes available for detection.

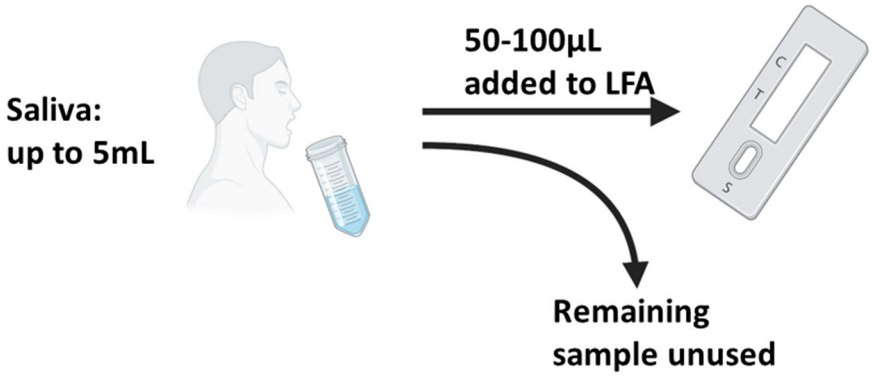

Figure 1.5. Opportunity to increase LFA sensitivity by increasing input sample volumes.

1.4 Improve Sensitivity of Rapid Covid-19 Antigen Test: Method Introduction

1.4.1 **Agglutination introduction**

When two multivalent components with specific binding interactions are mixed under the right concentration ratios, they can undergo agglutination, generating large aggregates similar to the polymerization process. Agglutination only requires the mixing of the two components yet is

effective in forming visible aggregates rapidly, making it a suitable approach for detection. The first application of agglutination in diagnostics dates back to the Widal test for typhoid fever developed in 1896, where inactivated *Salmonella typhi* is mixed with serum samples, prompting agglutination with target antibodies for *S typhi*-infected patients [70]. Due to its simplicity and visible readouts, agglutination tests have further expanded to various applications including blood typing [71], influenza virus screening [72], and detection of antibodies or other protein biomarkers [73–75]. The agglutination components also diversified into different biological reagents, such as red blood cells, antibody-coated latex beads, or bacteria with surface-displaying nanobodies [76]. However, most tests use the target analyte as one of the agglutination agents, and the readout is from the agglutination itself. As agglutination requires appropriate concentration ratios, target analytes need to be present at high concentrations, significantly limiting the test sensitivity.

1.4.2 **Method overview: SA-biotin-based agglutination assay**

We have found that agglutination could occur between streptavidin (SA), known to possess four biotin-binding sites, and antibodies conjugated with multiple biotins. Combining the new SA-biotin-based agglutination system and typical immunoassays, we propose a new format of COVID-19 agglutination assay, where the immunosandwich structures with biotinylated antibodies undergo agglutination with added SA and the agglutinated aggregates can be collected by filtration to report diagnostic signals. Since the agglutination is independent of target concentrations and the assay could accommodate large sample volumes, we anticipate the assay could achieve an enhanced LoD compared to LFAs. The relevant work is detailed in **Chapter 4**.

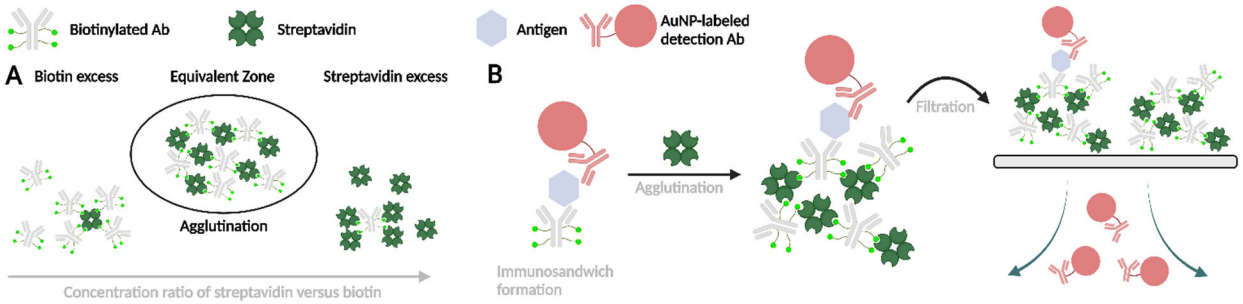

Figure 1.6. COVID-19 agglutination test: Method overview.

Chapter 2. HIV Reverse Transcriptase Activity Assay with Product Amplification Mediated by LAMP or CRISPR-Cas

2.1 Abstract

Sensitive HIV testing is critical for both early HIV diagnosis and routine HIV viral load monitoring in patients receiving antiretroviral therapy (ART), but the most sensitive approach, the HIV RNA rt-qPCR test, is limited to centralized laboratories. A sensitive point-of-care HIV test could expand the testing coverage, especially in low-resource settings. However, tests targeting HIV RNA experience significant challenges due to its low abundance and inherent instability. Here we developed an assay targeting the reverse transcription activity of the reverse transcriptase (RT) enzyme encapsulated inside HIV. Specifically, external RNA substrates were added for HIV RT to generate complementary DNA (cDNA), followed by amplification and detection mediated by LAMP or CRISPR-Cas systems. To guide the assay design, we first characterized the cDNA generation activity of HIV RT with qPCR. In the LAMP-mediated Product-Amplified RT activity assay (LamPART), the cDNA generation and LAMP amplification were combined into one pot with novel assay designs and demonstrated a LoD at 20 copies of HIV RT. When coupled with direct immunocapture of HIV RT for sample preparation and endpoint lateral flow assays for detection, LamPART detected down to 20 copies of HIV RT spiked in 25μL plasma (fingerstick volume) and was further validated on clinical samples. In the Cas-mediated Product-Amplified RT activity assay (CasPART), we tailored the substrate design to achieve a LoD of 2e4 copies (1.67fM) of HIV RT. Furthermore, as a sensitive phenotypic assay, CasPART was used to characterize the HIV RT inhibition under HIV drugs and differentiate responses between wild-

type and mutant HIV RT for potential drug resistance testing. Moreover, the CasPART assay can be readily adapted to target other enzymes for a wider range of pathogen detection and phenotypic characterization. As a proof-of-concept, we successfully used CasPART to detect the disintegration activity of HIV integrase with a sensitivity of 83nM.

2.2 Introduction

Infectious diseases persist as a global threat, and sensitive detection of the associated pathogens holds a central position in clinical management. HIV, with 39 million people infected worldwide and 1.3 million new cases in 2022, stands as one of the foremost challenges to global health [1]. Sensitive HIV testing is essential for both early HIV diagnosis and routine HIV viral load monitoring in patients receiving antiretroviral therapy (ART). However, the HIV RNA rt-qPCR test, the most sensitive method, is constrained to centralized laboratories due to laborious workflow and specialized instrumentation requirements. Bringing sensitive HIV testing to the point of care (POC) using fingerstick samples could expand the testing coverage, especially in low-resource settings. Existing POC HIV tests targeting HIV antigens and antibodies suffer from lower sensitivity and the window period of the human immune response, and they are not applicable for early infant diagnosis or viral load monitoring [6,7]. The development of various isothermal amplification techniques has brought nucleic acid amplification tests (NAAT) closer to POC applications. However, HIV RNA as the biomarker presents significant challenges due to its low abundance and inherent instability in plasma, which often translates to increased costs or reliance on complex instruments of the developed tests [3].

Most pathogens replicate their genetic materials via a combination of the host cell machinery and their own suite of enzymes, either encapsulated within the pathogen or encoded in their genome and subsequently expressed in the host. The pathogen-derived enzymes are typically specialized to facilitate distinct steps in the replication process and thereby their activities present an opportunity as biomarkers for pathogen detection. HIV, as a retrovirus, carries reverse transcriptase (RT) that possesses reverse transcription activity to convert its RNA genome into complementary DNA (cDNA) during replication[29]. Multiple assays have been developed in the

past to detect the cDNA generation activity of HIV RT for sensitive HIV diagnosis, which further expanded to viral load monitoring and drug resistance testing [36–39,45,77]. Compared to the HIV RNA, HIV RT offers several advantages as a biomarker. First, each HIV virion is reported to have 50-100 copies of RT, in contrast to two copies of HIV RNA, providing more targets available for detection [29,78]. In addition, HIV RT as a protein is inert to RNases abundant in plasma and less prone to degradation compared to RNA. Moreover, the conserved RT activity among HIV subtypes allows a broad coverage of HIV with diverse genetic sequences. However, the previous RT activity assays used PCR to amplify and detect the cDNA generated by HIV RT and ultracentrifugation to purify the virus from samples, thus limiting their use to higher-tier laboratories. In addition, the assays involved multiple separate steps including cDNA generation, RNA cleanup, and PCR amplification, adding to the assay complication for point-of-care applications.

Loop-mediated isothermal amplification (LAMP) is a highly sensitive and specific approach for rapid DNA amplification at a constant temperature [79]. In contrast to PCR, LAMP only requires a portable heater without thermal cycling, making it suitable for the point of care [15]. Here we developed a LAMP-mediated Product-Amplified Reverse Transcriptase activity assay (LamPART) by using LAMP to amplify and detect cDNA generated by HIV RT for simple yet sensitive HIV detection (Figure 2.1). While previous RT activity assays needed to separate the cDNA generation and amplification steps, here we combined them into one pot with novel assay designs to simplify the workflow. Furthermore, we integrated the one-pot LamPART with direct immunocapture of HIV RT for sample preparation and endpoint lateral flow assays for detection. The integrated workflow was further validated using HIV-negative plasma spiked with HIV RT as well as HIV-positive plasma samples.

In recent years, the CRISPR-Cas system has emerged as a prominent tool for nucleic acid detection, where the CRISPR RNA (crRNA) recognizes the target sequence, subsequently activating the Cas proteins and inducing collateral cleavage of reporters [80,81]. With its superior sensitivity and specificity, the system was employed in various molecular diagnostics applications [82]. However, the CRISPR-Cas system often requires a pre-amplification step of the target nucleic acid to improve the sensitivity to a clinically relevant range [83]. Here we combined the front-end enhancement provided by HIV RT and the high sensitivity and specificity of CRISPR-Cas nucleic acid detection and developed a Cas-mediated Product-Amplified Reverse Transcriptase activity assay (CasPART). Specifically, the crRNA-Cas12a complex is programmed to recognize the target strand generated by HIV RT and thereafter unleashes indiscriminate DNase activities that digest reporters and generate fluorescence signals (Figure 2.1). We optimized the substrate design to achieve higher sensitivity and demonstrated with both pure HIV RT and RT spiked into HIV-negative plasma. In addition to sensitive detection, CasPART as a quantitative phenotypic assay could be used to characterize HIV RT activities. We explored using CasPART to report the inhibition of drugs on wild-type HIV RT and different responses from mutants for potential drug resistance testing. Furthermore, the high programmability of the substrate and crRNA in CasPART allows the platform to be easily adapted for other enzyme targets. As a proof-of-concept, we adapted CasPART for HIV integrase by detecting its disintegration activity.

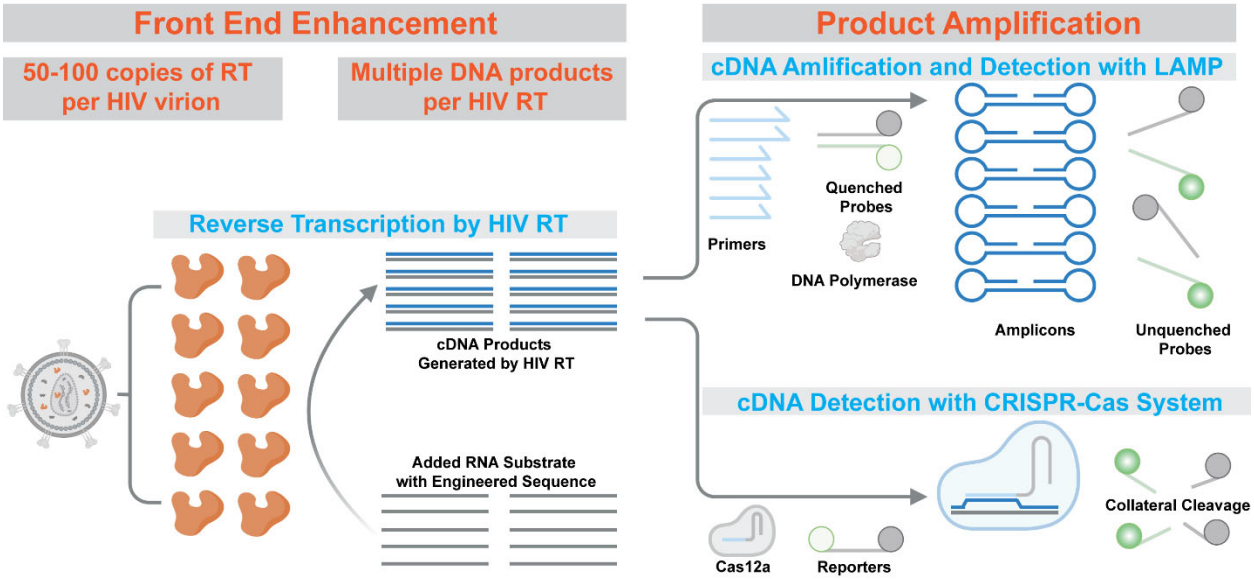

Figure 2.1. Illustrations of the proposed LAMP-mediated and Cas-mediated product-amplified reverse transcriptase activity assay.

2.3 Results and Discussion

2.3.1 **HIV RT activity characterization with qPCR**

As an enzyme, a single copy of HIV RT can potentially generate multiple copies of cDNA, essentially providing a front-end enhancement. To guide the design of the RT activity assay and maximize the detection sensitivity, qPCR was first used to characterize the cDNA generation ability of HIV RT. We adapted reported protocols and first made RNA substrates in-house from DNA templates [84]. HIV RT was then incubated with the RNA substrates and other reagents at 37°C for 2hr for cDNA generation. After heat inactivation, the sample was diluted and added to qPCR to quantify the copy number of cDNA generated by HIV RT. **Figure 2.2A** shows the real-time curves in the qPCR. The amplification from no-RT samples likely resulted from residual DNA templates in the added RNA stock or endogenous reverse transcription activity of the OneTaq DNA polymerase in qPCR [85]. All the positive samples with HIV RT showed

significantly lower Cq in qPCR compared to no-RT controls. As shown in **Figure 2.2B**, the copy number of cDNA and HIV RT exhibited a strong linear correlation, suggesting consistent cDNA per RT across a range of RT copy numbers. Moreover, one HIV RT generated 127.8 cDNA copies within 2hr, confirming the front-end enhancement from the catalytic activity of HIV RT. We next investigated the relationship of cDNA per HIV RT on incubation time and RNA substrate concentrations. The cDNA copy number per HIV RT decreased linearly when the incubation time was shortened from 2hr to 30min (**Figure 2.2B and Supplementary Figure 2.8**). 30-minute incubation was thereby selected to balance the assay time and frond-end enhancement. The cDNA copy number quickly rose when RNA concentrations increased from 0.05nM and started to saturate at 2nM (**Figure 2.2C and Supplementary Figure 2.9**). 5nM RNA was chosen to ensure the maximal front-end enhancement.

As we transitioned to LAMP for cDNA amplification, we characterized the cDNA per HIV RT against multiple RNA substrates of different sequences with established LAMP assays. Interestingly, the cDNA copy number per HIV RT varied among different sequences (**Figure 2.2D and Supplementary Figure 2.10**). The differences could be attributed to secondary structures of the RNA substrates that led to varied reverse transcription efficiency, or sequence preference of HIV RT as reported previously [86]. Nevertheless, sequence #2 with the highest cDNA copy number per HIV RT was selected for assay development aiming for high sensitivity.

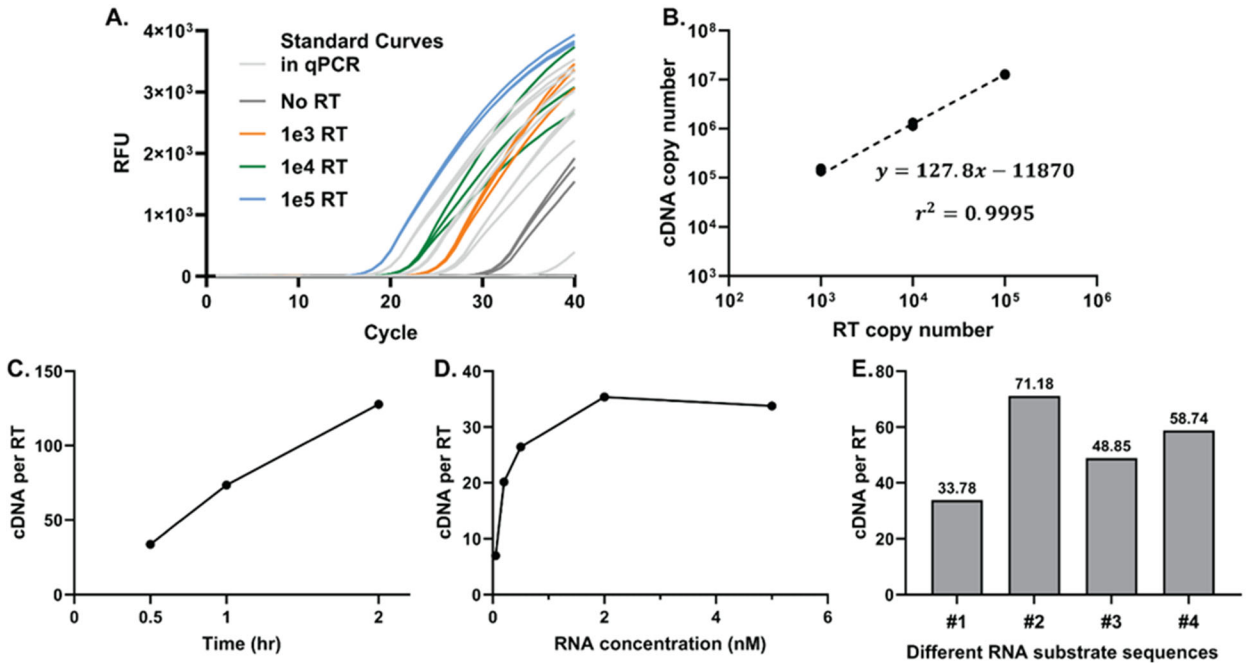

Figure 2.2. Characterization of HIV RT activity with qPCR.

(A) Real-time curves of qPCR quantifying the copy number of cDNA generated by HIV RT with 2hr incubation and 5nM RNA substrates. (B) The linear correlation between the copy number of cDNA and HIV RT. The slope of the fitted line was used to represent the average cDNA copy number per HIV RT. (C) The cDNA per HIV RT with different incubation time and 5nM RNA substrates. The linear correlation of cDNA per RT at each data point can be found in **Supplementary Figure 2.8**. (D) The cDNA per RT with different concentrations of RNA substrates and 0.5hr incubation. The linear correlation of cDNA per RT at each data point can be found in **Supplementary Figure 2.9**. (E) The cDNA per RT on different RNA substrate sequences with 0.5hr incubation and 5nM RNA. Sequence #1 was used in panel A-D. The linear correlation of cDNA per RT for sequences #2, #3, and #4 with 0.5nM, 2nM, and 5nM RNA substrates can be found in **Supplementary Figure 2.10**. All linear correlations were conducted in GraphPad Prism 10.

2.3.2 **Development of one-pot LamPART**

We aimed to combine cDNA generation by HIV RT and LAMP into one pot to simplify the assay workflow. Specifically, the reaction contains reagents for both reverse transcription and LAMP and would simply be incubated at 37°C for cDNA generation followed by 65°C for LAMP (**Figure 2.3A**). The LAMP assay employed sequence-specific probes to report amplification [56]. However, we initially encountered strong false positives in the absence of HIV RT (**Figure 2.3B**),

likely caused by a) innate reverse transcription activity of the DNA polymerase in LAMP at both 37℃ and 65℃ [87], and b) side products from primer dimers during 37℃ incubation that led to nonspecific amplification in LAMP (**Figure 2.3A**). TF Pol was used as the LAMP DNA polymerase since it was reported to be highly specific [15,56]. In addition, TF Pol showed less reverse transcription activity compared to Bst 2.0 WS as quantified by qPCR (**Supplementary Figure 2.11**). However, TF Pol still generated over 10^5 and 10^{10} copies of cDNA when incubated with 5nM RNA for 30min at 37℃ and 65℃, respectively (**Supplementary Figure 2.11**). To address the issue, first, an aptamer against the backbone of TF Pol was included in the reaction to inhibit TF Pol activity at 37℃ [88,89]. Second, to differentiate the cDNA product from the RNA substrate, the RNA sequence was truncated to be shorter than the LAMP footprint and missing F1 and partial F2 binding regions (**Figure 2.3C**). At 37℃, the FIP (F1-F2) primer functioned as the RT primer and hybridized with the truncated RNA substrate to generate the full-length cDNA under HIV RT. The melting temperature of the hybridization region was designed at around 45℃. At 65℃, the FIP-RNA hybrid dissociated, and the truncated RNA substrate became non-amplifiable in LAMP. Only the full-length cDNA generated by HIV RT could be amplified and detected. In addition, the cDNA had one loop structure incorporated, which removed the need for the F3 primer and one bumping step in LAMP that was suggested rate-limiting [90]. Furthermore, to address the issue of nonspecific amplification from primer dimers at 37℃, we introduced dockers to LAMP primers, specifically to the LB and B3 primers. The dockers are short DNA oligos complementary to the matching primer with melting temperatures around 55℃. The dockers could sequester the LB and B3 primers at 37°C to prevent extendable primer dimers and then release the primers at 65℃ for LAMP amplification (**Figure 2.3C**). The dockers were blocked on the 3' end to avoid introducing new extendable dimers. Interestingly, we found that cDNA per

HIV RT under LAMP conditions started to saturate at 50nM RNA instead of 2nM (**Supplementary Figure 2.12**). The discrepancy could be attributed to much higher primer concentrations in LAMP and primer dimers at 37℃ competing against RNA substrates to bind HIV RT, or higher dNTP concentrations in LAMP that chelated Mg^{2+} and thereby affected HIV RT activity. Regardless, 50nM RNA substrate was used in LamPART for a balance between HIV RT efficiency and false positives from TF Pol acting on RNA substrates.

With all the developments, the negative controls in the final assay all amplified after 30min which was then set as the cutoff time (**Figure 2.3D**). In preliminary LoD screening, the assay successfully detected all three replicates of 10-RT samples. In further LoD determination with 20 replicates, while only 11 replicates were positive for 10-RT samples, 19 replicates of 20-RT samples showed positive (**Figure 2.3E and Supplementary Figure 2.13**). All 20 replicates of negative controls were amplified later than the cutoff time. Therefore, the one-pot LamPART assay demonstrated a LoD at 20 copies of recombinant HIV RT, equivalent to a single virion. The whole assay is within an hour and requires only two temperature steps without any user intervention in between. In addition, the assay reagents do not include any reverse transcriptase, one of the most expensive components in an RT-LAMP assay [57]. Moreover, we anticipate the concept of primer dockers can be applied to other assays involving multiple steps at different temperatures, to sequester unwanted primers at certain steps and minimize unspecific amplifications.

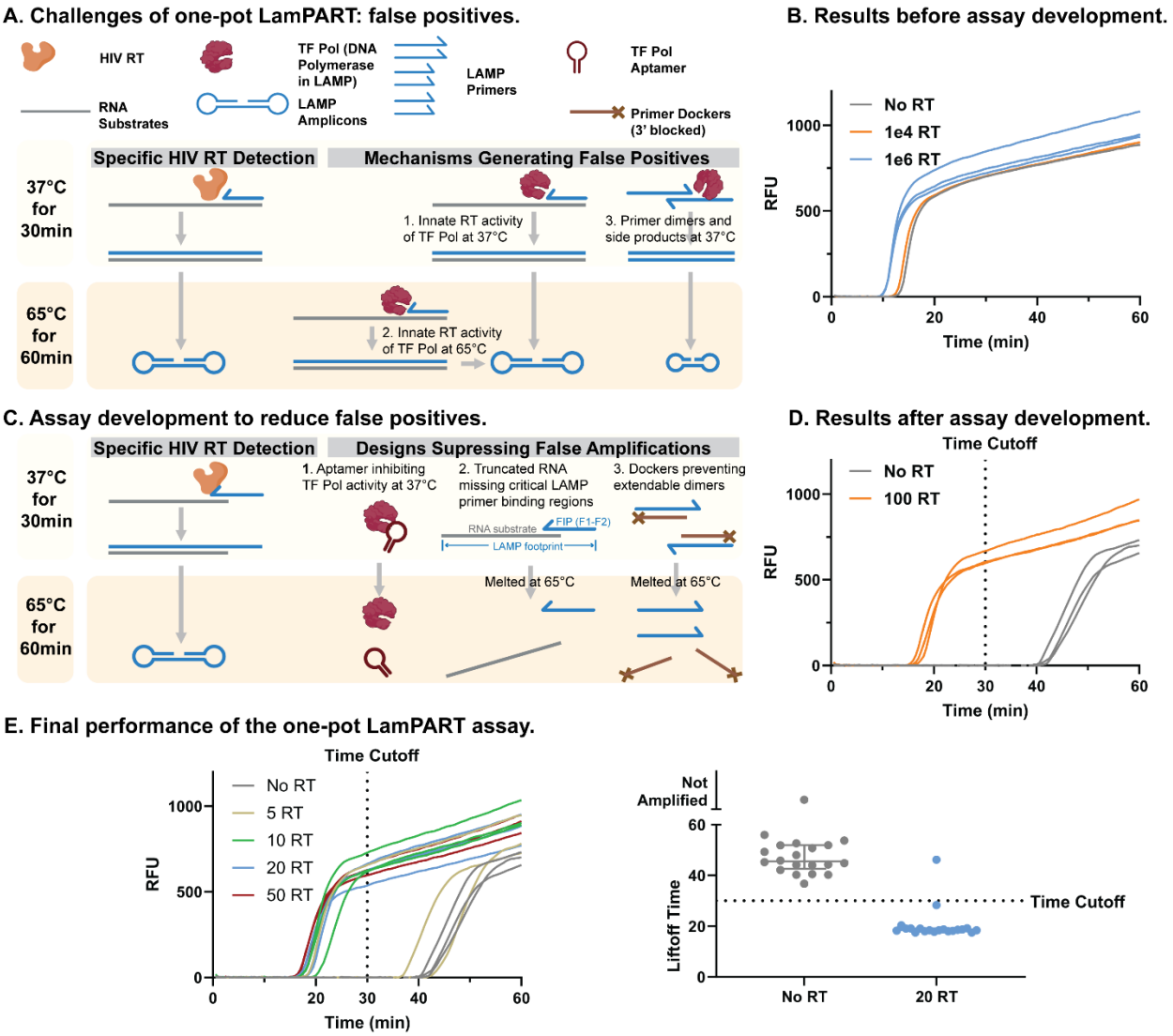

Figure 2.3. One-pot LamPART Assay.

(A) Illustrations of potential mechanisms in one-pot LamPART that could generate false positives. (B) One-pot LamPART results before assay development. (C) Assay designs that help suppress the false positives in one-pot LamPART. (D) One-pot LamPART results after assay development. (E) LoD determination of the final one-pot LamPART assay. Left, preliminary LoD screening with three replicates per sample. Right, LoD determination with 20 replicates of negatives and samples with 20 copies of HIV RT. The results of 20 replicates of 10-RT samples can be found in **Supplementary Figure 2.13**.

2.3.3 **Integrated workflow from sample to detection**

We developed direct immunocapture of HIV RT from plasma samples using anti-HIV-RT-coated magnetic beads for sample preparation (**Figure 2.4A**). Antibodies that do not inhibit HIV RT activity were first identified through PCR quantification of cDNA generated by free HIV RT versus HIV RT preincubated with antibodies (**Supplementary Figure 2.14**). The antibody was bound to anti-mouse-IgG-conjugated magnetic beads for immunocapture of HIV RT. To avoid false positives from unspecific capture of human polymerases that may have reverse transcription activity [91], 1% BSA was used to pre-block the beads and included during HIV RT capture for additional real-time blocking. To evaluate the performance of direct immunocapture, cDNA generated from HIV RT spiked into plasma and subsequently captured was quantified with qPCR and compared with free HIV RT. As shown in **Figure 2.4B**, the negative controls generated negligible cDNA, confirming the specificity of the immunocapture. The captured RT generated around half of cDNA compared to the positive controls. The loss could be due to imperfect capture efficiency or the inhibition of beads on the activity of bound RT. Finally, the immunocapture was integrated with the one-pot LamPART assay. The integrated workflow successfully detected 20 copies of HIV RT spiked into 25µL HIV-negative plasma (**Figure 2.4D**). To further simplify the workflow, endpoint lateral flow detection of LAMP amplicons was developed to replace real-time fluorescence. We adapted a published method where LAMP primers FIP and BIP were labeled with biotin and FITC, respectively [92]. The LAMP amplicons would be dual-labeled and subsequently detected in a commercial lateral flow strip (**Supplementary Figure 2.15**). As shown in **Figure 2.4C and D**, the endpoint lateral flow detection demonstrated the same sensitivity as real-time fluorescence in both the LamPART assay alone and the integrated workflow, where the

test lines remained clean for negative controls and appeared for positive samples with 20 HIV RT copies and above.

The integrated workflow demonstrated a LoD at 20 copies of recombinant HIV RT spiked into 25µL plasma (fingerstick volume). The whole workflow required minimal user steps and less than 2hr total turnaround time. The instrumentation only included a magnetic stand and a thermocycler that could run two temperatures combined with endpoint lateral flow detection. In addition, the workflow could be conducted in high throughputs by employing PCR strip tubes for sample processing combined with multi-channel pipettes (**Supplementary Figure 2.16**). Multiple areas of the workflow could continue to be developed in the future to facilitate simpler implementation. First, the antibody capture and washing steps can be automated in microfluid chips to further reduce user steps and shorten the total turnaround time. Second, the RNA substrates currently need to be stored in -80℃ freezers which is challenging for the point of care especially in low-resource settings. Future work could explore expressing the RNA substrates in phage-like particles to allow storage at higher temperatures or lyophilization [93]. Lastly, the assay reagents could be lyophilized and rehydrated at the point of testing to further minimize the user steps [94]. Nevertheless, the high sensitivity and simple procedures of the LamPART-based integrated workflow provided an alternative and promising option for sensitive HIV testing at the point of care.

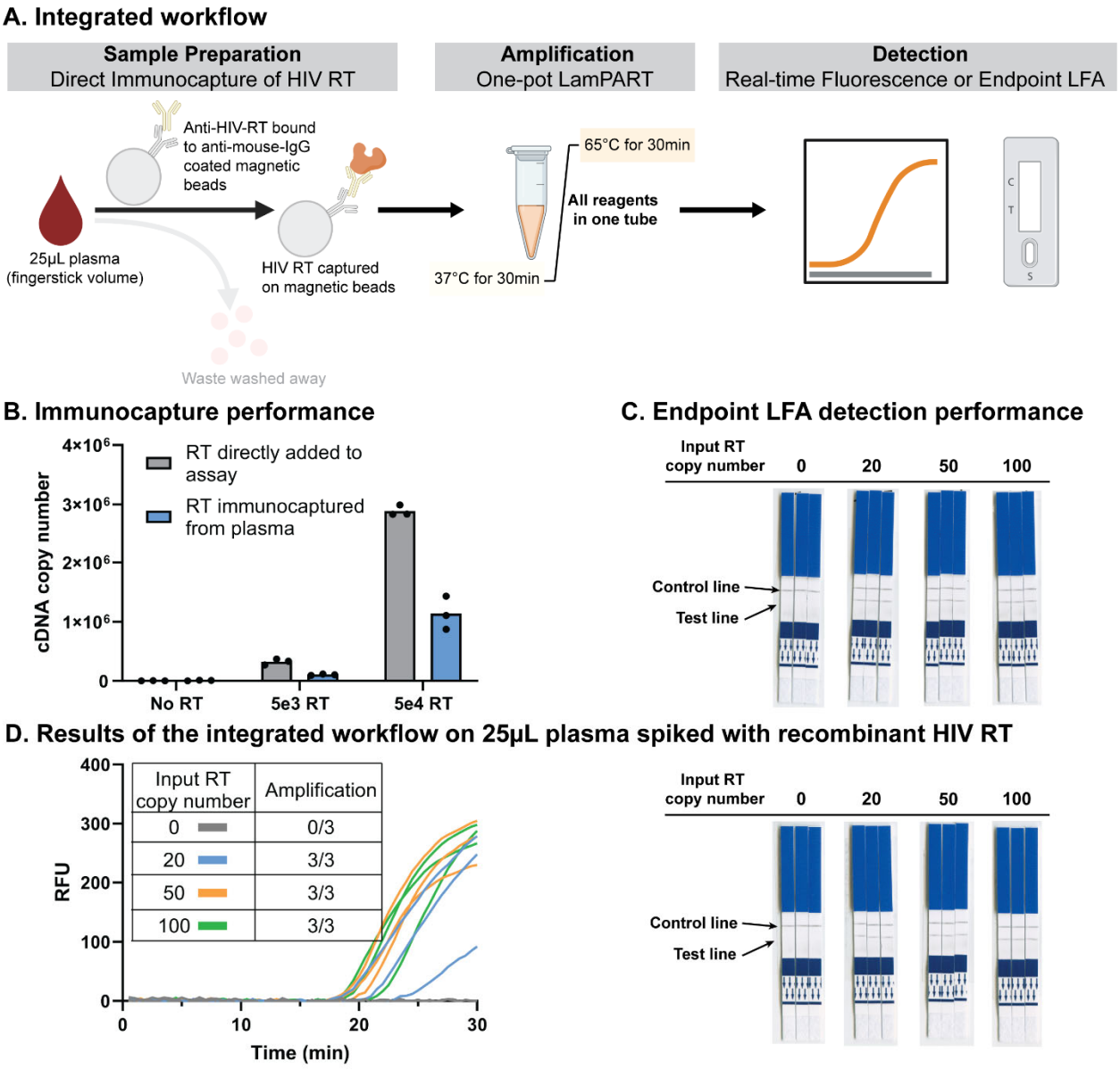

Figure 2.4. LamPART-based integrated workflow.

(A) Illustration of the integrated workflow. (B) PCR quantification of cDNA copy number generated by free freshly-diluted HIV RT versus HIV RT spiked into HIV-negative plasma and subsequently immunocaptured. (C) Performance of the endpoint lateral flow detection of the one-pot LamPART amplicons. (D) Results of the integrated workflow on 25µL HIV-negative plasma spiked with HIV RT. Left, integrated workflow with real-time fluorescence detection. Right, integrated workflow with LFA detection.

2.3.4 **Validation of integrated workflow on clinical samples**

The integrated workflow with real-time fluorescence detection was tested on 10 individual HIV-negative plasma samples and 6 HIV-positive ART-naïve samples with viral loads between 1000 and 5000cp/mL. For each sample, the workflow was run on three 25µL aliquots. As shown in **Figure 2.5**, for HIV-negative samples, 9 out of 10 showed negative results in all three replicates, and only one sample showed positive in one of the replicates. The results again confirmed the specificity of the workflow. However, for HIV-positive samples, only one sample showed consistent positive results in all replicates, while 4 samples showed positive in only one or two of the replicates and one sample showed negative in all replicates. The ability of the assay to detect some of the positive samples suggested the workflow was compatible with endogenous HIV RT. The lower-than-expected sensitivity could be attributed to several reasons including insufficient virus lysis, lower immunocapture efficiency due to inconsistent plasma matrix from different patients, or inhibition from antibodies in HIV-positive patients against HIV RT [95]. The lysis conditions could be further optimized in future development. The lysis step currently relies on 0.6% NP-40 in the lysis buffer and was included in the 30-minute incubation of the immunocapture step. The type and concentration of the detergents and the incubation time could be investigated thoroughly for a balance of sufficient virus lysis against retention of HIV RT activity and binding affinity of the capture Ab. In addition, the lysis could be separated from the immunocapture step, such as upon sample collection, to allow the use of higher detergent concentrations that could be subsequently diluted during immunocapture. Currently, the 25µL plasma was diluted two-fold with 25µL lysis buffer, and future work could explore increasing the dilution factor to minimize effects from inconsistent sample matrixes among patients. Moreover, an alternative approach for sample preparation could be immunocapturing the whole HIV virion by targeting the HIV surface

antigens, followed by lysis and HIV RT detection [96]. The approach of whole virus capture could remove the inhibition of human antibodies against HIV RT and HIV drugs for patients on ART. Nevertheless, the results showed that the integrated workflow may be promising in detecting HIV-positive samples with viral loads below 5000cp/mL from fingerstick volumes (25µL). Further development is needed for higher sensitivity and more robust performance.

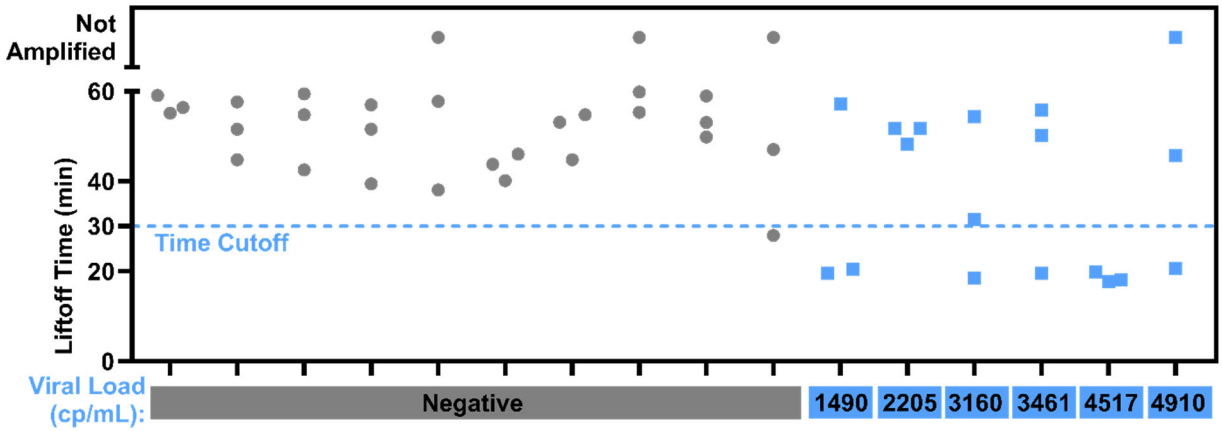

Figure 2.5. Test the LamPART-based workflow on clinical samples.
Results of the integrated workflow with real-time fluorescence detection on 10 HIV-negative and 6 HIV-positive ART-naïve samples. The liftoff time of three replicates per sample was plotted.

2.3.5 **Development of CasPART**

The emerging CRISPR-Cas system offered a simple and specific approach for nucleic acid detection but often required a step of pre-amplifying the target nucleic acid for improved sensitivity. We aimed to combine the front-end enhancement provided by HIV RT with the CRISPR-Cas detection system to develop a one-pot Cas12a-mediated HIV RT activity assay. At a constant temperature of 37°C, HIV RT extends on added substrates to generate target strands that can be specifically recognized by the crRNA-Cas12a machinery. The activated Cas12a then unleashes DNase I activity and cuts the reporters to generate fluorescence signals (**Figure 2.6A**).

We first identified a sequence region in the substrate used for LamPART with minimal hairpin structures through in-silico analysis and subsequently added a PAM sequence to allow Cas12a activation. We investigated using DNA- or RNA-substrates with DNA primers in CasPART and found that DNA substrates generated much higher positive signals (**Figure 2.6B**), likely due to the preference of Cas12a to double-stranded DNA over single-stranded DNA or DNA-RNA hybrid [97]. Since the background signals were lower with RNA substrates, we further tested using DNA-RNA chimeric substrates where the Cas12a activation region was DNA and the rest was RNA, aiming for high positive signals while maintaining low background signals. However, while the background signals stayed low, the positive signals were higher than the RNA substrates but lower than the DNA substrates. Therefore, DNA substrates were selected for assay development. Interestingly, a poly-T tail next to the activation region on the substrate was found to boost the Cas12a detection signals and was thereby included in the design (**Figure 2.6C**). Furthermore, we tested increasing the primer length to minimize the HIV RT extension required for Cas12a activation which could improve assay sensitivity. The positive signals increased as primers spanned into the activation region, but the background signals rose sharply when the overlap of the primer and the activation region changed from 10nt to 15nt, indicating a tipping point in the target strand for nonspecific cas12a activation (**Figure 2.6D**). The 20+10nt primer was thereby used in the final assay. Additionally, we tested including two cas12a activation regions in the substrate to potentially activate more Cas12a per HIV RT product for signal enhancement, as reported in Cas13a systems [98]. However, substrates with dual activation regions produced weaker signals and were thereby not adopted in the assay (**Supplementary Figure 2.17**). As shown in **Figure 2.6E**, the final CasPART assay with 2hr incubation detected down to 2e4 copies (1.67fM) of HIV RT directly added to the reaction. When combined with the direct immunocapture

for sample preparation, CasPART demonstrated the same LoD at 2e4 copies of HIV RT spiked into 25μL plasma (1.33fM), as shown in **Figure 2.6F**. Despite using DNA substrates that could be extended by human DNA polymerase, signals from the negative controls remained low owing to the specificity of the immunocapture.

The developed CasPART assay is a simple one-pot reaction at a constant temperature of 37°C with sensitivity at femtomolar levels for protein detection, among the highest in immunoassays [99]. The assay uses DNA substrates which are more stable than RNA and allow easier implementation. In addition, in future work, the fluorescence reporters could be replaced with lateral flow detections as demonstrated in other CRSPR-Cas systems to further simplify the workflow [100].

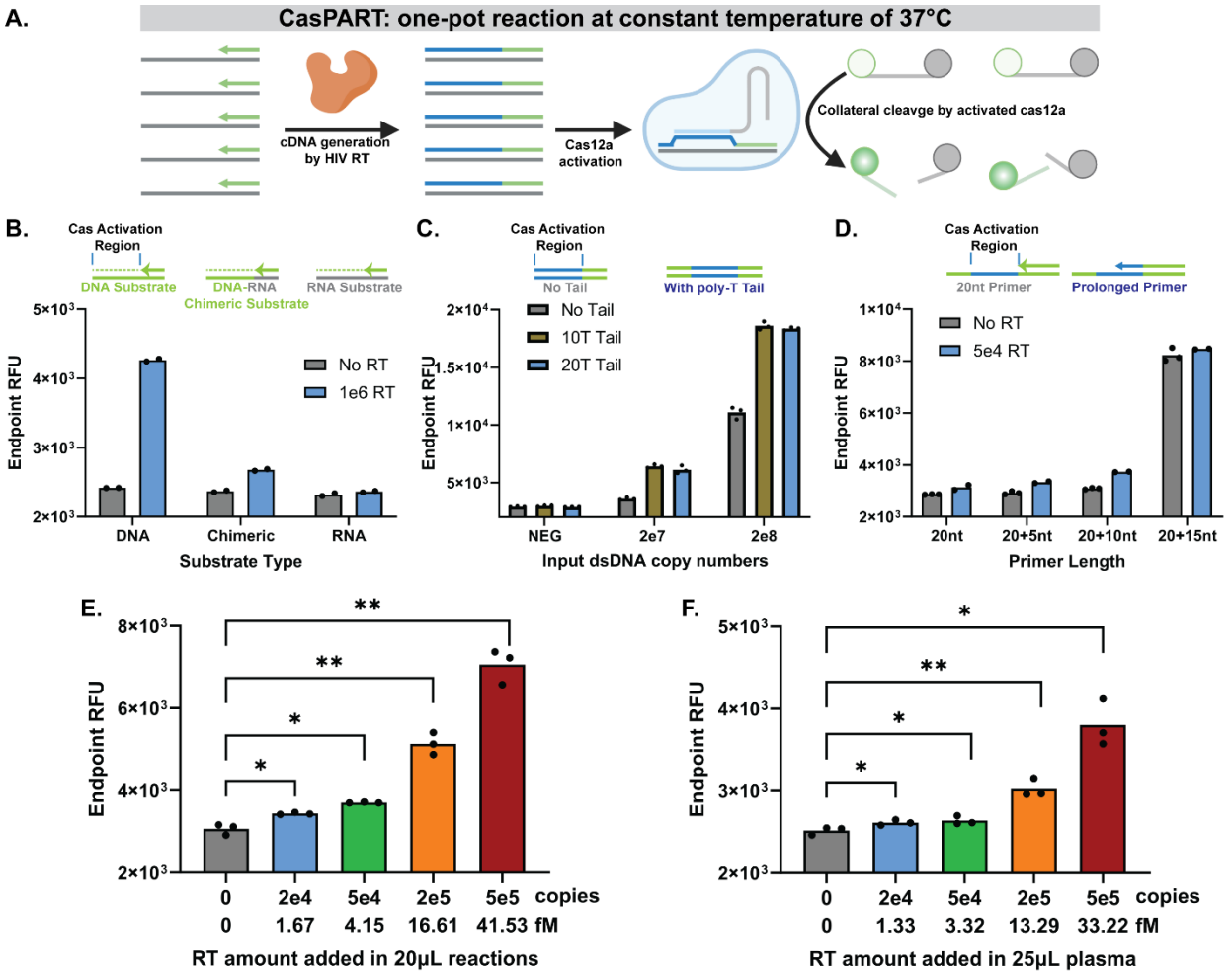

Figure 2.6. Development of the CasPART assay.

(A) Illustrations of the assay principle. (B) Endpoint fluorescence after 2hr incubation using DNA, RNA, and DNA-RNA chimeric substrates in CasPART. (C) Endpoint fluorescence after 2hr incubation of crRNA-Cas12a mixed with double-stranded DNA with or without poly-T tails. (D) Endpoint fluorescence of using primers with varied lengths in CasPART. (E) The final performance of CasPART with HIV RT. Endpoint fluorescence after 2hr incubation was plotted. Real-time curves of 5hr incubation and endpoint RFU at 0.5hr and 5hr can be found in **Supplementary Figure 2.18**. (F) Performance of CasPART integrated with immunocapture on HIV RT spiked into 25µL HIV-negative plasma. Endpoint fluorescence after 2hr incubation was plotted. Statistical significance in panels E and F was determined by unpaired t tests with Welch's correction and conducted in GraphPad Prism 10. * indicates $p < 0.05$ and ** indicates $p < 0.01$.

2.3.6 **Versatility of CasPART**

The quantitative detection of HIV RT products by crRNA-Cas12a made CasPART a sensitive phenotypic assay and offered an opportunity to characterize HIV RT activities in addition to detection. Therefore, we explored using CasPART to characterize the inhibition of HIV drugs on RT activities and responses of wild-type and mutant HIV RT to drugs for potential drug resistance testing. We first tested using CasPART to characterize the IC50 curves of HIV RT activities under Rilpivirine, a drug included in ART recommendations. Signals from samples with Rilpivirine (10^{-11}M – 10^{-5}M) were normalized against control samples with no drugs. As expected, assay signals were not inhibited with low Rilpivirine concentrations but decreased rapidly with higher concentrations, with an IC50 value at 58nM. The results demonstrated the potential of CasPART for the development and characterization of HIV RT inhibitors or drug adherence monitoring in patients [101]. Furthermore, we investigated the CasPART responses of wild-type (WT) and mutant (MUT) HIV RT to lamivudine triphosphate (3TC-TP), another drug often included in the ART regimen, for potential drug resistance testing. The mutant HIV RT carried an M184V mutation known to present resistance to 3TC-TP [102]. The assay incubation time was shortened to 30 minutes to avoid signal plateau and achieve a broader dynamic range. As shown in **Figure 2.7B**, signals from WT RT across a range of 5e5 to 5e7 copies were greatly reduced in the presence of 3TC-TP. Conversely, MUT RT signals remained similar with added 3TC-TP, demonstrating the successful detection of MUT RT using CasPART. Interestingly, the MUT HIV RT generated lower signals and exhibited a higher LoD in CasPART compared to WT. This could be due to purities of the MUT RT stock from a different source or the reduced RT activity induced by the mutation [103]. Nonetheless, the results demonstrated the ability of CasPART to detect drug resistance in HIV RT, bypassing the need to interpret genetic mutations and directly screening the

effectiveness of specific HIV RT drugs for individual patients. The substrate sequence could be further adjusted to match the targeted nucleotide for nucleoside RT inhibitors (NRTI). However, multiple issues need to be addressed in future work to enable clinical implementations. First, the sensitivity and dynamic range of the assay could not cover a broad range of HIV viral loads among patients. The issue could potentially be resolved by using larger-volume samples such as ones collected with Tasso devices [104], longer incubation time, and reporting the slope of the real-time curves instead of endpoint RFU (**Supplementary Figure 2.19**). In addition, the compatibility of HIV RT mutants and the immunocapture needs to be investigated. Furthermore, the overall lower activity of mutant HIV RT compared to wildtype poses challenges to detecting mutants mixed with wild-types. Regardless, the CasPART assay can differentiate mutant HIV RT from wildtypes and could be promising for drug resistance testing, especially in low-resource settings where other tests are not available.

In addition, the CasPART platform is highly adaptable to target other enzymes by tuning the substrate and CRISPR-Cas architecture to match the enzyme activity. As a proof-of-concept, CasPART was adapted to detect the disintegration activity of HIV integrase (IN). While the integration activity of HIV IN results in random products in vitro [105,106], the disintegration activity is reported to generate specific products and was used for HIV IN studies [107,108]. In disintegration, under the catalysis of HIV IN, the 3' hydroxyl group of S-Top5 in the added substrates attacks the adjacent phosphodiester bond in S-Top3 and generates the linked product, available for cas12a detection (**Figure 2.7D**). We adapted the substrate sequence in previous reports and added the crRNA-Cas12a activation sequence in CasPART [107]. Since the substrate contained all the crRNA-Cas12a activation sequence and only missed one phosphodiester bond at the disintegration site, the biggest challenge was the background signal caused by the nonspecific

activation of Cas12a. To address the issue, we varied the distance between the disintegration site and the PAM region on the substrate and found that a 10nt distance reduced the background signals to a similar level in the HIV RT detection assay (**Figure 2.7E**). Interestingly, substrates with 0nt, 5nt, and 20nt distances generated similarly high background signals, suggesting that the 10nt position may be a tipping point for nonspecific Cas12a activation, aligning with the results of varied primer lengths in the HIV RT detection (**Figure 2.6D**). As shown in **Figure 2.7F**, the final assay with the 10nt-distance substrates showed a LoD at 10^{12} copies (83nM) of HIV IN. The high LoD was possibly due to the slow activity of HIV IN, as quantified by qPCR (**Supplementary Figure 2.20**) and reported in the literature [105]. The slightly decreased signals at 10^{13} IN copies were likely caused by inhibition from the storage buffer of the IN stock. Nevertheless, the assay could be used to characterize and study the functions of HIV IN. More importantly, it demonstrated that the CasPART platform could be applied to other enzymes for broader applications, such as the DNA polymerase for hepatitis B virus (HBV), RNA-dependent RNA polymerase for SARS-CoV-2 and hepatitis C virus (HCV). The specificity of the assays can be further secured by the immunocapture of the targeted enzyme or the whole pathogen during sample preparation.

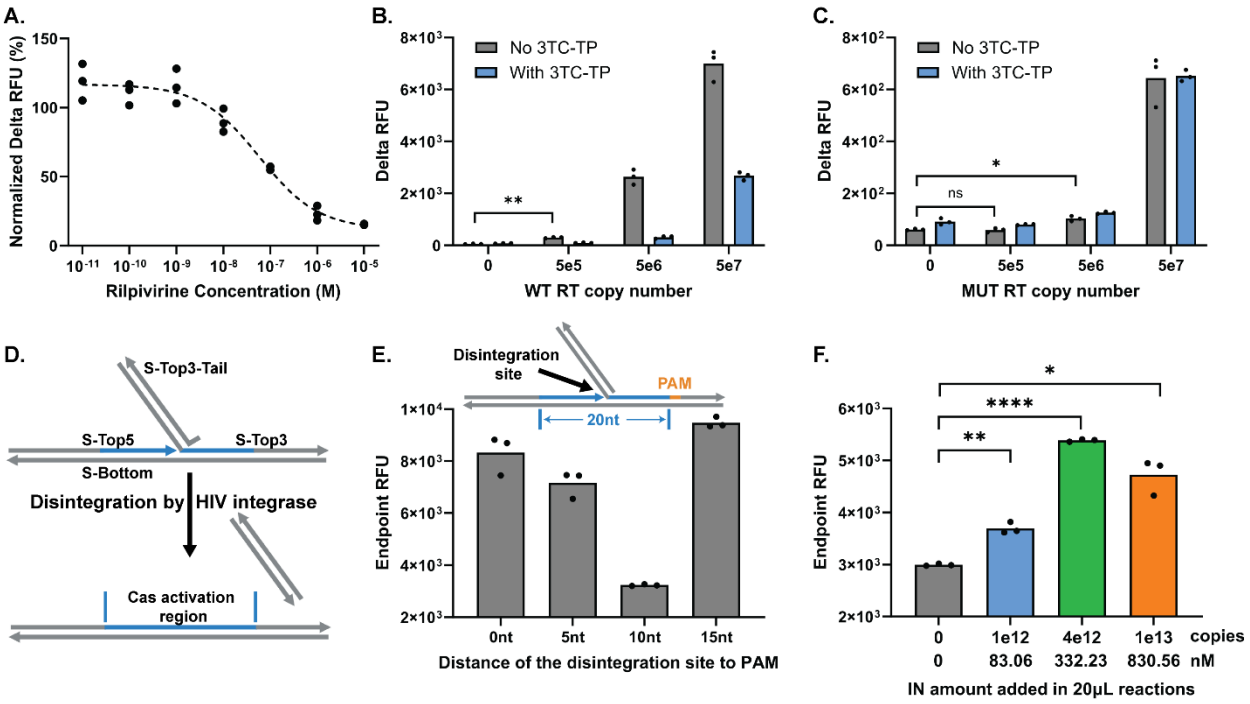

Figure 2.7. Versatile applications of CasPART.

(A) IC50 curves of Rilpivirine in inhibiting HIV RT activity using CasPART. Delta RFU (endpoint RFU minus starting RFU) at 1hr was used as CasPART signals. Signals from samples with Rilpivirine were normalized against control samples without Rilpivirine. The normalized signals were fitted to four-parameter logistic regression curves using GraphPad Prism 10. (B) and (C) Responses of wild-type and mutant HIV RT to 3TC-TP in CasPART. Delta RFU at 0.5hr was plotted for samples with or without 3TC-TP. Real-time curves of 5hr incubation can be found in **Supplementary Figure 2.19**. (D) Illustrations of adapting CasPART for detecting the disintegration activity of HIV integrase. (E) Background signals of using substrates with different distances between PAM and the disintegration site. (F) The final performance in detecting HIV integrase using cas12a. Reactions in panels E and F were incubated for 2hr. Statistical significance in panels B, C, and F was determined by unpaired t tests with Welch's correction and conducted in GraphPad Prism 10. * indicates $p < 0.05$, ** indicates $p < 0.01$, and **** indicates $p < 0.0001$.

2.4 Conclusions

We aimed to develop an HIV RT activity assay for sensitive HIV testing due to several advantages of RT as a biomarker, including higher copy number per virion, multiple cDNA products per RT, robustness in plasma samples, and conserved activity across subtypes. The cDNA generation

activity of HIV RT was first characterized with qPCR to guide assay designs. We found that cDNA per RT appeared linear over time, saturated at around 2nM RNA substrates, and varied among different substrate sequences. The sequence with the highest RT efficiency was selected for assay development, where one RT generated 71.18 copies of cDNA within 30 minutes, providing a front-end enhancement.

Based on the characterization of HIV RT activity, two formats of HIV RT activity assay, LamPART and CasPART, were then developed. In LamPART, LAMP was used to amplify cDNA products generated by HIV RT. With novel assay designs, we achieved a one-pot reaction requiring only 30min incubation at 37°C followed by another 30min at 65°C. The assay demonstrated a LoD of 20 copies of recombinant HIV RT, equivalent to a single virion. The one-pot LamPART assay was further integrated with direct immunocapture of HIV RT using antibody-coated magnetic beads and endpoint LFA detection of LAMP amplicons. The integrated workflow achieved detecting 20 copies of recombinant HIV RT spiked into 25µL HIV-negative plasma. When tested on clinical samples, the workflow detected some HIV-positive samples with viral loads below 5000cp/mL, but future development is needed for more robust performance. In CasPART, the front-end enhancement offered by HIV RT was combined with the sensitive and specific cDNA detection by the CRISPR-Cas system. The one-pot reaction only required incubation at a constant temperature of 37°C. The substrate design was tailored to improve assay sensitivity. The final assay, when combined with direct immunocapture for sample preparation, demonstrated a LoD of 2e4 copies (1.33fM) of recombinant HIV RT spiked into 25µL plasma. Furthermore, CasPART as a phenotypic assay enabled the characterization of HIV RT activities. We used CasPART to report the IC50 curves of Rilpivirine, an HIV drug targeting RT. In addition, CasPART successfully differentiated wild-type HIV RT from mutants with known resistance to

3TC-TP, another drug commonly included in ART regimens. Moreover, the inherent programmability of the CRISPR-Cas12 system allowed simple adaptation of CasPART for other enzyme targets. As a proof-of-concept, CasPART was adapted to detect the disintegration activity of HIV IN and achieved a sensitivity of 83nM. Since most pathogens encapsulate or encode their own suite of enzymes, the developed CasPART method holds potential for broader applications in infectious disease detection and phenotypic characterization.

2.5 Materials and Methods

In-house RNA synthesis DNA templates were ordered via IDT gBlocks and amplified with PCR using primers with added T7 promoter sequence, followed by purification with PureLink PCR Purification kits (Invitrogen, Cat. No.: K310001). RNA was generated from the purified DNA templates using T7 RNA polymerase (NEB, Cat. No.: M0251L) following the manufacturer's protocol. After incubating at 37°C for an hour, the RNA was purified using Monarch RNA Cleanup kits (NEB, Cat. No.: T2040L). To digest DNA templates in the RNA stock, purified RNA was added to DNase I reactions following the manufacturer's protocol (NEB, Cat. No.: M0303L). After incubating at 37°C for an hour, the RNA was purified using the Monarch kit. The DNA digestion step was repeated three times. The final RNA stock was quantified using the Qubit RNA High Sensitivity kit (Invitrogen, Cat. No.: Q32852). The length and integrity of the RNA were checked using Agilent High Sensitivity RNA ScreenTape (Agilent, Cat. No.: 5067-5579).

Quantify cDNA generation by HIV RT with qPCR Recombinant HIV reverse transcriptase was ordered from Millipore Sigma (Cat. No.: 382129-500U). The mass concentration of the stock was converted to molar concentrations based on a molecular weight of 117kDa provided by the manufacturer. The 10μL reverse transcription reaction contained 1X HIV RT buffer (50mM Tris-HCl at pH 8, 50mM KCl, 10mM $MgCl_2$, 2mM DTT, and 0.06% Triton X-100), 3mM DTT, 0.1%

Triton X-100, 2U/μL RNasin Plus (Promega, Cat. No.: N2615), 0.4mM dNTPs, 200nM primer, and RNA templates. The reaction was incubated at 37°C followed by 10min at 95°C for HIV RT inactivation and RNA degradation. The reaction was then diluted 10-fold in water and 2μL diluted sample was added to 25μL qPCR reactions for cDNA quantification. The qPCR reactions contained 0.625unit OneTaq Hot Start DNA polymerase (NEB, Cat. No.: M0481L), 1X OneTaq standard reaction buffer, 0.2mM dNTPs, 200nM forward primer, 200nM reverse primer, and 1X EvaGreen Dye (Biotium, Cat. No.: 31000). After an initial 2-minute heat spike at 95°C, the qPCR procedure includes 40 cycles of 15sec at 95°C, 15sec at 55°C and 30sec at 68°C.

LAMP-based HIV RT activity assay A 10μL LamPART reaction contained 1X HIV RT buffer, 3mM DTT, 0.1% Triton X-100, 2U/μL RNasin Plus, 1.4mM dNTPs, 800nM FIP and BIP, 400nM LB and LF, 160nM B3, 300nM UDP quencher, 200nM UDP fluorophore, 400nM LB docker, 160nM B3 docker, 500nM TQ21 aptamer, 50nM RNA substrates, 26.25μg/mL TF Pol. The master mix was incubated at 65°C for 5min and cooled down to room temperature before adding RNA substrates and TF Pol, to allow proper hybridization of the dockers to primers and the folding of the aptamer. After HIV RT was added, the reaction was incubated at 37°C for 30min followed by 65°C for 1hr.

Immunocapture of HIV RT 250μg M-280 Sheep Anti-Mouse IgG Dynabeads (ThermoFisher, Cat. No.: 11201D) were washed three times with 500μL binding buffer (1X TBS at pH=7.4, 1% BSA) and incubated in 50μL binding buffer with 7.5μg mouse anti-HIV-RT IgG (MyBioSource, Cat. No.: MBS531805) at 4°C with rotation overnight. The beads were then washed three times with 500μL binding buffer with 0.05% tween-20 and resuspended in 25μL lysis buffer (2X HIV RT buffer, 2% BSA, 1.2% NP-40). 25μL pooled HIV-negative plasma (BioIVT, Cat. No.: HUMANPLK2-0000291) was mixed with 25μL lysis buffer and spiked with different copy

numbers of HIV RT and 1uL beads. Samples were then transferred into 0.2mL PCR tube strips (USA Scientific, Cat. No.: 1402-4700) and incubated at room temperature with rotation for 30min for HIV RT capture. After capture, the beads were washed three times with 200μL wash buffer (1X RT buffer, 0.1% BSA, 0.6% NP-40) using multi-channel pipettes and strip-tube magnetic racks (NEB, Cat. No.: S1515S).

For experiments of quantifying capture efficiency with qPCR, 10μL reverse transcription was added to the washed beads, followed by the same steps described in the section of quantifying cDNA generation activity of HIV RT by qPCR. The results were compared with freshly diluted HIV RT directly added to the reactions. For experiments demonstrating integrated workflow with LamPART, 10μL LamPART reaction described in the section of LAMP-based HIV RT activity assay was added to the washed beads, followed by incubation at 37°C for 30min and 65°C for 1hr.

Endpoint lateral flow detection of CasPART The 10μL LamPART reaction was prepared the same as above except that no UDP quenchers or fluorophores were used and biotin-labeled FIP and FITC-labeled BIP were used. The reaction was incubated at 37°C for 30min followed by 65°C for 30min. The amplicons were detected using PCRD Flex Lateral Flow Strips (Abingdon Health, Cat. No.: FG-FD51676) following the manufacturer's protocol. Specifically, the 10μL post-amplification reaction was added to 140μL extraction buffers provided in the kit. The lateral flow strip was then dipped inside the buffer for 10min. The strips were scanned using an Epson V700 Photo Scanner.

Test LamPART-based integrated workflow on clinical samples 10 HIV-negative plasma samples and 6 HIV-positive ART-naïve samples with viral loads between 1000 and 5000 cp/mL were provided by the Center for AIDS Research (CFAR) at the University of Washington. The viral load values were provided by CFAR. Samples were thawed and aliquoted upon arrival and

stored in a -80°C freezer until testing. Each test started with 25µL plasma and followed the steps described in the LamPART-based integrated workflow with real-time fluorescence detection. Three tests were conducted per sample.

CasPART 100nM LbCas12a (NEB, Cat No.: M0653T) and 100nM crRNA was incubated in 1X HIV RT buffer at 25°C for 15min to form the Cas12a-crRNA complex. 10µL Cas12a-crRNA complex was then mixed with 10µL HIV RT reaction. The final 20µL reaction contained 1X HIV RT buffer, 5mM $MgCl_2$, 5mM DTT, 0.4mM dNTPs, 500nM reporters, 50nM RT substrate, 200nM RT primer, and 50nM of the Cas12a-crRNA complex. The reaction was incubated at 37°C with fluorescence measurements every 2min. For experiments testing CasPART integrated with immunocapture, HIV RT was spiked into 25µL HIV-negative plasma and immunocaptured as described in the section of HIV RT capture. After capture, 20µL CasPART reaction described above was added to the beads followed by incubation at 37°C with fluorescence measurements every 2min.

IC50 curves of Rilpivirine in CasPART The CasPART assay was prepared as described above except the reaction used 0.5µM dNTPs and included 5e6 copies of HIV RT. Rilpivirine was diluted in DMSO and 2µL was added to the reaction to limit DMSO concentrations in the assay. The reaction was incubated at 37°C for 1hr with fluorescence measurements every 2 minutes. Delta RFU (fluorescence change; endpoint RFU minus starting RFU) was used as assay signals. Signals from test samples with Rilpivirine were normalized against the average of the control samples (no Rilpivirine). The normalized signals were fitted to four-parameter logistic regression curves using GraphPad Prism 10.

Responses of WT and MUT HIV RT in CasPART to 3TC-TP The CasPART assay was prepared as described above except that lamivudine triphosphate (3TC-TP), ordered from Sierra

Bioresearch, was included at 0.4mM in the final reaction. The mutant HIV RT was kindly provided by the NIH HIV Reagent Program (Cat. No.: ARP-3195). The reaction was incubated at 37°C for 5hr with fluorescence measurements every 2min. The delta RFU at 30min was calculated by the endpoint RFU at 30min minus the starting RFU.

CasPART adaption for HIV IN detection To allow proper hybridization of the oligos into the substrate structure, 1μM of S-Top5, S-Top3, S-Top3-Tail, and S-Bottom was mixed in 1X HIV RT buffer and cooled down from 95°C to 4°C at a rate of 1°C per 3min. The prepared substrate was then stored in the fridge until use. HIV integrase was kindly provided by the NIH HIV Reagent Program (Cat. No.: HRP-20203). The assay was prepared the same as described in CasPART including the buffer conditions and the crRNA sequence, except that 50nM disintegration substrates were used instead of the RT substrates. The reaction was incubated at 37°C for 2hr with fluorescence measurements every 2min.

2.6 Acknowledgment

This work was supported by NIH/NIAID grants AI140460. I would like to thank all collaborators on this project: Enos C. Kline for designing the RNA substrate sequence and accompanying LAMP used in the final assay, designing the UDP probe, providing TF Pol materials and the aptamer information, and providing advice throughout the project; Shane D. Gilligan-Steinberg for validating one of the LAMP assay candidates tested in the project, helping with sample acquisition, and providing advice throughout the project; Dr. James J. Lai for helping with materials from NIH HIV Reagent program, helping with sample acquisition, and providing advice throughout the project; Dr. Ian T. Hull for providing advice throughout the project; Dr. Ayokunle O. Olanrewaju for sharing the materials and protocols of testing RT inhibitors and providing advice on potential

drug resistance testing with CasPART; Dr. Nuttada Panpradist for providing advice throughout the project; Dr. Barry R. Lutz for overseeing and guiding the project.

We thank Bob Atkinson for his initial design in sequence #2 and the accompanying LAMP assay. We thank Joe Henthorn for his design in sequence #4 and the accompanying LAMP assay. We thank Cara Brainerd and Cosette Craig for sharing the materials and protocols of testing Rilpivirine. We thank Dr. Joanne D. Stekler and Dr. Paul K. Drain for their clinical advice on the project. We thank Dr. Paul Yager, Dr. James I. Mullins, Dr. Patrick Stayton, and Dr. Xiaohu Gao for their advice on the project. Research reported in this publication was supported by the University of Washington/Fred Hutch Center for AIDS Research, an NIH-funded program under award number AI027757 which is supported by the following NIH Institutes and Centers: NIAID, NCI, NIMH, NIDA, NICHD, NHLBI, NIA, NIGMS, NIDDK. The content is solely the responsibility of the authors and does not necessarily represent the official views of the National Institutes of Health. The following reagents were obtained through the NIH HIV Reagent Program, Division of AIDS, NIAID, NIH: Human immunodeficiency virus type 1 HXB2 reverse transcriptase/MI84V heterodimeric protein, recombinant from Escherichia coli, ARP-3195, contributed by Dr. Vinayaka Prasad and Dr. Mark Wainberg; Integrase (F185K/C280S) protein from human immunodeficiency virus type 1 (HIV-1) NL4-3, recombinant from Escherichia coli, HRP-20203, contributed by DAIDS, NIAID. Schematics in the manuscript were created with BioRender.com.

2.7 Supplementary Information

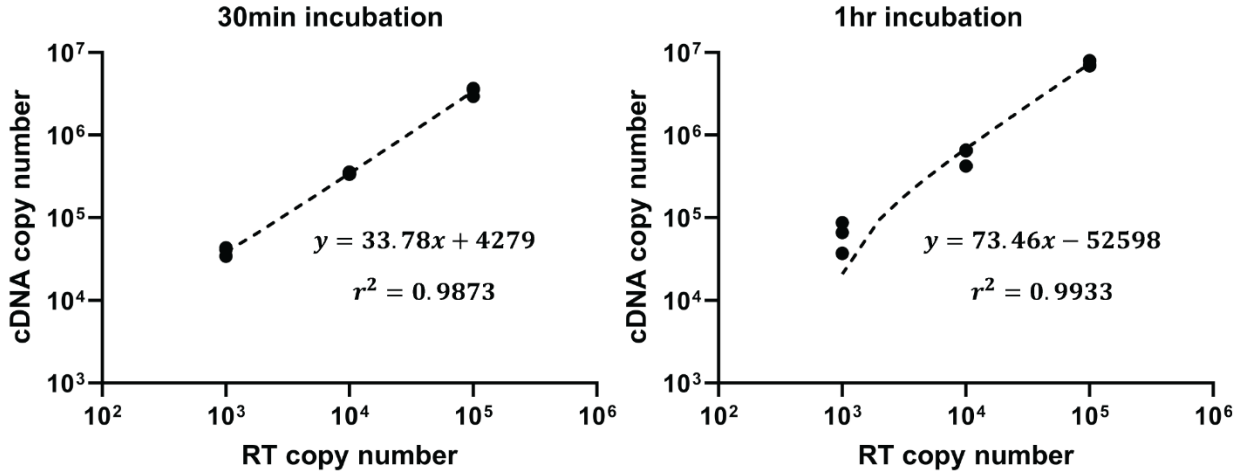

Figure 2.8. Linear correlations of cDNA copy number versus HIV RT copy number with 30min or 1hr incubation.

5nM RNA substrates were used.

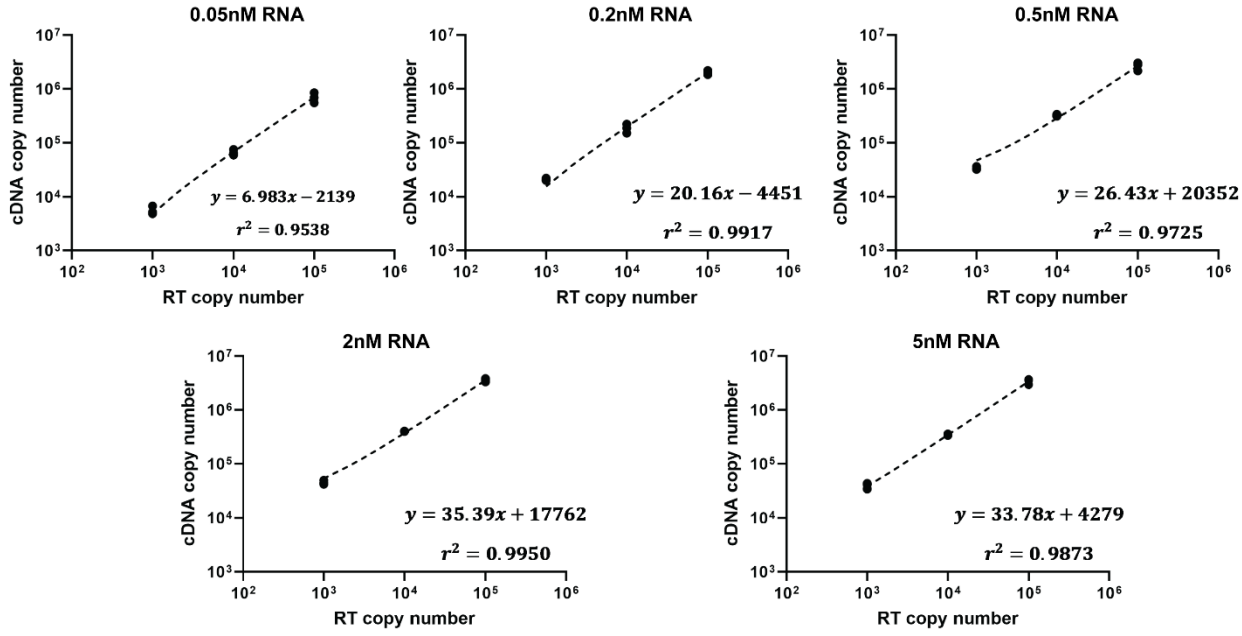

Figure 2.9. Linear correlations of cDNA copy number versus HIV RT copy number with different concentrations of RNA substrates.

The RT reaction was incubated for 30min.

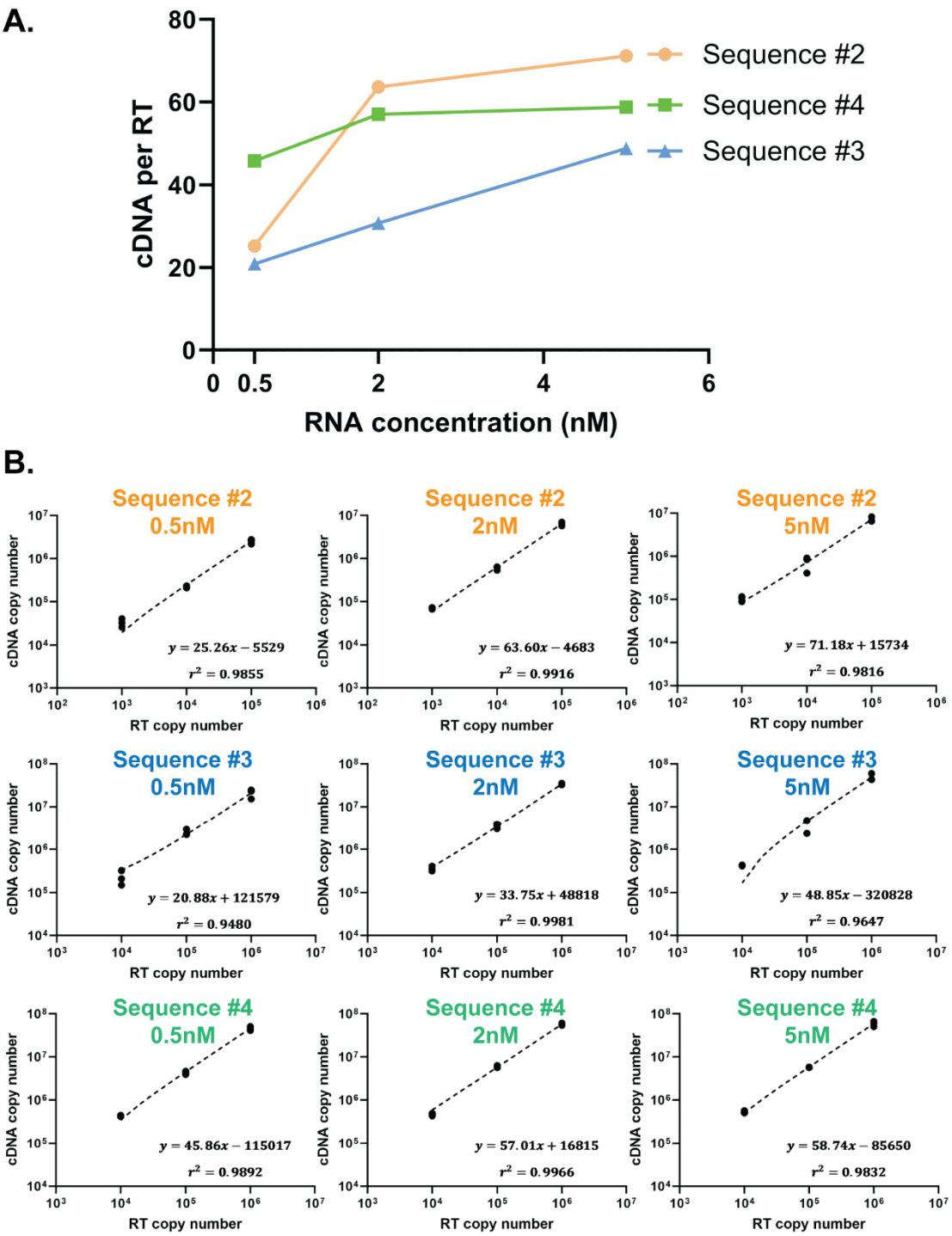

Figure 2.10. HIV RT efficiency on different sequences.

(A) The cDNA per RT with 0.5nM, 2nM and 5nM of RNA sequence #2, #3 and #4. (B) The linear correlations of cDNA copy number against HIV RT copy number at each data point in panel A.

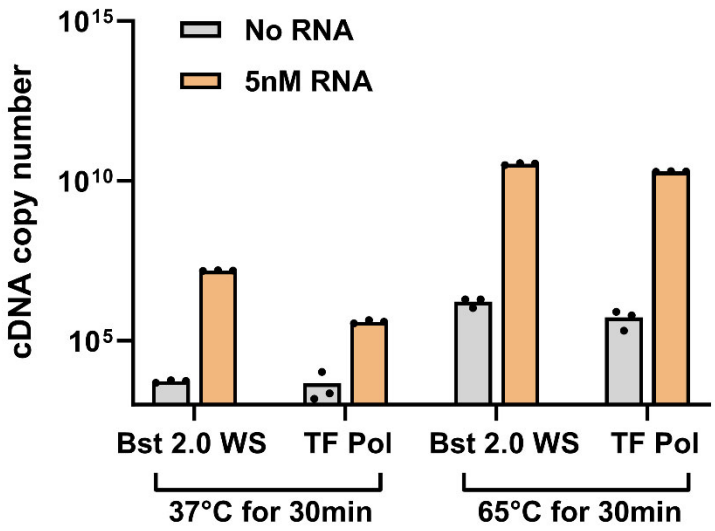

Figure 2.11. Innate reverse transcription activity of Bst 2.0 WarmStart (WS) and TF Pol.

Bst 2.0 WS and TF Pol at concentrations used in LAMP were added to the same reverse transcription reaction used to quantify cDNA generation by HIV RT, with 5nM RNA sequence #2 as the substrate. After incubating at 37°C or 65°C for 30min, the reaction was heated at 95°C for 20min to inactivate Bst2.0 WS or TF Pol, followed by dilution and qPCR quantification, the same protocol used to quantify cDNA generation by HIV RT.

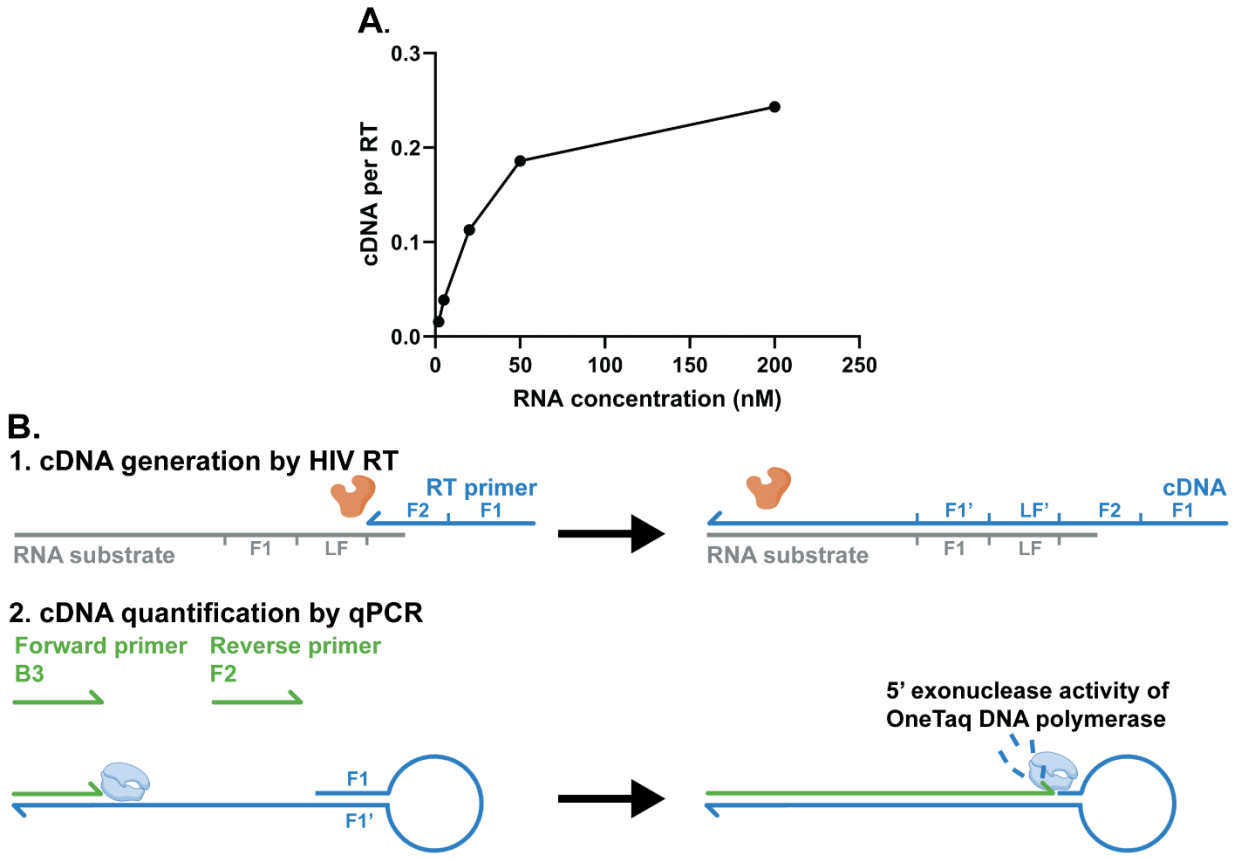

Figure 2.12 The cDNA copy number per HIV RT under LAMP conditions.

(A) The cDNA per HIV RT versus RNA concentrations under LAMP conditions, as quantified by qPCR. Note that the cDNA per HIV RT was much less compared to results in **Figure 2.2**, which could be due to the PCR quantification artifact illustrated in panel B. (B) Due to the truncated RNA substrate design and use of FIP (F1-F2) as the RT primer, the cDNA generated by HIV RT contains a hairpin loop structure on the 5' end. While the cDNA is amplifiable in qPCR owing to the 5' exonuclease activity of the OneTaq DNA polymerase in PCR, the cDNA template may have a lower amplification efficiency compared to the qPCR reference standards which do not have the hairpin structure, inducing an artifact of lower quantification outcomes. Nevertheless, the quantification artifact does not affect the overall trend of the curve in panel A.

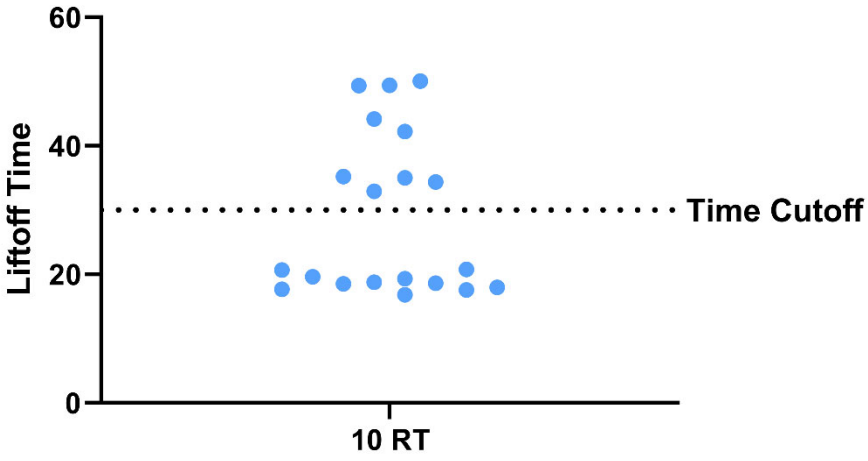

Figure 2.13 Results of 20 replicates of one-pot LamPART with 10 copies of HIV RT.

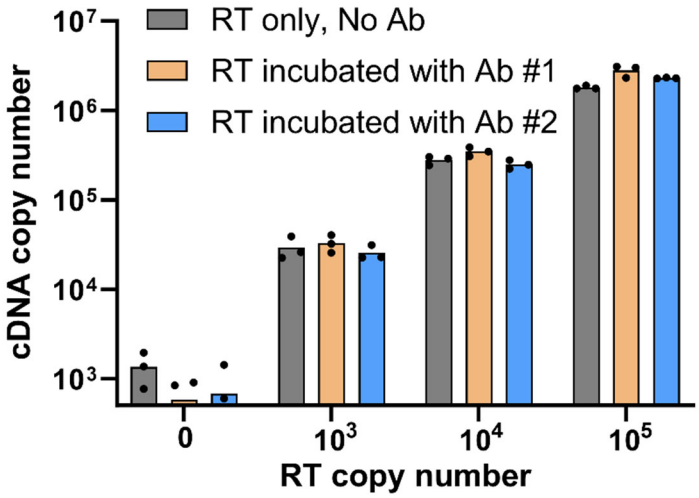

Figure 2.14 The cDNA copy number generated by free HIV RT versus HIV RT preincubated with antibodies.

Free HIV RT or HIV RT mixed with 15µg/mL of antibody #1 (MyBioSource, Cat. No.: MBS531805) or antibody #2 (MyBioSource, Cat. No.: MBS601420) in buffer (1X TBS at pH=7.4, 1% BSA) was incubated in a rotator at room temperature for 30min, followed by quantifying cDNA generation by qPCR as described in HIV RT activity characterization. Ab #1 was selected to move forward for assay development.

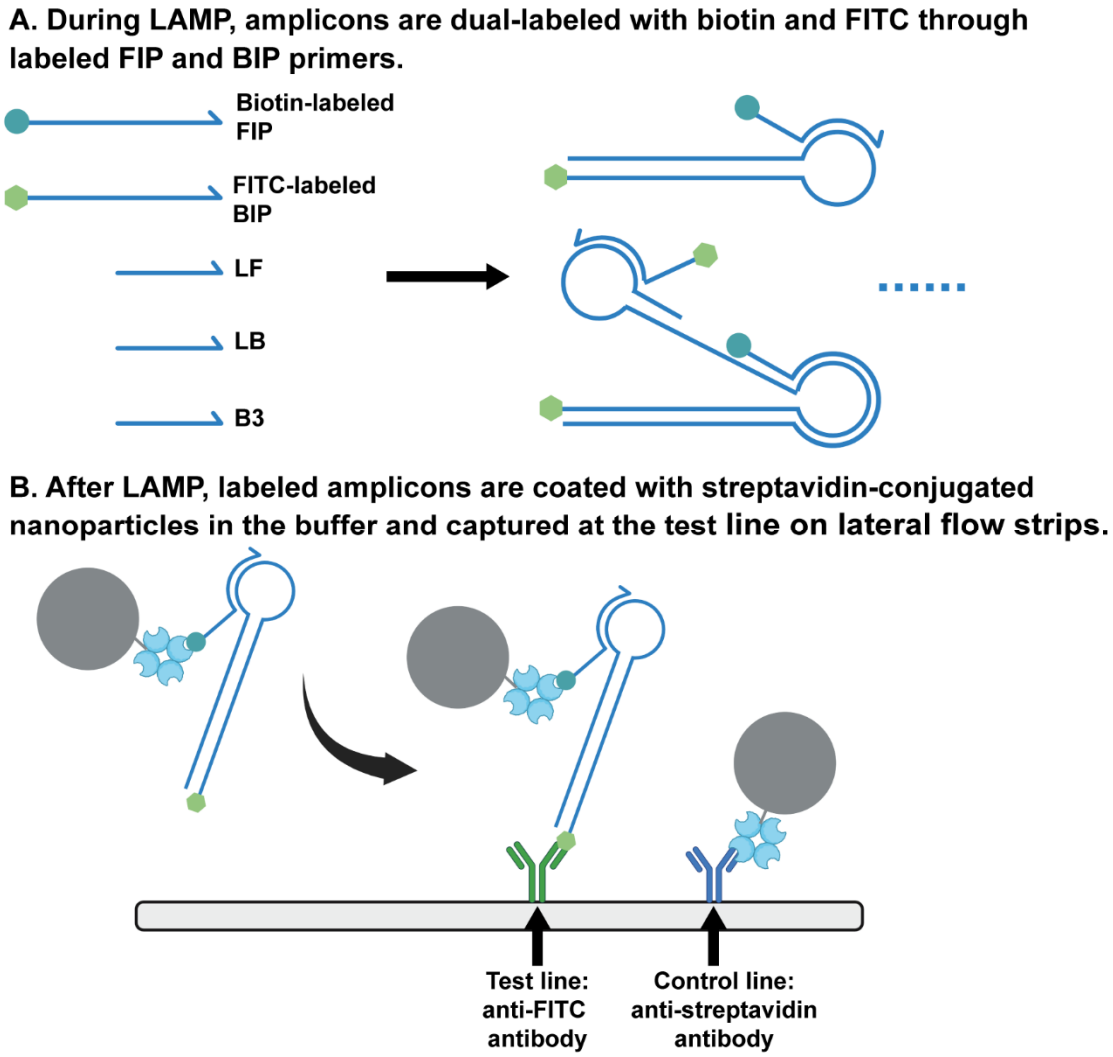

Figure 2.15 Illustrations of the endpoint lateral flow detection of LAMP amplicons.

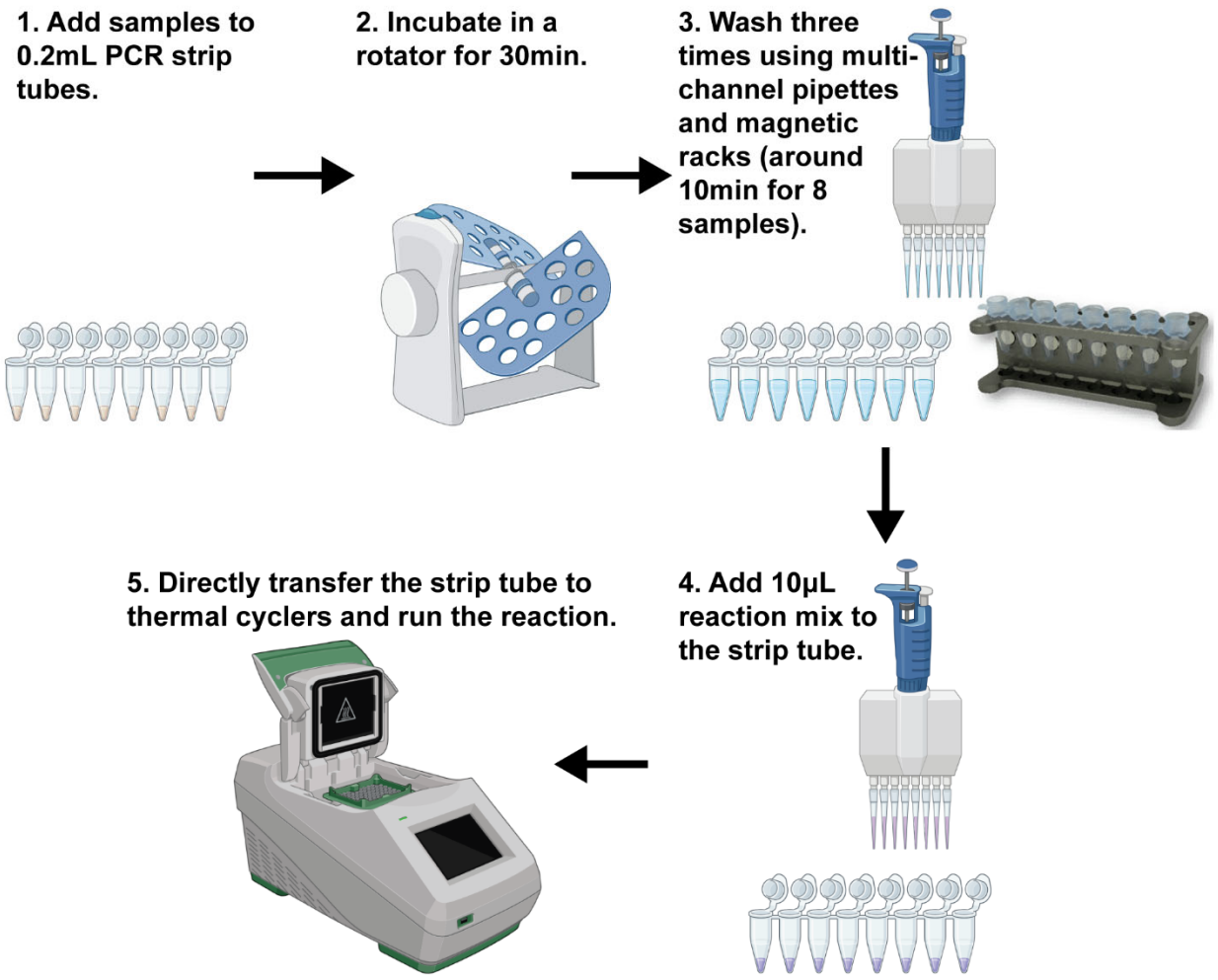

Figure 2.16 High-throughput testing with the integrated workflow by using strip tubes and multi-channel pipettes.

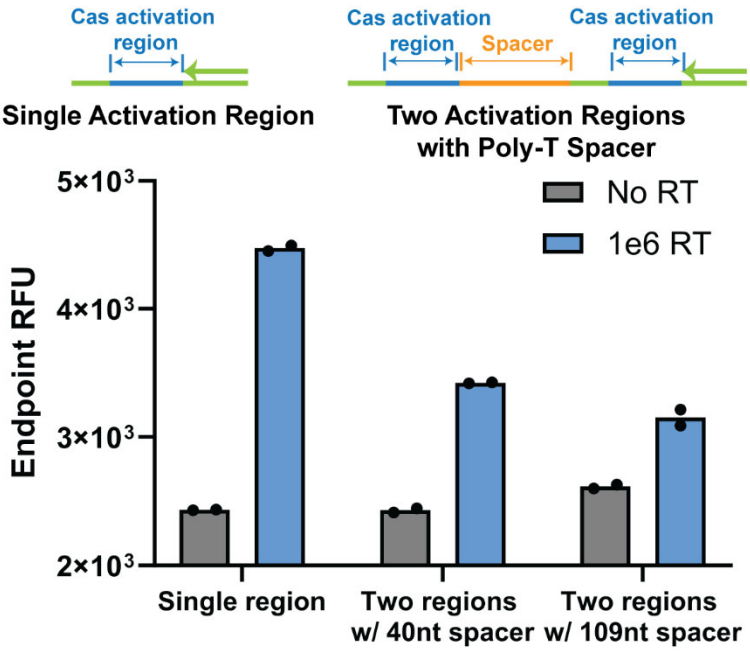

Figure 2.17 CasPART signals of using substrates with two activation regions versus a single activation region.

A poly-T spacer was included between activation regions to avoid steric hindrance.

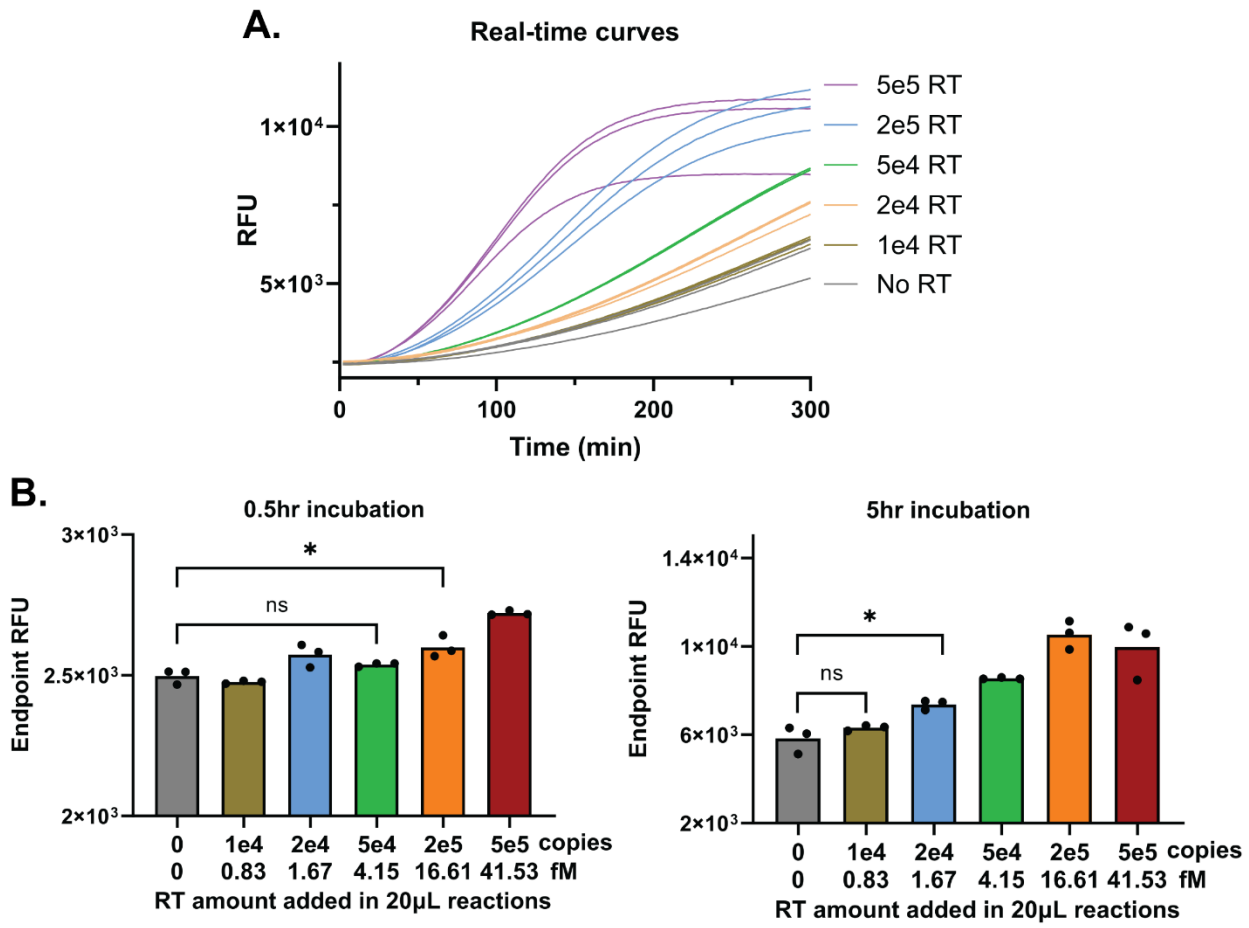

Figure 2.18 Real-time curves of CasPART.

(A) Real-times curves of final CasPART performance with HIV RT in buffers during 5hr incubation. (B) Endpoint RFU after 0.5hr incubation (left) and 5hr incubation. Compared to 2hr incubation, LoD with 0.5hr incubation increased to 2e5 copies of HIV RT (16.61fM). LoD with 5hr incubation did not decrease due to higher background signals. Statistical significance was determined by unpaired t tests with Welch's correction and conducted in GraphPad Prism 10. * indicates $p < 0.05$.

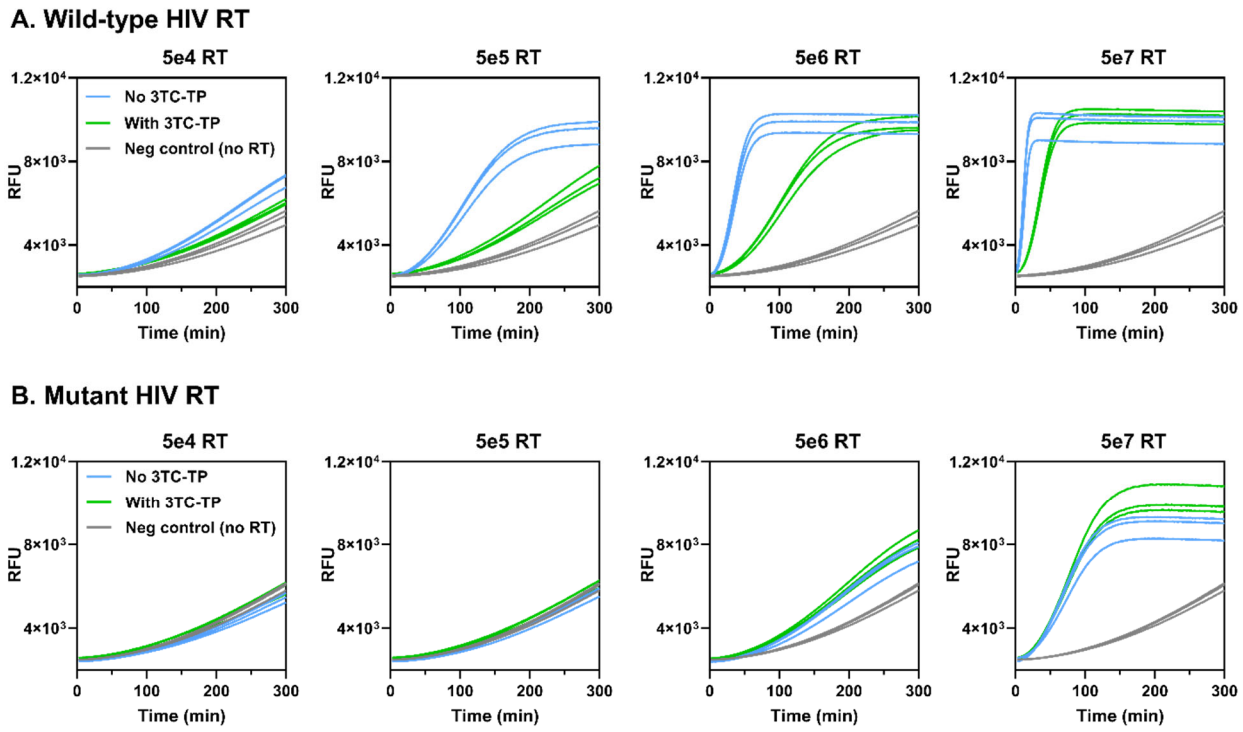

Figure 2.19 Real-time curves of HIV RT responses to 3TC-TP in CasPART during 5hr incubation. (A) Wild-type HIV RT. (B) Mutant HIV RT.

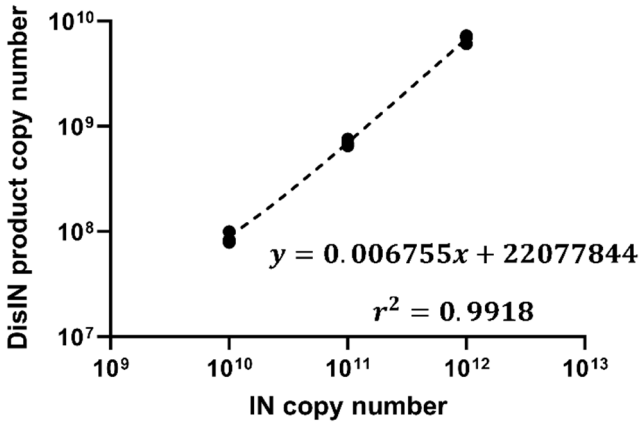

Figure 2.20 The linear correlation of disintegration product copy number versus integrase copy number, as quantified by qPCR.

2.8 Appendix: Sequence Table

Characterization of cDNA generation by HIV RT with qPCR		
Sequence #1	RNA template	GGGAGACAUUAGCCAUUUCAACCCAUGCGUUUGAGGAGAAGCGCU UUCUGAUAACCGGUGGUCUCCCAUCAGGUUGUGCAGCGACCUCAA UGCUAAACACUAUAAUGAAUAAUAUAAUAAUUAGGGCGGGUUUG UAUCUCACGUAUAAAAAUUUUGAAUUUGAUGAUGUGAAGGUGUU GUCGUACGGAGAUGAUCUCCUUGUGGCCACAAAUUACCAAUUGGA UUUUGAUAAGGUGAGAGCAAGCCUCGCAAAGACAGGAUAUAAGAU AACUCCCGCUAACACAACUUCUACCUUUCCUCUUAAUUCGACGCU UGAAGACGUUGUCUUCUUAAAAAGAAAGUUUAAGAAAGAGGGCCC UCUGUAUCGGCCUGUCAUGAAC
	RT primer/ PCR Rev primer	CGTCGAATTAAGAGGAAAGGTAG
	PCR Fwd primer	TTTGATAAGGTGAGAGCAAGC
Sequence #2	RNA template	GCCGGCCUAGCUGUGAUAAGUCUAUCUCUCUUUCCACGGGCUAUG GAAUCGCUACAGGAGGUUAGAGAGUCGAUACGUGCGCUAUGUGCU CGGCUAUAUCUAAGCAAGCUUUCCUCCGAUACCCAUCGCGUAGAG GA
	RT primer/ PCR Rev primer	GCTCACACTACTCCTCTACGC
	PCR Fwd primer	CCGGCCTAGCTGTGATAAGTC
Sequence #3	RNA template	GUGGGAAGUUCAAUUAGGAAUACGAUGCAUAUUUUUCAGUUCCCU UAGAUCUGCAUUCACCAUACCUAGUAAACAAUGAGACACCAGGAG AUAUCAGUACAAUGUGCUGAUGGAAAGGAUCACCAGCAAUAUUAG CAUGACAAA
	RT primer/ PCR Rev primer	TGGGAAGTTCARTTAGGAATAC
	PCR Fwd primer	GGCTCTAAGATTTTTGTCATGCT
Sequence #4	RNA template	GUGUUGUUCUGUCUGUCUUCCCACCUCCUUCUCCUUCUUCUUGAG UGAAGUGUGUGAGAGGUGGUGAGAGUGAGCACUUCCUCUUCUUCU GUUGUUGUCUCCCUCUUCUUCGUGGUGAGUG
	RT primer/ PCR Rev primer	CACTCACTCACACTCACCAC
	PCR Fwd primer	GTGTTGTTCTGTCTGTCTTC
One-pot LamPART		
Sequence #2, full length		GCCGGCCUAGCUGUGAUAAGUCUAUCUCUCUUUCCACGGGCUAUG GAAUCGCUACAGGAGGUUAGAGAGUCGAUACGUGCGCUAUGUGCU CGGCUAUAUCUAAGCAAGCUUUCCUCCGAUACCCAUCGCGUAGAG GAGUAGUGUGAGCGUGGGAUAUGUACGACGACCG
Sequence #2, truncated design		GCCGGCCUAGCUGUGAUAAGUCUAUCUCUCUUUCCACGGGCUAUG GAAUCGCUACAGGAGGUUAGAGAGUCGAUACGUGCGCUAUGUGCU

		CGGCUAUAUCUAAGCAAGCUUUCCUCCGAUACCCAUCGCGUAGAGGA
LAMP primers	FIP	GTGCTCGGCTATATCTAAGCAGCTCACACTACTCCTCTACGC
	BIP	ATAGCGCACGTATCGACTCTCTATCTCTCTTTCCACGGGCTA
	UDPtag-LF	ACCACACCTACCACCACTAATAACTAAAGCTTTCCTCCGATACCCATC
	LB	TAACCTCCTGTAGCGATTCCA
	B3	CCGGCCTAGCTGTGATAAGTC
	F3 (not included in final LamPART)	CGGTCGTCGTACATATCCCAC
Probes	UDP quencher	CTGTCGTAGGTGGTTGGGTTCGGAAGTGGTCAGG/3IABkFQ/
	UDP fluorophore	/56-FAM/CCTGACCACTTCCGAACCCAACCACCTACGACAGACCACACCTACC ACCACTAATAACTAA
Aptamer	TQ21	TTCTCGGTTGGTCTCTGGCGGAGCGATCATCTCAGAGCATTCTTAGCGTTTTGTTCTTGTGTATGATTCGCTTTTCCC
Dockers	LB docker	GCTACAGGAGGTTA/3ddC/
	B3 docker	ACAGCTAGGCCGG/3ddC/
Endpoint lateral flow detection		
FIP		/5BiosG/GTGCTCGGCTATATCTAAGCAGCTCACACTACTCCTCTACGC
BIP		/56-FAM/ATAGCGCACGTATCGACTCTCTATCTCTCTTTCCACGGGCTA
CasPART		
Substrate (10T-tail)		TTTTTTTTTTTTGAGGAGGTTAGAGAGTCGATACGTGCGCTATGTGCTCGGCT
20nt+10nt primer		AGCCGAGCACATAGCGCACGTATCGACTCT
crRNA		/AlTR1/rUrArArUrUrUrCrUrArCrUrArArGrUrGrUrArGrArUrArGrGrArGrGrUrUrArGrArGrArGrUrCrGrArUrA/AlTR2
Reporter		/56-FAM/TTATT/3IABkFQ/
20nt primer		AGCCGAGCACATAGCGCACG
20nt+5nt primer		AGCCGAGCACATAGCGCACGTATCG
20nt+15nt primer		AGCCGAGCACATAGCGCACGTATCGACTCTCTAAC
HIV integrase detection		
S-bottom		TCTCTCTCTCTTTGAGGAGGTTAGAGAGTCGATACGTGCGCTAT
S-Top3-Tail		ACTGCTAGAGATTTTCCACA
S-Top3 (10nt distance; final)		TGTGGAAAATCTCTAGCACTAACCTCCTCAAAGAGAGAGAGA
S-Top5 (10nt distance; final)		ATAGCGCACGTATCGACTCT
S-Top3 (0nt distance)		TGTGGAAAATCTCTAGCACAAAGAGAGAGAGA
S-Top5 (0nt distance)		ATAGCGCACGTATCGACTCTCTAACCTCCT
S-Top3 (5nt distance)		TGTGGAAAATCTCTAGCACTCCTCAAAGAGAGAGAGA
S-Top5 (5nt distance)		ATAGCGCACGTATCGACTCTCTAAC
S-Top3 (15nt distance)		TGTGGAAAATCTCTAGCAACTCTCTAACCTCCTCAAAGAGAGAGAGA
S-Top5 (15nt distance)		ATAGCGCACGTATCG

Chapter 3. Large-Volume RT-LAMP Enables Extraction-Free Amplification of HIV RNA from Fingerstick Plasma

3.1 Abstract

Point-of-care nucleic acid amplification test (NAAT) can significantly expand testing coverage, critical in infectious diseases diagnostics and monitoring. The development of various isothermal amplification techniques such as LAMP greatly simplifies NAATs, but the cumbersome nucleic acid extraction step remains a bottleneck for the point-of-care. Extraction-free amplification bypasses the extraction step and enables directly adding crude samples into the assay. However, the small assay volumes combined with the need for sample dilution limits the added sample quantity, leading to an inevitable sensitivity loss. Here we propose running isothermal amplification at larger reaction volumes to accommodate larger sample quantities, thereby improving sensitivity in extraction-free amplifications. We demonstrated by developing large-volume RT-LAMP for extraction-free amplification of HIV RNA from fingerstick plasma. We first found that reaction volumes up to 1mL did not compromise LAMP performance. We then developed dilution conditions to achieve preserved LoD of RT-LAMP in the presence of plasma. Subsequently, we showed the successful detection of 24 copies of HIV RNA in inactivated virus in 500μL RT-LAMP in the presence of 20μL plasma (fingerstick volumes). In addition, the reagent cost was estimated and compared with existing 20μL RT-LAMP kits. Moreover, the large-volume LAMP exhibited superior tolerance to a wide range of inhibitors in the sample, showing the potential to streamline various point-of-care workflows.

3.2 Introduction

Nucleic acid amplification test (NAAT) has been an indispensable tool in infectious disease diagnostics and monitoring. Bringing NAAT to the point-of-care could significantly expand testing access, especially in low-resource settings [5]. NAAT typically starts with nucleic acid extraction where target DNA or RNA is purified from sample inhibitors, followed by nucleic acid amplification where target sequences are exponentially amplified to detectable levels. Conventionally, polymerase chain reaction (PCR), the gold standard nucleic acid amplification method, has limited NAATs to centralized laboratories due to its dependence on specialized instrumentation with precise temperature cycling controls. The development of multiple isothermal amplification methods has brought NAAT closer to the point of care [14]. For example, loop-mediated isothermal amplification (LAMP) operates at a constant temperature of around 65°C and only requires a portable heater [15,79]. However, the laborious nucleic acid extraction step remains a substantial challenge for point-of-care. While various approaches, such as paper membranes or microfluidics coupled with silica beads, magnetic beads, or sequence-specific probes, have been demonstrated to streamline nucleic acid extraction [19–22], they often follow a multi-step lyse-bind-wash-elute paradigm, which escalates the device complexity and testing costs.

Alternatively, extraction-free nucleic acid amplification bypasses the complicated nucleic acid extraction step and directly introduces crude samples into the amplification reaction. In extraction-free amplification, samples are often pretreated by dilution coupled with enzymes (e.g., proteinase K), chemicals (e.g., detergents), or heating, to ensure maintained amplification efficiency [46,109]. Extraction-free amplification has been successfully demonstrated using LAMP with various human samples such as blood [49], urine [54], nasal swab [15], and saliva [55]. For example,

Curtis *et al.* developed a method for HIV detection where whole blood was diluted 4-fold with lysis buffer and directly added into an RT-LAMP assay [24]. However, the limitations in reaction volumes and the dilution required during sample pretreatment place restrictions on the quantity of samples that can be added to an assay, leading to an inevitable sensitivity loss in extraction-free tests.

NAATs have been traditionally run at 10-20μL volumes. The requirements for small reaction volumes are likely associated with historical constraints of rapid thermal cycling in polymerase chain reaction (PCR) and lower costs with less reagent consumption. Expanding the reaction volume can facilitate the inclusion of larger sample quantities for improved sensitivity in extraction-free amplification assays, but the potential of large-volume NAAT remains uncertain. Isothermal amplification techniques such as LAMP only require a single reaction temperature, eliminating the volume limitation tied to thermal cycling. Additionally, the cost could be drastically reduced by employing in-house or lower-cost reagents, offering a promising opportunity to run isothermal amplification assays at larger reaction volumes [57]. While prior studies have demonstrated RT-LAMP at 100μL volumes with a limit of detection (LoD) comparable to standard 20μL reactions, its performance at even larger volumes remains unexplored [110].

HIV, with 39 million people infected worldwide and 1.3 million new cases in 2022, persists as a major threat to global health [1]. Sensitive HIV testing is required for both early HIV diagnosis and routine HIV viral load monitoring in patients receiving antiretroviral therapy (ART) [3]. However, the HIV RNA rt-qPCR test, the most sensitive testing approach, is limited to higher-tier laboratories. A sensitive point-of-care HIV test using fingerstick samples can expand the testing coverage, especially in low-resource settings. Here we propose directly adding fingerstick plasma

(~20μL) to large-volume RT-LAMP assays for sensitive HIV testing at the point-of-care. This novel approach bypasses the laborious RNA extraction step while accommodating the whole fingerstick plasma sample through expanded reaction volumes. We hypothesize that large-volume RT-LAMP assays could maintain similar amplification LoD while diluting out inhibition from plasma matrix. In this study, the performance of large-volume reactions was first investigated with DNA targets. Subsequently, the dilution conditions for preserving RT-LAMP LoD with added plasma was then developed using standard 20μL reaction volumes. This enabled us to demonstrate the performance of large-volume RT-LAMP in the presence of 20μL plasma (fingerstick volumes). Furthermore, the reagent cost for large-volume RT-LAMP was estimated and compared with existing RT-LAMP kits of standard reaction volumes. Finally, we tested the performance of large-volume reactions against other inhibitors including albumin and GuSCN, to explore broader applications at the point of care.

3.3 Results and Discussion

3.3.1 **Performance of large-volume LAMP with DNA targets**

We first used DNA targets to test if large-volume LAMP could maintain the same performance. We designed and optimized a LAMP assay targeting the HIV *pol* region. The assay used in-house TF Pol as the DNA polymerase to reduce the cost and intercalating dye for real-time detection [56]. At 20μL reaction volumes, the assay demonstrated a LoD of 200 DNA copies, and no non-specific amplification was observed within 1hr (**Figure 3.1A**). The reaction volume was then expanded while the assay reagent concentrations were kept unchanged, to test if the large-volume reaction could uphold the established LoD. Since the instrumentation for running nucleic acid amplification assays only allowed reaction volumes up to 50uL, the larger-volume LAMP was

instead incubated in a heating block set at 65°C for an hour (**Figure 3.1B and Supplementary Figure 3.5**). The reaction was capped with a layer of mineral oil to avoid evaporation, and the heating block was filled with water for consistent heating. After 1hr, 20μL of the reaction was collected for endpoint fluorescence measurements and gel electrophoresis. As shown in **Figure 3.1C**, LAMP at 200uL volumes also achieved amplification at 200 DNA copies, equivalent to the LoD at 20μL reaction volumes. The specificity of the amplification was confirmed through gel electrophoresis analysis **Figure 3.1D**). In addition, no false positives were observed in the negative controls. When the reaction volume was further increased to 1mL, the assay LoD stayed the same at 200 copies (**Figure 3.1C and D**). Moreover, the turbidity of the positive reactions, a known phenomenon of LAMP [50], became visible even to the naked eye thanks to the large reaction volume (**Figure 3.1E**).

The results showed that large reaction volumes up to 1mL did not compromise LAMP performance. While larger reaction volumes may appear to dilute the DNA targets, the assay reagents such as primers and polymerases were kept at the same concentrations and in abundant excess relative to the target. Consequently, the initiation events of specific amplification may not be impacted. However, large-volume LAMP could pose an increased risk of side reactions due to a larger number of reagents. The side reactions could lead to exponential non-specific amplifications or simply occupy and consume assay reagents, resulting in false positives or sensitivity loss [111]. Compared to other isothermal amplification methods, LAMP may be more resilient to false positives since the amplification relies on distinctive loop structures, mitigating the risk of scaling up reaction volumes. Besides, the reagent concentrations in large-volume LAMP could potentially be decreased to minimize side reactions. Moreover, beyond preserved assay LoD,

large-volume LAMP offers stronger signal intensity in positive reactions, thereby allowing a more forgiving detection setup which is especially beneficial in point-of-care applications.

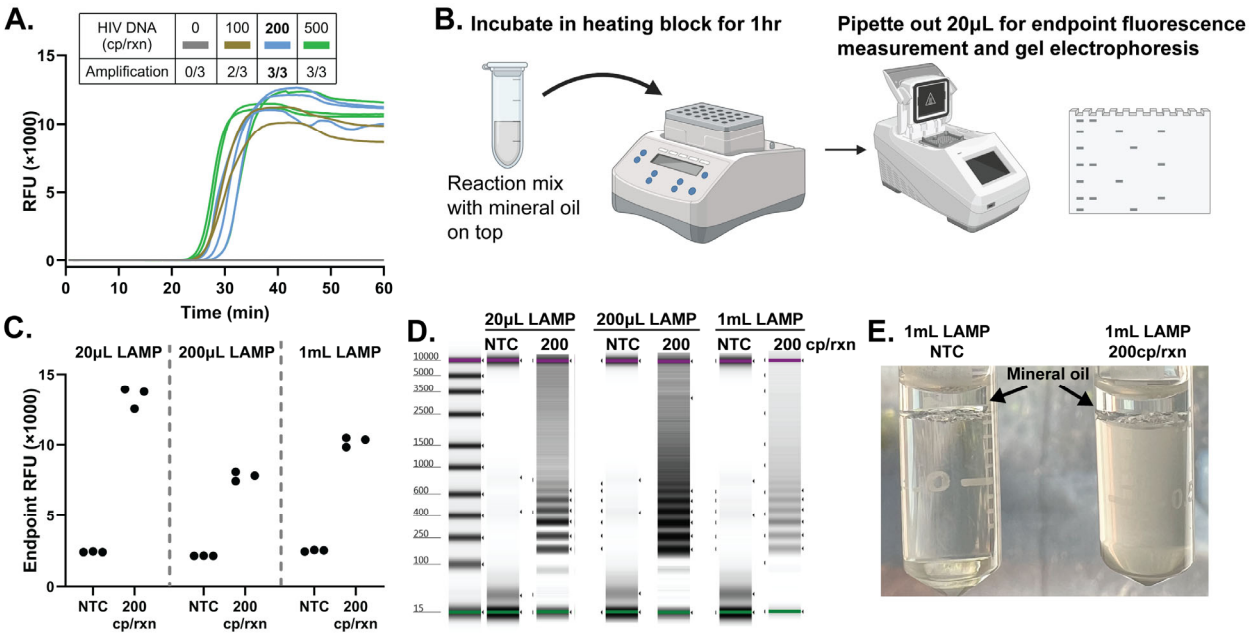

Figure 3.1. Performance of Larger-Volume LAMP.

(A) Real-time curves with baseline subtraction of 20µL LAMP to establish the assay LoD. (B) Workflow of running large-volume LAMP and endpoint analysis. (C) Endpoint fluorescence of 20µL reaction mixtures collected from 20µL, 200µL, and 1mL LAMP. (D) Representative gel electrophoresis results of 20µL, 200µL, and 1mL LAMP reactions. Results from all three replicates can be found in **Supplementary Figure 3.6**. (E) Pictures of 1mL LAMP reactions post-amplification.

3.3.2 **Preserved LoD of 20µL RT-LAMP with plasma**

The 20µL LAMP assay was adapted for RNA targets with added RNase inhibitor and WarmStart RTx for reverse transcription, following reported protocols [15]. Using HIV RNA extracted from inactivated virus stock as the template, the RT-LAMP demonstrated a LoD of 24 RNA copies, comparable to the lowest in reported assays (**Figure 3.2A**) [24–27]. The lower LoD of the assay with RNA targets compared to double-stranded DNA targets (**Figure 3.1A**) could be attributed to

more efficient primer binding to single-stranded RNA. For DNA targets, LAMP initiation relied on primers invading the double-stranded DNA which was suggested as the rate-limiting step [90]. In addition, the inherent RNase H activity of reverse transcriptase could degrade the RNA in the cDNA-RNA hybrid and facilitate subsequent primer binding [112,113].

We next explored the conditions to enable maintaining the RT-LAMP LoD in the presence of human plasma. One significant challenge was the high abundance of RNases in plasma that could instantly degrade RNA targets. Detergents and reducing agents such as Triton X-100 and DTT were reported to inhibit RNase functions [47]. In addition, detergents could facilitate virus lysis and prevent plasma coagulation at elevated temperatures [114]. We first tested the tolerance of the assay to Triton X-100 and DTT and found that 1% Triton X-100 and 2mM DTT did not impact assay performance and was therefore included in the assay (**Supplementary Figure 3.7**). To test assay compatibility with plasma, the inactivated HIV virus was used as the target to simulate conditions with clinical samples where HIV RNA remained encapsulated inside the virus until lysis. The assay with inactivated HIV virus yielded the same LoD as extracted RNA, confirming complete virus lysis (**Figure 3.2B**). Different percent of plasma were then spiked into the assay to investigate plasma dilution required for preserving assay LoD. The assay demonstrated the same LoD with 4% plasma while experiencing failed or substantially delayed amplification at LoD levels with 10% plasma (**Figure 3.2B and Supplementary Figure 3.8**). Therefore, 25-fold plasma dilution combined with 1% Triton X-100 and 2mM DTT enabled preserved LoD in RT-LAMP. Although harsher conditions may be required to completely inactivate RNases in plasma [115], the dilution and additives employed here could impede RNases acting on the RNA targets, allowing the reverse transcription to outpace RNA degradation and thereby maintaining assay LoD.

Furthermore, to reduce reagent costs which were critical for larger-volume reactions, the WarmStart RTx and the RNase inhibitor, the most expensive components in the formula (Supplementary Table 1), were replaced with lower-cost reagents from alternative sources. The temperature for reverse transcription with the lower-cost reagents was screened and subsequently determined at 50°C (**Supplementary Figure 3.9**). As shown in **Figure 3.2C**, the new assay demonstrated the same LoD at 24 copies of HIV RNA in inactivated virus in the presence of 4% plasma. Therefore, we moved forward with the lower-cost reagents.

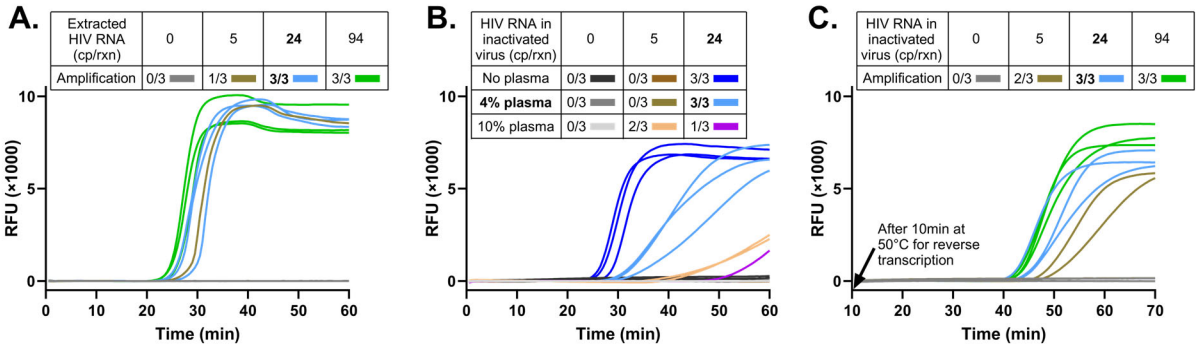

Figure 3.2. Preserved LoD of 20µL RT-LAMP with plasma

(A) Real-time curves of RT-LAMP with extract HIV RNA. (B) Real-time curves of RT-LAMP with inactivated HIV virus without or with human plasma. Real-time curves with 94 copies of the inactivated virus can be found in **Supplementary Figure 3.8**. (C) Real-time curves of RT-LAMP with inactivated HIV virus in the presence of 4% human plasma using lower-cost reagents. All real-time curves are with baseline subtraction.

3.3.3 Large-volume RT-LAMP with fingerstick plasma volumes

25-fold plasma dilution translates to 500µL reaction volumes for 20µL plasma (fingerstick volumes). Although 1mL LAMP showed the same assay performance (**Figure 3.1C and D**), the addition of reverse transcriptase and 10-minute incubation at 50°C posed increased risks of side reactions in larger-volume RT-LAMP. Therefore, the performance of 500µL RT-LAMP was first tested. As shown in **Figure 3.3**, the RT-LAMP assay of 500µL reaction volumes demonstrated the

same amplification LoD at 24 copies of extracted RNA, and no non-specific amplification was observed for negative controls. When 20µL plasma was spiked into the assay, the 500µL RT-LAMP maintained the same LoD at 24 copies of HIV RNA in inactivated virus (**Figure 3.3**). The results confirmed the successful amplification of HIV RNA in the presence of 20µL plasma through 500µL RT-LAMP assays.

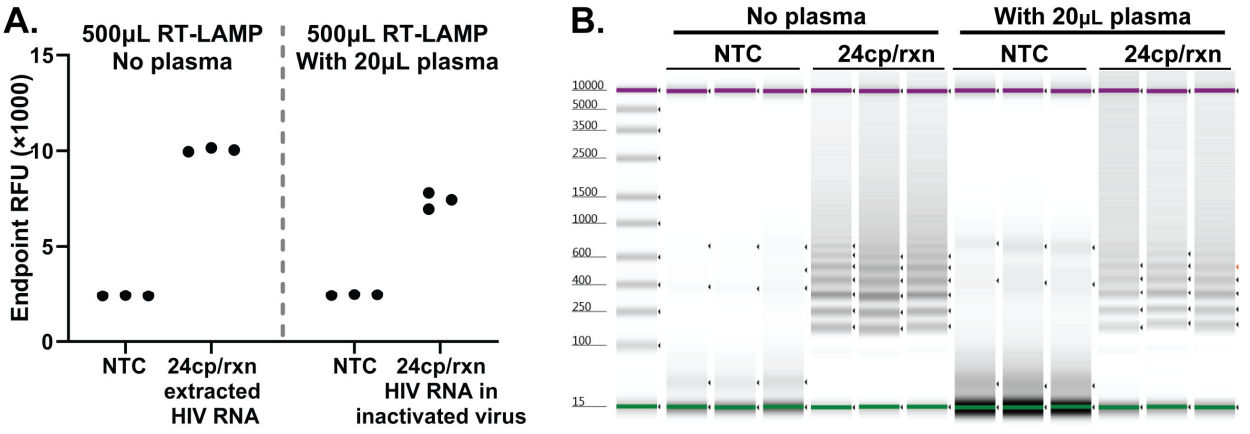

Figure 3.3. Performance of 500µL RT-LAMP without or with 20µL plasma (fingerstick volumes).
(A) Endpoint fluorescence of 20µL reaction mixtures collected from the 500µL RT-LAMP. (B) Gel electrophoresis results.

Besides technical performance, another risk for large-volume reactions is the exploded reagent cost. We estimated the cost for the 500µL RT-LAMP based on the retail prices of the reagents. The total cost was reduced from $35.18 to $14.78 by shifting to the lower-cost reagents described in **Figure 3.2C** (

Table 3.1 and Supplementary Table 3.2). Despite a 25-fold volume increase, the final cost of $14.78 for 500µL reactions was merely 1.64-3.13 times the price of existing 20µL RT-LAMP kits for SARS-CoV-2 (**Supplementary Table 3.3**). In addition, the reagent cost could potentially further decrease with large-scale production. Moreover, future work could explore switching to in-house RNase inhibitors and reverse transcriptase for substantial cost reduction [116,117].

Nevertheless, the results showed that reagent costs for large-volume reactions can be reduced dramatically by using in-house or lower-cost reagents, ultimately in close alignment with existing 20µL tests.

Table 3.1. Cost estimate for the 500µL RT-LAMP.
All cost was based on the retail price of the largest product size listed on the vendor website accessed on Oct. 15th, 2023**.**

Reagents	Vendor	Amount for 500µL rxn	Cost for 500µL rxn
Water	N/A	N/A	N/A
Buffer	In-house	N/A	N/A*
dNTPs	Syd Lab	2.8µmol	$0.3150
Primers	IDT	1.1nmol	$0.0425
20X EvaGreen	Biotium	25µL	$1.1350
Triton X-100	Promega	0.5µL	$0.0001
DTT	Promega	1µmol	$0.0022
TF Pol DNA polymerase	In-house	26.25µg	N/A*
RNase Inhibitor	MCLab	500unit	**$2.8325**
Reverse Transcriptase	MCLab	2000unit	**$10.4500**
Total			**$14.7773**

* The buffer and TF Pol DNA polymerase were made in-house. The associated cost of materials and human labor could not be estimated but should be negligible compared to the total cost listed here.

3.3.4 **Large-volume LAMP with other inhibitors**

Since the large-volume LAMP can dilute inhibition from the sample matrix while maintaining the same amplification LoD, we hypothesized that large-volume LAMP could tolerate higher inhibitor

concentrations in samples compared to standard 20µL reactions. As a proof-of-concept, the performance of 20µL and 200µL LAMP was tested against two common inhibitors, human albumin, present in crude samples such as plasma and whole blood, and guanidine isothiocyanate (GuSCN), often employed during nucleic acid extraction and needed to be stringently removed [118]. For human albumin, 20µL LAMP started experiencing amplification failures at the LoD level (200 DNA copies) when 8mg/mL albumin was included in 5µL samples (**Figure 3.4A**). In contrast, 200µL LAMP successfully maintained the LoD even in the presence of 40mg/mL plasma in the 5µL samples (**Figure 3.4B**). The results confirmed that human albumin was a major inhibitor in plasma and highlighted the superior tolerance of large-volume LAMP. Similarly, while the 20µL LAMP performance was compromised with 400mM GuSCN in 5µL samples, the 200µL LAMP could accommodate 800mM GuSCN in the sample (**Figure 3.4C and D**). Additionally, we repeated the tests with hemoglobin, a known inhibitor in human blood (**Supplementary Figure 3.10**) [119]. Although the 20µL LAMP appeared to maintain the LoD with 20mg/mL hemoglobin in the sample, the fluorescence in positive reactions was barely detectable, likely due to hemoglobin-induced quenching [51]. However, when the same sample was added to 200µL LAMP, the endpoint fluorescence in positive reactions was significantly higher than the negative controls. The results with hemoglobin showed the added advantage of large-volume LAMP in diluting potential inhibitory effects on signal detection, particularly valuable for point-of-care applications.

In summary, the findings demonstrated that large-volume LAMP had the capacity to tolerate higher concentrations of a wide range of inhibitors in samples added to the reactions. Therefore, large-volume LAMP could be employed in various point-of-care applications, including extraction-free nucleic acid amplification from crude samples, skipping rigorous washing steps

during nucleic acid extraction, or enabling harsher conditions for pathogen lysis followed by direct amplification. Moreover, the reaction volume could be further increased as needed to accommodate higher sample dilutions.

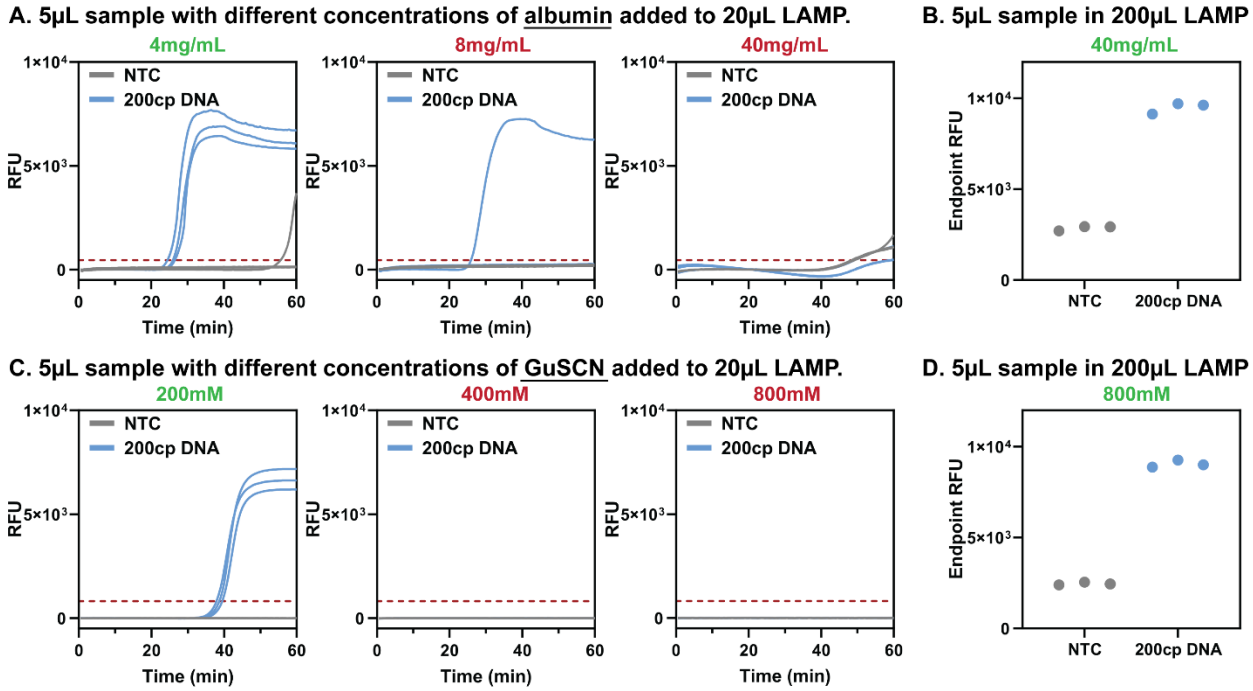

Figure 3.4. Large-volume LAMP with other inhibitors.

(A) Real-time curves of 20µL LAMP when 5µL samples with different concentrations of albumin were added to the reactions. (B) Endpoint fluorescence of 20µL mixtures collected from 200µL LAMP when 5µL samples with 40mg/mL albumin were added to the reaction. (C) Real-time curves of 20µL LAMP when 5µL samples with different concentrations of GuSCN were added to the reactions. (D) Endpoint fluorescence of 20µL mixtures collected from 200µL LAMP when 5µL samples with 800mM GuSCN were added to the reaction.

3.4 Conclusions

We proposed a novel approach for sensitive point-of-care HIV testing by directly adding fingerstick plasma samples into a large-volume RT-LAMP, to bypass the complicated RNA extraction step. We first examined the feasibility of large-volume LAMP using DNA targets and found that increasing reaction volumes up to 1mL did not compromise assay performance. We

then used RT-LAMP at 20μL reaction volumes to develop the dilution conditions for preserved LoD in the presence of plasma. By including 1% Triton X-100 and 2 mM DTT in the reaction and diluting plasma 25-fold, the RT-LAMP successfully maintained the LoD at 24 copies of HIV RNA in inactivated virus. Subsequently, the RT-LAMP reaction volume was scaled up to 500μL and demonstrated the same LoD in the presence of 20μL plasma (fingerstick volumes). Research is ongoing to integrate the large-volume RT-LAMP into a point-of-care sample-to-result device. In addition, we estimated the reagent cost for the 500μL RT-LAMP reaction based on retail prices. With in-house and more economical reagents, the cost was reduced to $14.78, aligning closely with existing 20μL RT-LAMP kits for SARS-CoV-2. Finally, the large-volume LAMP demonstrated the ability to tolerate higher concentrations of diverse inhibitors and can potentially be applied to streamline various point-of-care workflows.

3.5 Materials and Methods

20μL LAMP assays The 20μL LAMP contained 50mM bicine at pH 8.3, 10mM $(NH_4)_2SO_4$, 50mM KCl, 8mM $MgSO_4$, 1.4mM dNTPs, 1X EvaGreen Dye (Biotium, Cat. No.: #31000), 0.1% Triton X-100, 52.5μg/mL TF Pol, 0.6μM FIP, 0.6μM BIP, 0.3μM LF, 0.3μM LB, 0.2μM F3, 0.2μM B3. 2uL DNA templates were added to 18μL reaction mixtures. The reaction was run at 65°C for an hour in BioRad CFX96 Touch Deep Well Real-Time PCR Detection system. All primers were ordered from IDT with the following sequences.

FIP: CCTGGTGTCTCATTGTTGATGCATATTTTTCAGTYCCYTTAGAT.

BIP: AGATATCAGTACAATGTGCTGGCTCTAAGATTTTTGTCATGCT.

LF: TACTAGGTATGGTGAATGCAG

LB: GATGGAAAGGATCACCAGCAATATT

F3: TGGGAAGTTCARTTAGGAATAC

B3: CATACAARTCATCCATGTATTG

Large-volume LAMP assays The large-volume (200µL or 1mL) LAMP was prepared with the same reagent concentrations described in the 20µL LAMP assays. 2uL DNA templates were added to 198µL or 998µL reaction mixture for 200µL or 1mL LAMP assays, respectively. The reaction was briefly vortexed after DNA templates were added and capped with 200µL mineral oil (Millipore Sigma, Cat. No.: 69794-500ML). The reactions inside 2mL centrifuge tubes were incubated in a heating block filled with water set at 65°C. After an hour, the tubes were removed from the heating block. 20µL of the reactions were collected into PCR strip tubes for fluorescence measurements in the same BioRad CFX96 system used in 20µL LAMP assays. The fluorescence was measured at 65°C to be consistent with 20µL LAMP assays. The gel electrophoresis analysis was performed using Agilent D5000 ScreenTape in an Agilent 2200 TapeStation system, following the manufacturer's protocol.

RNA template and quantification The inactivated HIV virus stock was a customized order from ZeptoMetrix (Cat. No.: 0801032CFHI) by incubating the HIV-1 culture fluid (ZeptoMetrix, Cat. No.: 0801032CF) at 56°C for 1hr. HIV RNA templates were extracted from the virus stock with QIAamp Viral RNA Kits (Qiagen, Cat. No.: 52904) following the manufacturer's protocol. Extracted RNA was aliquoted and stored at -80°C until use.

20µL RT-LAMP in the presence of plasma The 20µL RT-LAMP reaction was prepared the same as the LAMP reaction with the addition of 0.5unit/µL of RNasin Plus (Promega, Cat. No.: N2615) and 0.3unit/µL of WarmStart RTx (NEB, Cat. No.: M0380L). 2µL RNA templates were added to 18µL reaction mixture followed by incubation at 65°C for 1hr. When testing with plasma, the reaction included 2 mM DTT and 1% Triton X-100. DTT (Promega, Cat. No.: V3151) solutions were aliquoted and stored at -20°C until use. 2µL diluted plasma (BioIVT, Cat. No.:

HUMANPLK2-0000291) was added to 16μL reaction mixture, followed by adding 2μL inactivated HIV virus.

For RT-LAMP with lower-cost reagents, the reaction was prepared the same except that WarmStart RTx was replaced with 4unit/μL of QuantumScript HD Reverse Transcriptase (MCLab, Cat. No.: SSIII-200) and RNasin Plus was replaced with 1unit/μL of RNase Inhibitor (MCLab, Cat. No.: RNIN-200). The reaction was incubated at 50°C for 10min followed by 65°C for 1hr.

Large-volume RT-LAMP 500μL RT-LAMP contained the same reagent concentrations as described in 20μL RT-LAMP with lower-cost reagents. 2uL extracted HIV RNA was added to 498μL reaction mixtures. The reaction was briefly vortexed and capped with 200μL mineral oil. The reaction was submerged in a water bath set at 50°C for 10min and immediately transferred to a heating block filled with water for incubation at 65°C for 1hr, followed by endpoint analysis described in large-volume LAMP. For reactions with plasma, 20μL plasma was added to 478μL reaction mixtures followed by adding 2μL inactivated HIV virus.

3.6 Acknowledgement

This work was supported by NIH/NIAID grants AI140460. I would like to thank all collaborators who contributed to this project: Shane D. Gilligan-Steinberg for designing and validating the assay used in this project, quantifying the RNA stock concentration, and contributing to the cost estimation; Wookyeom Kim for testing the large-volume LAMP with other inhibitors and analyzing the data; Enos C. Kline for designing and validating the assay used in this project, providing TF Pol materials, and contributing to sourcing lower-cost reagents; Dr. Ian T. Hull and Dr. James J. Lai for providing advice throughout the project; Dr. Barry R. Lutz for overseeing and guiding the project.

We thank Dr. Joanne D. Stekler and Dr. Paul K. Drain for their clinical advice on the project. We thank Dr. Erin Heiniger, Kevin Jiang, Sujatha Ramachandran Kumar for their advice on the project. We thank Dr. Gaurav Kumar Gulati for sharing the materials of the inactivated HIV virus. We thank Dr. Paul Yager, Dr. James I. Mullins, Dr. Patrick Stayton, and Dr. Xiaohu Gao for their advice on the project. Schematics in the manuscript were created with BioRender.com.

3.7 Supplementary Information

Figure 3.5. Pictures of the setup for running large-volume LAMP reactions.
The 2mL tubes were incubated in a heating block set at 65°C filled with water, with another metal block on top to avoid tubes floating out.

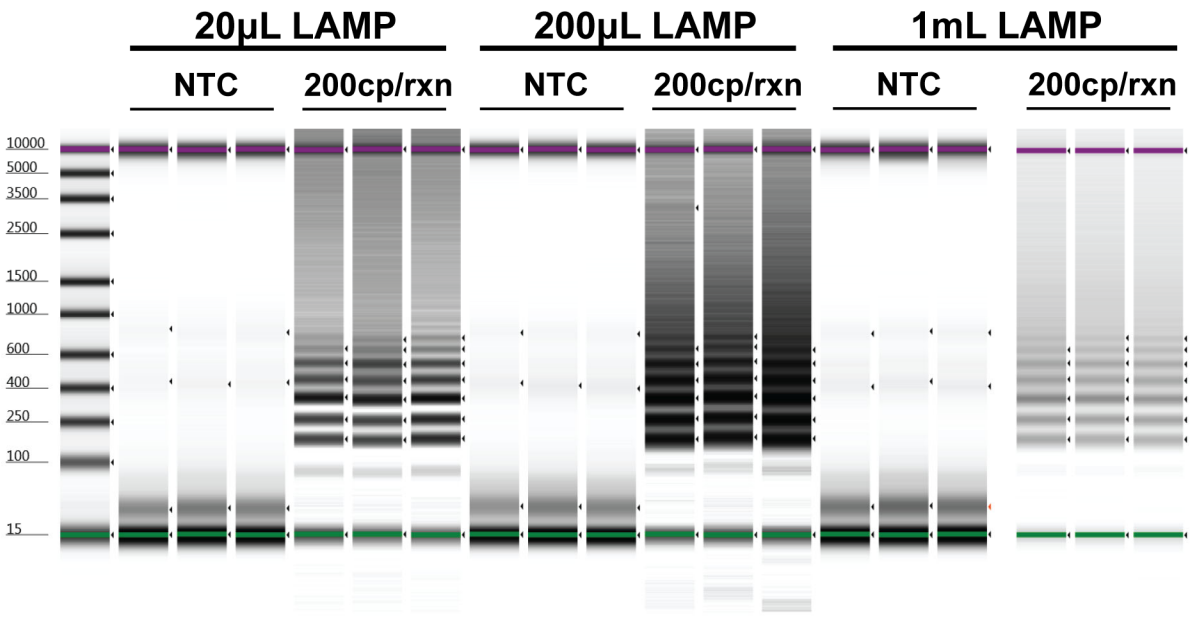

Figure 3.6. Gel electrophoresis results for all three replicates of 20µL, 200µL, and 1mL LAMP

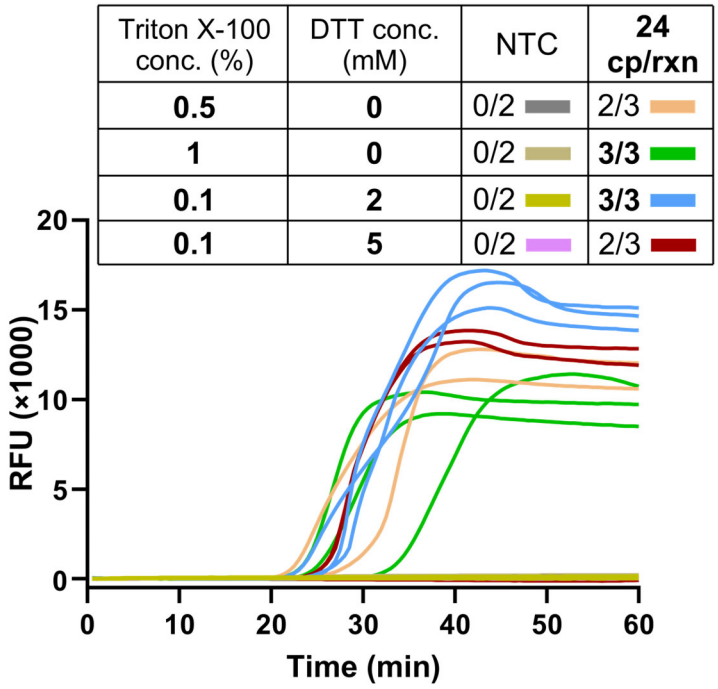

Figure 3.7. Performance of the 20µL RT-LAMP assay with extracted RNA in the presence of Triton X-100 and DTT at different concentrations.

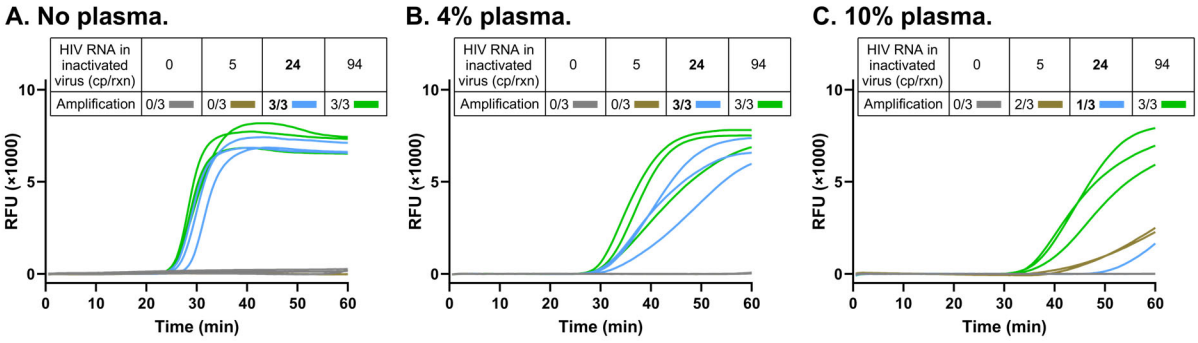

Figure 3.8. Full real-time curves of the 20µL RT-LAMP assay without plasma and with 4% and 10% plasma.

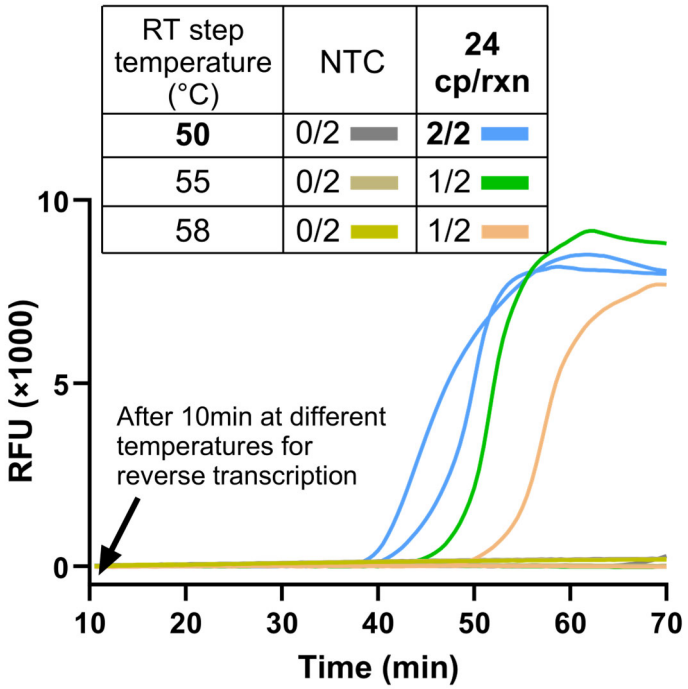

Figure 3.9. Screening the temperature for the reverse transcription step when switching to the lower-cost reagents.

Table 3.2. Reagent cost for 500uL RT-LAMP reactions before switching to lower-cost reagents.
All cost was based on the retail price of the largest product size listed on the vendor website accessed on Oct. 15th, 2023.

Reagents	Vendor	Amount for 500µL rxn	Cost for 500µL rxn
Water	N/A	N/A	N/A
Buffer	In-house	N/A	N/A
dNTPs	Syd Lab	2.8µmol	$0.3150
Primers	IDT	1.1nmol	$0.0425
20X EvaGreen	Biotium	25µL	$1.1350
Triton X-100	Promega	0.5µL	$0.0001
DTT	Promega	1µmol	$0.0022
TF Pol DNA polymerase	In-house	26.25µg	N/A
RNasin Plus	**Promega**	**250unit**	**$9.8500**
WarmStart RTx	**NEB**	**150unit**	**$23.8395**
Total			**$35.1843**

Table 3.3. Prices of existing SARS-CoV-2 RT-LAMP kits.
Price per test was based on retail prices for the largest product size list on vendor websites, accessed on Oct. 15th, 2023.

Vendor	Product	Cat. No.	Price per Test
NEB	SARS-CoV-2 Rapid Colorimetric LAMP Assay Kits	E2019S	**$8.21**
Invitrogen	Colorimetric ReadiLAMP™ Kit, SARS-CoV-2	A52544	**$4.72**
RayBiotech	COVID-19 Rapid Isothermal PCR Kit	RT-LAMP-B-100	**$9.00**

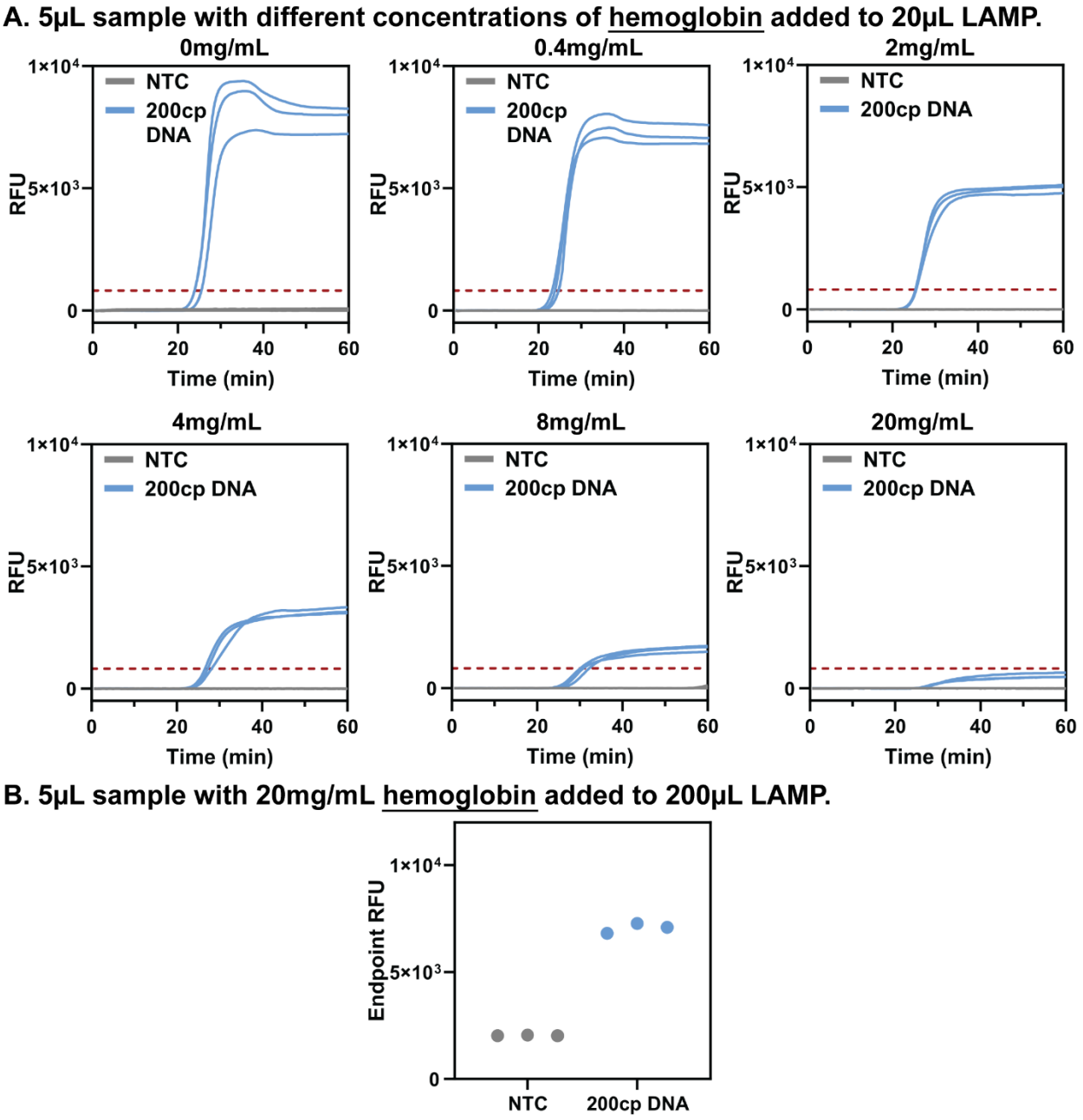

Figure 3.10. Large-volume LAMP with hemoglobin.

(A) Real-time curves of 20μL LAMP when 5μL samples with different concentrations of hemoglobin were added to the reactions. (B) Endpoint fluorescence of 20μL mixtures collected from 200μL LAMP when 5μL samples with 20mg/mL hemoglobin were added to the reactions.

Chapter 4. A Simple Agglutination System for Rapid Antigen Detection from Large Sample Volumes with Enhanced Sensitivity

4.1 Abstract

Lateral flow assays (LFAs) provide a simple and quick option for diagnosis and are widely adopted for point-of-care or at-home tests. However, their sensitivity is often limited. Most LFAs only allow 50μL samples while various sample types such as saliva could be collected in much larger volumes. Adapting LFAs to accommodate larger sample volumes can improve assay sensitivity by increasing the number of target analytes available for detection. Here, a simple agglutination system comprising biotinylated antibody (Ab) and streptavidin (SA) is presented. The Ab and SA agglutinate into large aggregates due to multiple biotins per Ab and multiple biotin binding sites per SA. Dynamic light scattering (DLS) measurements showed that the agglutinated aggregate could reach a diameter of over 0.5μm and over 1.5μm using poly-SA. Through both experiments and Monte Carlo modeling, we found that high valency and equivalent concentrations of the two aggregating components were critical for successful agglutination. The simple agglutination system enables antigen capture from large sample volumes with biotinylated Ab and a swift transition into aggregates that can be collected via filtration. Combining the agglutination system with conventional immunoassays, an agglutination assay is proposed that enables antigen detection from large sample volumes using an in-house 3D-printed device. As a proof-of-concept, we developed an agglutination assay targeting SARS-CoV-2 nucleocapsid antigen for COVID-19 diagnosis from saliva. The assay showed a 10-fold sensitivity enhancement when increasing sample volume from 50μL to 2mL,

with a final limit of detection (LoD) of 10pg/mL (~250fM). The assay was further validated in negative saliva spiked with gamma-irradiated SARS-CoV-2 and showed an LoD of 250 genome copies per µL. The proposed agglutination assay can be easily developed from existing LFAs to facilitate the processing of large sample volumes for improved sensitivity.

4.2 Introduction

Lateral flow assays (LFAs) have been widely used as point-of-care or self-diagnostic tests, due to their ease of use, rapid turnaround time, and low cost [99]. However, compared to nucleic acid amplification tests (NAATs) or enzyme-linked immunosorbent assays (ELISA), LFAs often result in lower sensitivity, thus limiting their applications for early diagnosis [99]. The sensitivity of most LFAs is inescapably limited by their ability to accommodate only 50-100μL of samples, while various non-invasive samples such as saliva, nasal swab elution, and urine often provide much larger volumes. Adapting LFAs to accommodate larger sample volumes can improve sensitivity by loading more target analytes. Various techniques have been explored to concentrate target analytes from samples, such as isotachophoresis [67], osmosis [64], immunomagnetic capture [120,121], electrokinetic separation [65,122], and phase extraction [66]. For example, Golden *et al.* reported concentrating the malaria antigen in plasma through the capture of stimuli-responsive polymer-antibody conjugates at porous membranes [68]. Although these methods have significantly improved assay sensitivity, they often require elaborate device fabrication, complicated manual operations, or long processing time, hindering their potential for use in point-of-care settings. Therefore, there is still a need for a simple yet effective system to concentrate target analytes from large sample volumes to improve assay sensitivity.

Agglutination refers to the assembly of two multivalent components into large aggregates via specific binding interactions under appropriate concentration ratios. Agglutination only requires mixing the two components and is effective in generating visible large aggregates within a short time. Since the first agglutination-based diagnostic for typhoid fever in 1896 [70], agglutination tests have expanded to different applications such as blood typing [71], influenza virus screening [72], and detection of antibodies or other protein biomarkers [73–75]. However, most agglutination

tests use the target analyte as one of the agglutination agents, and the signal is from the agglutination itself. Since agglutination requires appropriate concentration ratios, target analytes need to be present at high concentrations, which limits the test sensitivity. In addition, running multiple dilutions of the sample or assay reagents is needed to find the agglutination zone, which increases the labor intensity. Moreover, red blood cells or latex beads are often used for agglutination to allow visible readout, which requires complicated conjugation methods and adds the complication of reagent stability and consistency [123].

Here, a new and simple agglutination system is presented using biotinylated antibody (Ab) and streptavidin (SA). The agglutination is facilitated by multiple biotins per Ab and four biotin binding sites per SA, generating large aggregates that can be concentrated by filtration (**Figure 4.1A**). We characterized the agglutination process through both experiments and Monte Carlo modeling. Furthermore, a new format of agglutination assay is proposed by combining immunoassays and the simple agglutination system (**Figure 4.1B**). Specifically, biotinylated capture Abs and gold-nanoparticle-labeled detection Abs will generate immunosandwich structures in the presence of the target antigen. Upon addition of SA, the immunosandwich complex will undergo agglutination and the aggregated structures can be collected by filtration and detected in an in-house 3D-printed device. In this format, while the selectivity of the Ab pair ensures the specificity towards target analytes, the agglutination is independent of the analyte, and the ratio of biotinylated capture Ab and SA can be well-controlled to ensure efficient agglutination without running multiple dilutions. As the new agglutination assay only requires standard biotinylation of Abs, it can be easily developed from existing LFAs. Since the proposed agglutination assay allows capturing antigens from large sample volumes, we hypothesize that the

assay can achieve a better limit of detection (LoD) compared to conventional LFAs by detecting more analytes.

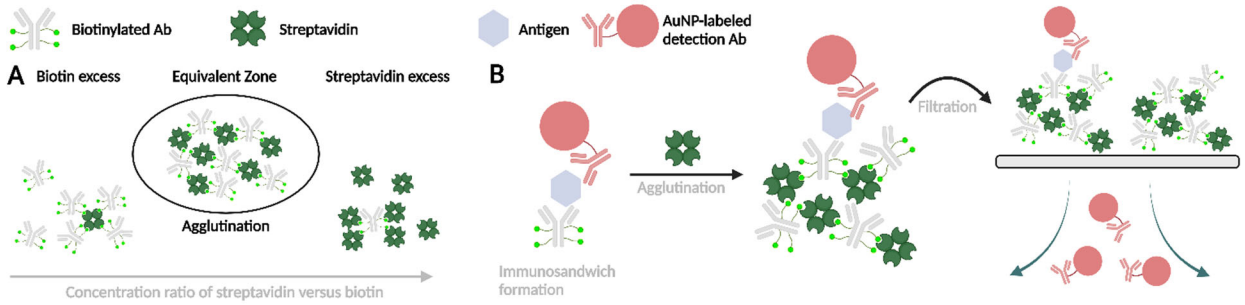

Figure 4.1. Biotin-SA-based agglutination system and the proposed agglutination assay.

The coronavirus disease 2019 (COVID-19) pandemic has caused over 6 million deaths globally since its outbreak. Despite the development of effective vaccines, as of February 8, 2023, there are still over 200,000 daily new cases globally, according to the World Health Organization (WHO) [58]. Therefore, diagnosis remains critical in controlling the spread of infection. Rapid COVID-19 antigen tests are widely adopted to detect SARS-CoV-2 nucleocapsid antigen from nasal swab samples. In addition to nasal swab detection, saliva testing has been drawing attention as a minimally invasive alternative sample type. In addition, most studies using RT-PCR have found similar sensitivities using saliva samples compared to nasal swabs [69]. Notably, up to 5mL of saliva can be collected from the average person by spitting, making it suitable for increasing the sample volume to improve sensitivity [63]. However, existing saliva-based LFAs miss the opportunity to use large sample volumes and reportedly have diagnostic sensitivity less than 50% [124,125]. As a proof-of-concept, we developed an agglutination assay detecting SARS-CoV-2 nucleocapsid antigen for COVID-19 diagnosis from saliva. We compared the assay performance with the conventional LFA format and further validated the assay in saliva matrix.

4.3 Results and Discussion

4.3.1 **SA-biotin-based agglutination system**

The agglutination system comprised of biotinylated Ab and SA. Commercial biotin-dPEG$_4$-TFP (tetrafluorophenyl) ester was used for the biotinylation of anti-SARS-CoV-2 nucleocapsid Ab. By tuning the biotin linker:Ab molar ratios during conjugation, Abs with 8, 5, and 3 biotins per Ab were generated. Since SA exhibits 4 biotin binding sites, we hypothesized that agglutination could occur between SA and biotinylated Abs. As shown in **Figure 4.2**, when the 8-biotin Ab was mixed with increasing concentrations of SA, the particle diameter measured using dynamic light scattering (DLS) changed from several nanometers to over 0.5 micrometers before returning to the nanometer level. Similar trends were observed in other agglutination systems, such as the Heidelberger-Kendall curve describing the extent of antigen-antibody agglutination as a function of their concentration ratios [76]. The sharp increase of the particle size to near-micron-level diameters suggested that the SA-biotin-based agglutination system was effective in generating large aggregates from protein monomers. As expected, the agglutination peak appeared when the molar ratio of the biotins and SA binding sites was near unity, suggesting that equal concentrations facilitated the agglutination. No agglutination peak was observed for 5-biotin and 3-biotin Abs, and particle size remained at the nanometer level (**Supplementary Figure 4.7**). This suggested that higher valency was critical for agglutination.

To explore key design parameters of the SA-biotin-based agglutination system, we sought to model the agglutination process. Numerous models have been developed on different agglutination systems. However, most models focused on the agglutination kinetics and temporal evolution, which involved parameters such as binding rate constants that needed to be experimentally determined [76,126,127]. Goldberg *et al.* modeled the equilibrium state of antibody-antigen

agglutination by introducing the reaction extent (p; the fraction of antigen sites that have reacted), but the model could only be applied when p was below a critical reaction extent [128,129]. Here, we adapted the Goldberg model's assumptions in conjugation with a Monte Carlo approach to simulate the process. A detailed description of the model can be found in Supplementary Information. Briefly, the model inputs included the number of Ab and SA, the number of biotins per Ab, the number of biotin binding sites per SA, and the reaction extent p. We chose the fraction of SA sites that were reacted during agglutination to represent p. To experimentally estimate p, we used the HABA reagent to measure the remaining free SA sites after agglutination, resulting in p around 0.4 when the molar ratio of biotins and SA sites ranged from 0.5 to 2 (**Supplementary** Figure 4.8 **and**

Table **4.4**). Hence, p was set to 0.4 in the model. For the model output, the number of total Ab and SA within an aggregate was used to represent the aggregate size. **Figure 4.2** presented the modeled size distribution when the Ab number was kept at 10,000 and the SA number was varied for different concentration ratios. With 8-biotin Ab, the modeled agglutination peak appeared when the concentration ratio was at 0.9, 1.0, and 1.1, where all the Ab and SA were essentially agglutinated into one large aggregate. The slightly larger aggregate size at higher concentration ratios was due to a higher input number of SA. Whereas for 5-biotin Ab and 3-biotin Ab, the agglutination peak was not observed in the model (**Supplementary Figure 4.7**). The modeled results aligned well with the DLS results, which confirmed that agglutination peaks were most likely to appear when the molar ratio of reacting sites was near unity, and higher valency of the components was critical for agglutination.

Since higher valency is expected to promote agglutination, we further tested using commercial poly-streptavidin (poly-SA) for agglutination. Poly-SA consists of multiple SAs crosslinked

together via polymers. Although the exact valency and molar concentration were unknown, the estimated poly-SA molecular weight was 30-300 times that of single SA, suggesting a much higher valency. We mixed different concentrations of poly-SA with biotinylated Abs and empirically identified the agglutination peak using DLS. As shown in **Figure 4.2**, the peak sizes with poly-SA were all larger than those using SA. Additionally, the poly-SA agglutination occurred with both 5-biotin and 3-biotin Abs, which did not aggregate with SA, and the median sizes of the agglutination peaks were 1.23µm and 0.65µm, respectively. The same effects were observed using our model simulation when increasing the SA valency to 100 (**Supplementary Figure 4.9**). Moreover, the measured median size of the agglutination peak using 8-biotin Ab and poly-SA reached 1.68µm. Therefore, we selected 8-biotin Ab and poly-SA to move forward with the development of the agglutination assay as it had the largest agglutination size.

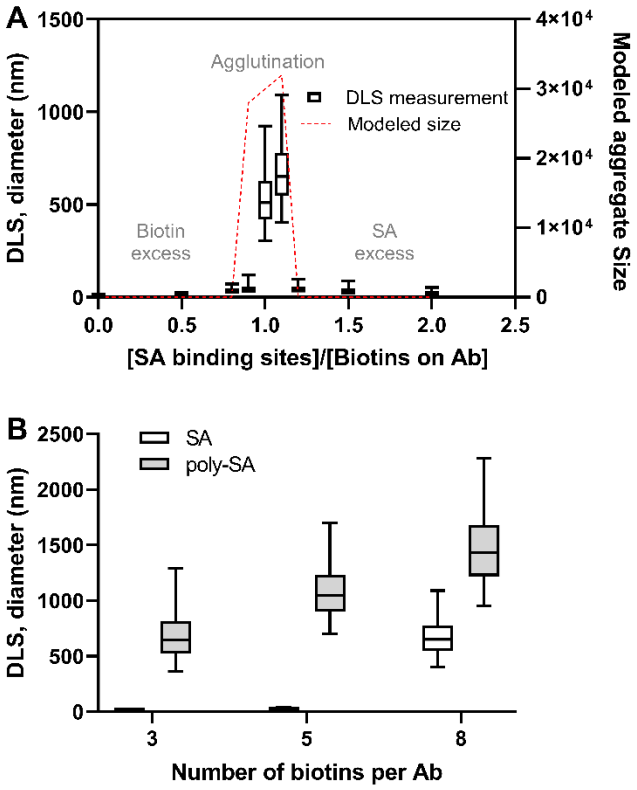

Figure 4.2. Agglutination characterization.

(A) Results of 8-biotin Ab agglutinating with SA at different concentration ratios. Left vertical axis shows DLS measurements of the aggregate size. Right vertical axis shows the median values of the modeled aggregate size, where the modeled size refers to the total number of Ab and SA within the aggregate. (B) DLS measurements of the peak sizes of Ab with different biotinylation levels agglutinating with SA or poly-SA. In both panels, the whiskers of the DLS measurements extend to 2% and 98% of the distribution, and the boxes cover the interquartile intervals while the middle lines represent the median values.

4.3.2 **Filtration of agglutinated products**

We next tested the separation of the agglutinated aggregate from the solution by filtration. After evaluating different filters, we selected glass microfiber filters with a particle retention size of 1.5μm due to their high loading capacity and relevant cutoff size. To test filtration efficiency, agglutinated samples were pushed through the selected filter in a syringe filter holder, and total protein concentrations before and after filtration were measured with the bicinchoninic acid (BCA) assay. The results were compared with the PBS control and non-agglutinated samples (biotin-Ab or poly-SA only). As shown in **Figure 4.3**, for agglutinated aggregates, the filtration flowthrough had non-detectable protein concentrations, showing that simple filtration was effective in capturing the agglutinated aggregates from the solution. The filtered flowthrough for biotin-Ab-only and poly-SA-only samples contained 51% and 63% of total proteins, respectively, as quantified with standard curves of the same biotin-Ab and poly-SA (**Supplementary Figure 4.10** and **Figure 4.11**). The protein loss likely resulted from non-specific binding to the filter. The results showed that agglutination enabled effective protein capture by filtration.

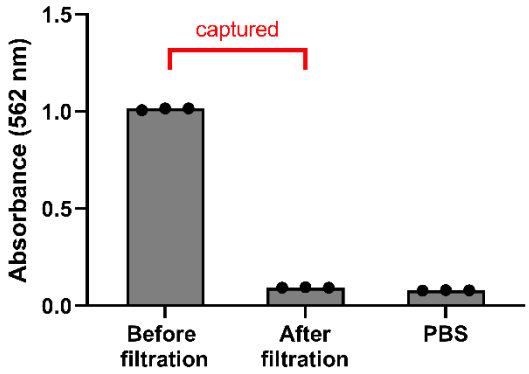

Figure 4.3. Filtration of the agglutinated aggregates.
BCA assay measurements are plotted for agglutinated samples before and after filtration and compared to PBS control.

4.3.3 **Agglutination assay development and performance**

Based on the simple agglutination system and effective separation of agglutinated aggregates via filtration, we designed an agglutination assay that can accommodate large sample volumes. Similar to conventional immunoassays, biotinylated capture Ab and AuNP-labelled detection Ab were added to the sample to form sandwich structures with the antigen (**Supplementary Figure 4.12**). The sample was pulse-vortexed for 15 seconds to ensure thorough mixing. After incubation, poly-SA was spiked into the sample solution to trigger agglutination with the biotinylated capture Ab. The whole sample was then transferred to a 3D-printed filtration device (**Figure 4.4**) where the aggregate was captured on the filter surface together with the immunosandwich structure, generating signals for the detection of the antigen. To minimize background signals caused by nonspecific absorption of detection Ab onto the filter paper, filters were pre-blocked with 1% casein, and the running buffer also included 1% BSA.

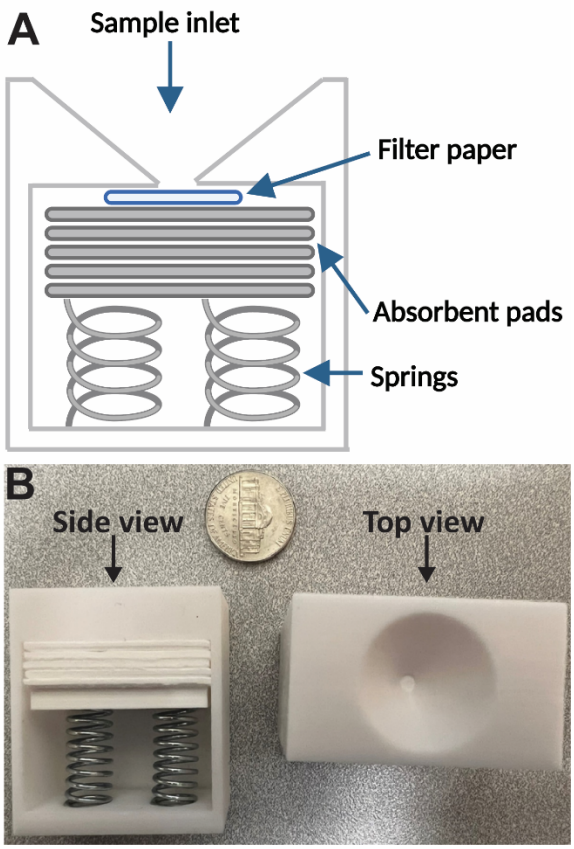

Figure 4.4. Filtration device.
(A) Schematics of the filtration device design. (B) Pictures of the device. A five-cent coin is used for scale.

To evaluate the performance of the agglutination assay at different sample volumes, we selected the detection limit of the target concentration as the comparison standard since it is clinically the most relevant. We first developed in-house LFAs using the same antibody pair to provide a benchmark limit of detection (**LoD**). Representative strip images and quantified band intensities are shown in **Figure 4.5**. With 50µL samples, the LoD was 50pg mL^{-1} as determined by the quantified line intensity, similar to other published SARS-CoV-2 nucleocapsid LFAs [130–132]. We then tested the agglutination assay using 50µL samples with the same Ab concentrations. The positives showed a circle pattern as expected, and the intensity maintained relatively uniform across the region based on the line plots (**Supplementary Figure 4.14**). The LoD was 100pg mL^{-}

[1], slightly higher than the LoD of LFAs. The higher LoD was likely due to higher background noise caused by the rough surface of the filter paper compared to the smooth nitrocellulose used in LFAs. Nevertheless, the comparable level of LoD validated the feasibility of the proposed new format of the agglutination assay.

We next explored the ability of this agglutination assay to accommodate large sample volumes. We selected a 2mL sample volume as it is reported to be a feasible volume for saliva collection [133,134]. When the same assay conditions for 50μL were applied to 2mL samples, the whole workflow took over an hour, and the signals from negative controls were extremely high. We hypothesized that the filtration region was clogged due to a large number of agglutinated aggregates that trapped the AuNPs and generated high background signals. To solve the issue, the diameter of the filtration region was increased from 1.5mm to 2.5mm by readjusting the device's sample port diameter. Antibody concentrations were also decreased to reduce background signals. The final flow time was about 5 minutes for 2mL samples, and the negative controls remained clean. Furthermore, the LoD of the assay with 2mL samples decreased to 10pg mL^{-1} (~250fM), showing a 10-fold enhancement in detection compared to using 50μL samples. The LoD improvement of approximately 10-fold fell short of the 40-fold improvement that might be predicted based solely on the larger number of antigens in the 40-fold sample volume. This may have been due to a reduction of antibody binding efficiency at the reduced antibody concentration in the 2mL sample test and/or increased signal dispersion of the larger flow-through area in the 2mL sample test.

The biggest challenge we encountered with increased sample volumes was high background signals. Besides reducing antibody concentrations, an alternative assay format is to add the AuNP-labeled detection Ab in the end, after the antigen capture, agglutination, and filtration, to avoid the

unspecific binding of the detection Ab to the large aggregates or other proteins in the sample. However, the agglutinated aggregates may hide the captured antigen from the detection Ab due to steric hindrance. The fast flow time may also limit the binding between the detection Ab and antigen. On the other hand, in the current format, both antibodies bind the antigens in a homogenous solution, which allows binding all available analytes with fast kinetics. Therefore, the alternative format was not tested. Regardless, while multiple aspects of the assay, such as incubation time, can be further optimized to improve the sensitivity, the relative comparison of the three formats validated the feasibility of the proposed agglutination assay and its ability to improve assay LoD with larger sample volumes.

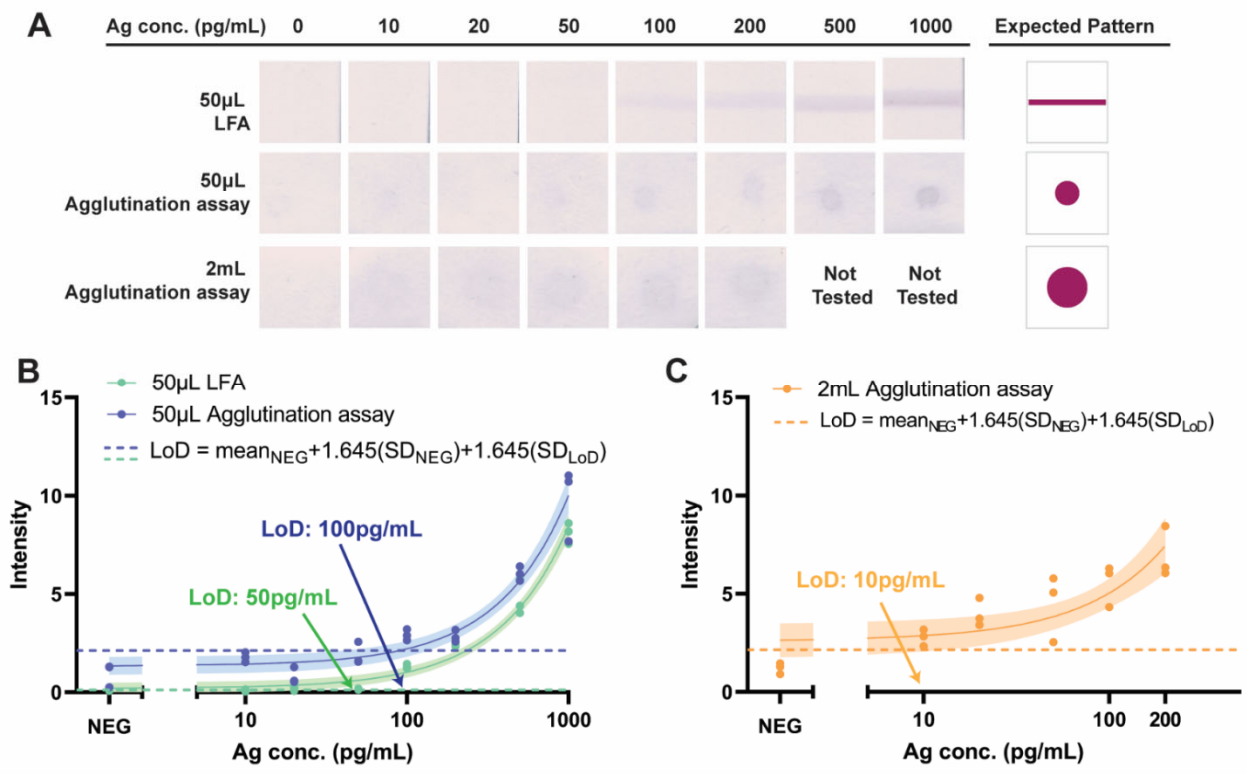

Figure 4.5. Agglutination assay performance.

The assay workflow is shown in **Supplementary Figure 4.12**. (A) Representative scanned images of the 50µL LFAs, 50µL agglutination assays, and 2mL agglutination assays. A uniform contrast is added for display purposes. Raw images without added contrast from all replicates (N=3) are shown in

Supplementary Figure 4.15. (B) The quantified intensity of the 50µL LFA and 50µL agglutination assay results. (C) The quantified intensity of the 2mL agglutination assay results. All intensities are quantified using ImageJ. The dotted horizontal lines represent the cut-off value for LoD determination and SD represents the standard deviation. All LoD determination in the three assay formats followed the same method described in the reference [135]. The solid dots represent the individual value for each replicate (N=3), and the curves and shades represent the best-fit lines with linear regression and their 95% confidence bands.

4.3.4 **Assay validation in saliva matrix**

We used pooled saliva collected from healthy donors to validate the assay compatibility with the saliva matrix. Saliva is known to be viscous due to its high mucin content [136,137]. In initial attempts, saliva was simply diluted and added to the agglutination assay. However, the flow time was over two hours and background signals were high, likely due to filter clogging from mucin aggregates or other large particles in saliva. *N*-Acetyl-L-cysteine (NALC) in alkaline phosphate buffer is reported to reduce the viscosity of mucoprotein solutions mediated through the sulfhydryl group reducing disulfide bonds [138]. We found that incubating saliva with NALC buffer helped reduce the viscosity and homogenize the sample. An additional prefiltration step with common 0.45µm syringe filters further helped remove any remaining large components in saliva such as food particles and microorganisms. In the final assay, 2mL saliva was mixed with 0.5mL lysis buffer with a final concentration of 10mM NALC and 1% Triton X-100 for reducing saliva viscosity and lysing the SARS-CoV-2 virus, respectively. After incubating for 15 minutes, the sample was prefiltered with syringe filters and then transferred to the agglutination assay (**Supplementary Figure 4.13**).

We first evaluated the assay LoD using negative saliva spiked with SARS-CoV-2 nucleocapsid antigen. As shown in **Figure 4.6**, the assay was able to detect concentrations as low as 10pg mL^{-1} antigen, the same as the LoD in the buffer, suggesting that the assay was compatible with the saliva

matrix. We further tested the assay with negative saliva spiked with gamma-irradiated SARS-CoV-2. The stock concentration of the inactivated virus was quantified using a commercial SARS-CoV-2 RT-qPCR kit (**Supplementary Figure 4.16**). The agglutination assay was able to detect 250 genome copies per μL of inactivated virus (**Figure 4.6**). The lower variance of the signal intensities with inactivated viruses may suggest that the antibody pair binds more strongly towards native antigens versus the recombinant ones. One SARS-CoV-2 virus is reported to contain about 1800 copies of nucleocapsid protein [139]. The LoD of 250 genome copies per μL corresponds to 35pg mL^{-1} nucleocapsid antigen, which is on par with the observed 10pg mL^{-1} LoD. The slightly higher LoD with inactivated viruses could result from incomplete lysis during the assay or antigen degradation during the inactivation process of the stock. Nevertheless, the WHO target product profiles (TPP) for point-of-care COVID-19 tests set the acceptable LoD at 1000 genome copies per μL [140], which is higher than the 2mL agglutination assay LoD. The LoD of 10pg mL^{-1} nucleocapsid antigen and 250 genome copies per μL of virus in saliva was well within the range of the reported viral load in saliva samples [141,142].

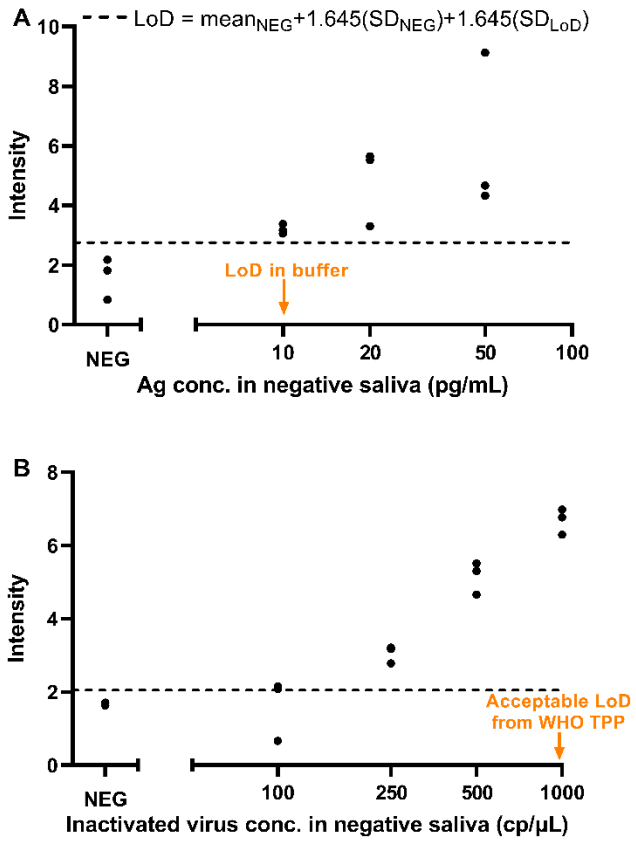

Figure 4.6. Agglutination assay in saliva matrix.

(A) The quantified intensity of agglutination assay detecting recombinant SARS-CoV-2 nucleocapsid antigen spiked into saliva. (B) The quantified intensity of agglutination assay detecting inactivated SARS-CoV-2 virus spiked into saliva. The acceptable LoD from the WHO target product profile (TPP) is 1000 copies μL^{-1} [140]. The dotted horizontal lines represent the cut-off value for LoD determination and SD represents the standard deviation. Scanned raw images for all replicates can be found in **Supplementary Figure 4.17 and Figure 4.18**.

In summary, we started with testing in the buffer and demonstrated that the new agglutination assay showed comparable detection limit to LFAs when using the same 50µL sample volume, and a 10-fold lower LoD when the sample volume was increased to 2mL. Besides the ability to accommodate large sample volumes and improve LoD, the run time for the agglutination assay was also fast (about 5 minutes for 2mL samples) due to the vertical flow. Moreover, the

agglutination assay could be easily converted from existing LFAs by biotinylating the capture antibody to enable agglutination with poly-SA. We further validated the assay with saliva matrix. The LoD was the same as in the buffer and well within the clinical range. Although the assay required an additional prefiltration step, multiple commercially available saliva collection devices incorporate filtration during sample collection [143,144]. Our results suggest that an agglutination assay using 2mL saliva shows promises for sensitive SARS-CoV-2 antigen detection from saliva samples.

There are a few limitations that need to be addressed in future work. During assay development, we encountered high background signals when scaling up the sample volume, which may be caused by clogged filters. In addition to optimizing antibody concentrations and the filtration region diameter, future work could explore increasing the aggregate size with even higher valency or including multiple binding pairs besides SA and biotin, such as nucleic acid hybridizations. This may enable the use of filters with larger pore sizes and higher loading capacity. Additionally, the current assay workflow includes multiple user steps, and the filter needs to be removed from the device to observe the assay result, adding to the complexity for the point of care. The issues can potentially be resolved with improved device design, such as a spinning disk system that can automate assay steps and drive the filtration with centrifugation [145]or the detection region could be covered by a transparent film to allow direct observation of the assay results. Alternatively, the device could include a detachable part that can be simply removed after the assay to expose the filter region. Nevertheless, the proposed agglutination assay is simple to develop from existing LFAs and can be easily scaled up to accommodate different sample volumes.

4.4 Conclusions

We have developed a simple agglutination system comprising biotinylated Ab and SA or poly-SA. The agglutinated aggregates can reach sizes over 1 micron and be effectively separated from the solution via simple filtration. Moreover, with both experimental measurements and Monte Carlo modeling, we verified that higher valency and equal concentrations of agglutinating pairs facilitated agglutination, which can be applied to the development of other agglutination systems. Further, we developed an agglutination assay that can accommodate large sample volumes. Using the COVID-19 antigen test as a proof-of-concept, the assay showed a 10-fold enhancement in sensitivity with 2mL samples compared to 50μL samples. The final assay was able to detect down to 10pg mL^{-1} SARS-CoV-2 nucleocapsid antigen and 250 genome copies per μL of inactivated virus spiked into saliva. The new agglutination assay can be simply developed from existing LFAs by biotinylating the capture Ab to enable agglutination. Although further simplification in the assay workflow is needed, we anticipate that the proposed agglutination assay can be applied to improve LFA sensitivity for different applications where large sample volumes are available.

4.5 Materials and Methods

Antibody Biotinylation Biotin-dPEG$_4$-TFP ester (Quanta Biodesign, Cat. No. 10009) was dissolved at 33mM in DMSO upon arrival and stored at -20°C. Anti-SARS-CoV-2 nucleocapsid monoclonal antibody (Exonbio, Cat. No.: NP_11A7) was diluted to 6.67μM in 500mM sodium bicarbonate buffer (pH 9.6) and spiked with the biotin linker stock. The final molar ratio of biotin linker to antibody was at 20, 50, or 80 to achieve different biotinylation levels. The reaction was incubated at 4°C overnight. The biotinylated antibody was purified into 1xPBS using Zeba Micro Spin Desalting Columns 7K MWCO (Thermo Scientific, Cat. No.: 89877) following the

manufacturer's protocol. The biotinylation level on the antibody was quantified with HABA assay (Sigma-Aldrich, Cat. No.: H2153) following the manufacturer's protocol.

Agglutination Characterization 33.3nM biotinylated antibody was mixed with different concentrations of streptavidin (Sigma-Aldrich, Cat. No: 189730) or polystreptavidin R (Antibodies-Online, Cat. No.: ABIN4370319) in PBS and incubated at room temperature for 15 minutes. Particle size was then measured via dynamic light scattering.

Monte Carlo Simulation See Supplementary Information for model details. In all simulations, the Ab number was 10,000, and the reaction extent p was set to 0.4. The valency of SA and poly-SA was set to 4 and 100, respectively. The number of SA or poly-SA and the number of biotins per Ab were varied for different simulation conditions.

Experimental Estimation of Reaction Extent HABA (TCI America, Cat. No: H0586) was dissolved in 0.01M NaOH to make a 10mM HABA stock. 0.3mM HABA in 1xPBS was spiked into standard dilutions of SA and absorbance at 500nm was measured to generate a standard curve. Agglutinated reactions were spiked with 0.3mM HABA to quantify the remaining free SA concentrations.

Filtration Efficiency of Agglutinated Aggregate Samples of 20ug mL^{-1} Ab only, 48μg mL^{-1} poly-SA only, and a mix of them both were incubated for 15 minutes. Whatman Grade 934-AH glass microfiber filter (Cytiva, Cat. No.: 1827-025) was put inside a syringe filter holder (Sartorius, Cat. No.: 16517-E). 10mL of 10ug mL^{-1} BSA in PBS flowed through the filter to passivate the filter and reduce unspecific binding, followed by 10mL PBS, to wash the filter and minimize BSA in the final flowthrough. 500μL sample was immediately added to the syringe filter, and the flowthrough was collected. Total protein concentration in the remaining non-filtered sample and the filtered flowthrough was measured using the Micro BCA Protein Assay Kit (Thermo Scientific,

Cat No.: 23235) following the manufacturer's protocol (test tube procedure), except that only 75μL sample was used. The BCA assay was added to a 96-well plate to measure A562 using BioTek Synergy Neo reader.

SARS-CoV-2 Nucleocapsid LFA 2mg mL^{-1} Polystreptavidin R was deposited onto nitrocellulose (Sartorius, Cat. No. 1UN95ER100020NT) as the capture line using a Biodot ZX1010 Dispense System. After drying overnight, the nitrocellulose was pre-blocked by soaking in PBS with 1% casein for 2 hours at room temperature followed by a 10-minute soaking in 1xPBST buffer. After drying overnight, the nitrocellulose was then assembled with absorbent pads on backing cards and cut into 4mm-wide lateral flow strips.

Anti-SARS-CoV-2 nucleocapsid monoclonal Ab (Bioss, Cat. No.: bsm-41411M) conjugated with gold nanoparticles (custom conjugation provided by the vendor) was used as the detection antibody. The recombinant SARS-CoV-2 nucleocapsid protein (AcroBiosystems, Cat No.: NUN-C5227-1mg) in PBS with 1% BSA and 1% Triton X-100 was spiked with 1μg mL^{-1} biotinylated capture Ab and 5μg mL^{-1} detection Ab, and pulse-vortexed for 15 seconds for mixing. After incubating for 15 minutes, 50μL sample was added to the lateral flow strip, followed by 50μL PBST as wash buffer.

SARS-CoV-2 Nucleocapsid Agglutination Assay The assay device was printed with a 3D printer (Original Prusa i3 MK3S+). The Whatman Grade 934-AH glass microfiber filter was pre-blocked by soaking in 1xPBS with 1% casein for 2 hours at room temperature, followed by 10 minutes in 1xPBST buffer. The filters were then dried overnight and cut into quarters. The filter was placed under the sample port of the device, followed by 5 layers of absorbent pads (Cytiva, Cat. No., 8115-2250). Two springs were used to hold the layers together to ensure close contact.

For 50μL agglutination assays, the reaction was prepared the same as in the LFA using the same Ab concentrations. After a 15-minute incubation, 0.5μL of 240μg mL^{-1} poly-SA was spiked into the reaction and pulse-vortexed for 15 seconds for mixing. After another 15 minutes, the sample was added to the agglutination device, followed by 50μL PBST wash. For 2mL agglutination assays, all the procedures were the same except that 0.5μg mL^{-1} biotinylated capture Ab and 0.2μg mL^{-1} detection Ab were used. 500μL PBST was used as the washing buffer. The diameters of the sample port in the agglutination device for 50μL and 2mL assays were 1.5mm and 2.5mm, respectively.

Quantification of Inactivated SARS-CoV-2 Stock Concentration with RT-qPCR Gamma-irradiated SARS-CoV-2 was obtained from BEI Resources (Cat. No.: NR-52287). RNA was extracted using QIAmp Viral RNA kits (Qiagen, Cat. No.: 52904) and added to the FDA-EUA-approved Smart Detect™ SARS-CoV-2 rRT-PCR kit (InBios International, Inc.) for quantification following the manufacturer's protocol. The PCR reactions were run on a Bio-Rad CFX96 real-time detection system. Synthetic SARS-CoV-2 RNA control from Twist Biosciences (Cat. No.: MT007544.1) was used as the standard.

Agglutination Assay with Saliva Matrix Pooled saliva was collected from volunteers with no reported COVID-19 symptoms and stored in a -80°C freezer before use. Sample collection was approved by the University of Washington IRB (Study STUDY00010543). After thawing, 2mL saliva was spiked with recombinant SARS-CoV-2 nucleocapsid antigen or inactivated virus and mixed with 0.5mL lysis buffer, resulting in a final buffer condition of 0.1M sodium phosphate (pH=8), 10mM NALC, 1% Triton X-100 and 1% BSA. The sample was incubated for 15 minutes and then filtered with a 0.45μm syringe filter (PALL, Cat. No.: 4654). The sample was then spiked

with capture Ab and detection Ab, followed by poly-SA, in accordance with the agglutination assay protocol.

Signal Quantification All strip images were scanned using an Epson V700 photo scanner. The signal intensities were quantified in ImageJ and mean intensity with the background signal subtracted was reported. For LFAs, a rectangle 73 pixels wide and 25 pixels long was centered over the test line as the region of interest (ROI). Rectangles of the same size 50 pixels above and below the ROI were selected as the background. The averaged mean intensity from the two background regions was used for background subtraction. In cases where lines were not visible, the distance between the test lines and the bottom of the strips was used to identify the test line region. For the 50μL agglutination assay results, the procedure was the same except a circle with a diameter of 24 pixels was used instead of a rectangle. For 2mL agglutination assay, a circle with a diameter of 65 pixels was used, and two regions 100 pixels away from the ROI on the filter, either in the x or y direction, were selected as the background.

4.6 Acknowledgment

This work was supported by NIH/NIAID grants AI140460 and AI163282. I would like to thank all the collaborators who contributed to this project: Dr. Nuttada Panpradist for collecting the saliva samples and quantifying the inactivated virus stock concentrations, Jack Henry Kotnik for collecting the saliva samples and quantifying the band intensities of the assay results, Dr. Richard C. Willson and Dr. Katerina Kourentzi for generously sharing their antibody pair screening information, Zoe Chau and Joanne Liu for their literature review on SARS-CoV-2 viral load in saliva and existing COVID-19 LFAs, Dr. James J. Lai and Dr. Barry R. Lutz for their guidance in this project. I would like to thank all collaborators above for editing the manuscript. We would like to thank InBios International, Inc. for generously providing the Smart Detect SARS-CoV-2 rRT-PCR kits. Schematics in this chapter were created with BioRender.com.

4.7 Supplementary Information

Monte Carlo Modeling of the Streptavidin-Biotin-Based Agglutination System

Overview We aimed to model the size distribution at the equilibrium state of the streptavidin-biotin-based agglutination system. Specifically, we adapted the assumptions in the Goldberg model and used the Monte Carlo approach to predict the size distribution in the agglutination system at the reaction extent p. Briefly, in a binding event, a free biotin site and a free streptavidin (SA) site was randomly chosen to react, with corresponding size changes of the bound aggregate. During a single simulation run, this randomized binding event was repeated until the reaction extent was met, and the simulation run generated a size distribution of the agglutinated aggregates. The single simulation run was then repeated 1000 times, and the averaged output was used as the model result.

Assumptions:

1. Any unreacted biotin site had the same reactivity, regardless of the size of the aggregate that the biotin was attached to. The same applied to the SA binding sites.
2. An unreacted biotin site within an aggregate cannot react with any other unreacted SA binding site in the same aggregate. In other words, intra-aggregate reactions did not occur.
3. The reaction did not stop until the reaction extent was met.

The first two assumptions were adapted from the Goldberg model. The third assumption was added for our Monte Carlo approach. While multiple factors could contribute to the termination of the agglutination reaction, such as steric hindrance and diffusion limitations, it was challenging to accurately model the factors and their impacts on the agglutination system. Instead, the reaction extent p, adapted from the Goldberg model, was experimentally measured and used as the

termination condition in the simulation. This assumption aligned with our goal to model the equilibrium state only, rather than the kinetic pathway that led to the equilibrium state.

Input Parameters

Ab	**Number of starting antibodies.**	**Ab=10000 in all simulations.**
b	Number of biotins per Ab.	Varied in different conditions.
SA	Number of starting streptavidin.	Varied in different conditions.
s	Number of biotin binding sites per SA.	s=4 for streptavidin. s assumed as 100 for poly-SA.
p	Fraction of SA sites reacted during agglutination.	p=0.4 in all simulations.

Due to computing power limitations, Ab was set to be 10000 only. However, since we were modeling the equilibrium state with an experimentally measured reaction extent p and strong biotin-streptavidin binding, we anticipated that the scales of concentrations (numbers) of reactants should not have a major impact on the relative distribution of the agglutinated aggregates.

Output Parameters The output was a matrix **M** containing the sizes and numbers of the aggregates. Since it was unrealistic to model the actual diameter of the aggregate, we used the number of Ab and SA within the aggregate to represent its size.

Simulation Workflow The workflow below was repeated 1000 times in our simulation, and the averaged output was used as the model result.

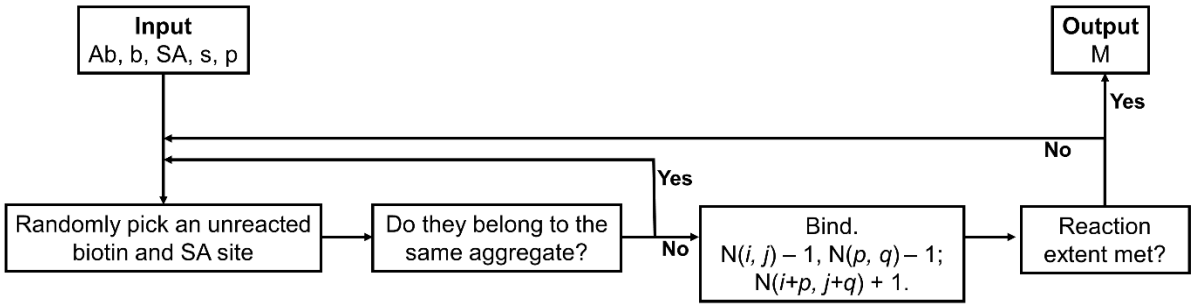

N(*i, j*) refers to the number of the aggregate that the chosen biotin site was attached to, and have i molecules of Ab and j molecules of SA. N(*p, q*) refers to the number of the aggregate that the chosen SA site was attached to, and has p molecules of Ab and q molecules of SA. After binding, both N(*i, j*) and N(*p, q*) decrease by 1, while N(*i*+*p, j*+*q*) increases by 1. The simulation was run in Matlab.

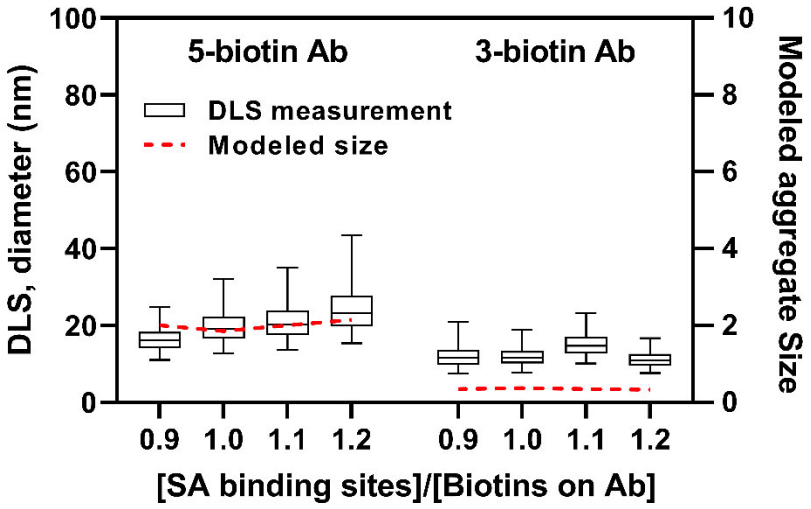

Figure 4.7. Results of 5-biotin Ab and 3-biotin Ab agglutinating with SA.

The left y-axis shows DLS measurements of the aggregate size. The right y-axis shows the median values of the modeled aggregate size, where the modeled size refers to the total number of Ab and SA within the aggregate.

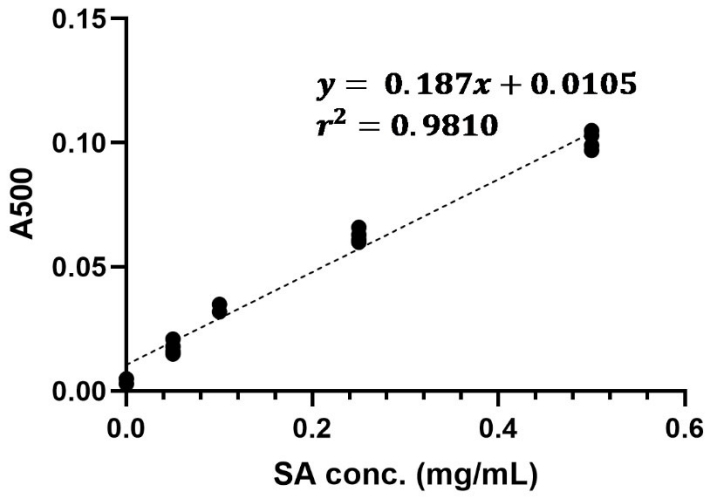

Figure 4.8. The standard curve of quantifying SA concentrations with HABA assay.
Y axis refers to the absorbance at 500nm from the HABA assay measurements.

Table 4.4. Estimation of reaction extent p in 8-biotin Ab agglutinating with SA.
The remaining SA concentration was quantified using the standard curve in **Figure 4.8**.

[Biotins on Ab]/ [SA binding sites]	Added SA conc. (mg/mL)	Remaining SA conc. (mg/mL)	Reaction Extent, p
0.5	0.556	0.360	**35.2%**
0.8	0.348	0.198	**43.1%**
1	0.278	0.151	**45.8%**
1.5	0.185	0.108	**41.7%**
2	0.139	0.088	**36.9%**

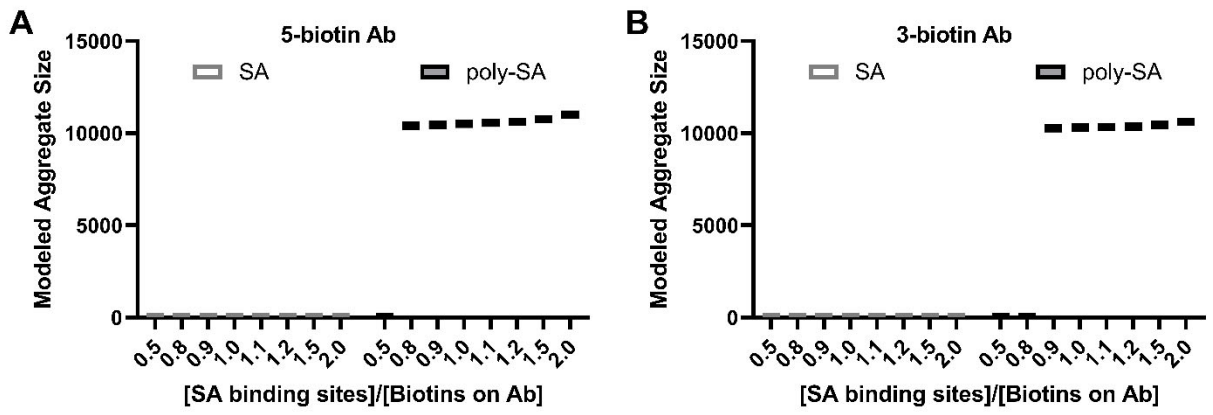

Figure 4.9. Model results of using SA versus poly-SA.

The valency of poly-SA was assumed at 100. (A) Model results of 5-biotin Ab. (B) Model results of 3-biotin Ab.

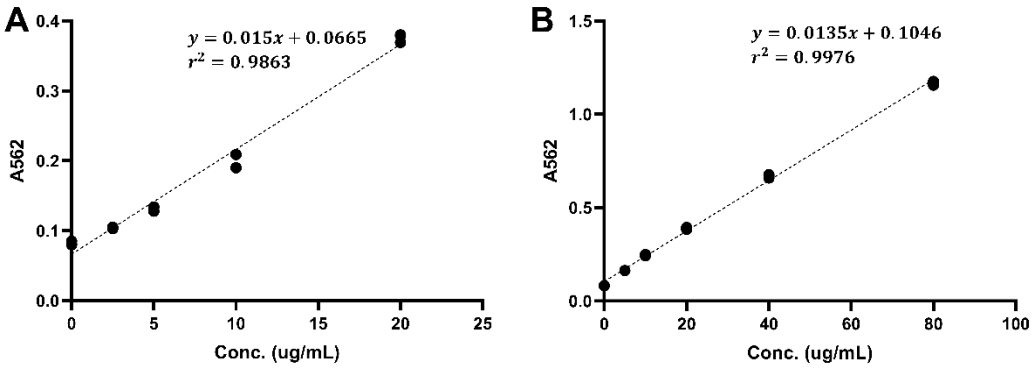

Figure 4.10. Standard curves of measuring total protein concentrations with BCA assay.
(A) Standard curve of biotin-Ab only. (B) Standard curve of poly-SA only.

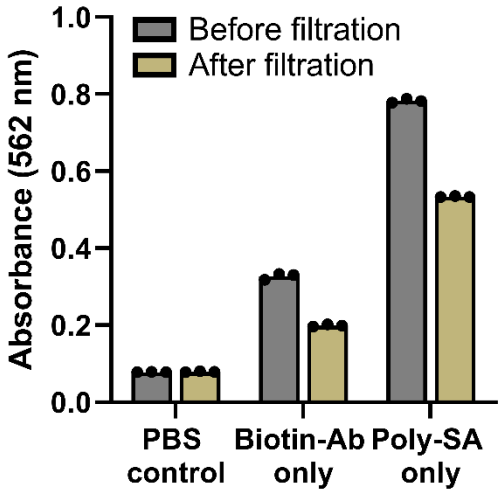

Figure 4.11. Filtration of non-agglutinated samples.
Total protein concentrations in samples of biotin-Ab only and poly-SA only were measured before and after filtration using the BCA assay. The filtrated flowthrough contained 51% and 63% of total proteins for biotin-Ab-only and poly-SA-only samples respectively, as quantified with the standard curves in **Figure 4.10**. The protein loss likely resulted from unspecific binding to the filter.

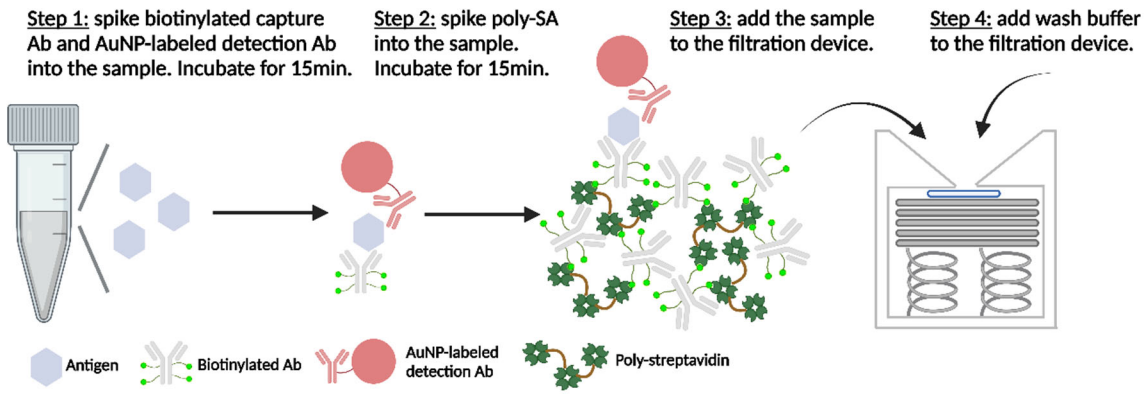

Figure 4.12. Workflow of the 50μL or 2mL agglutination assay using buffers spiked with antigens as the samples.

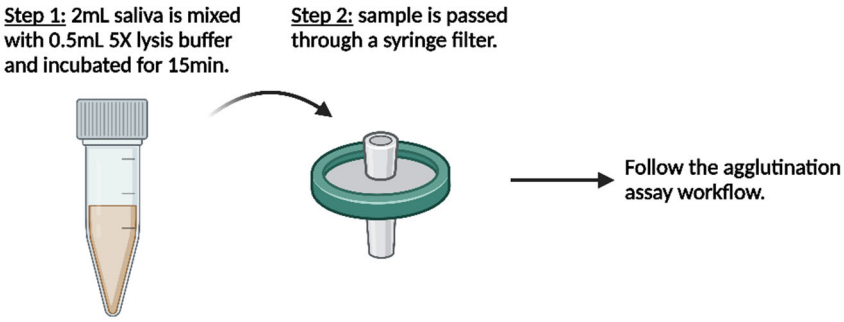

Figure 4.13. Workflow of testing the agglutination assay using 2mL saliva.
After the filtration (step 2), the sample goes through the workflow described in **Figure 4.12**.

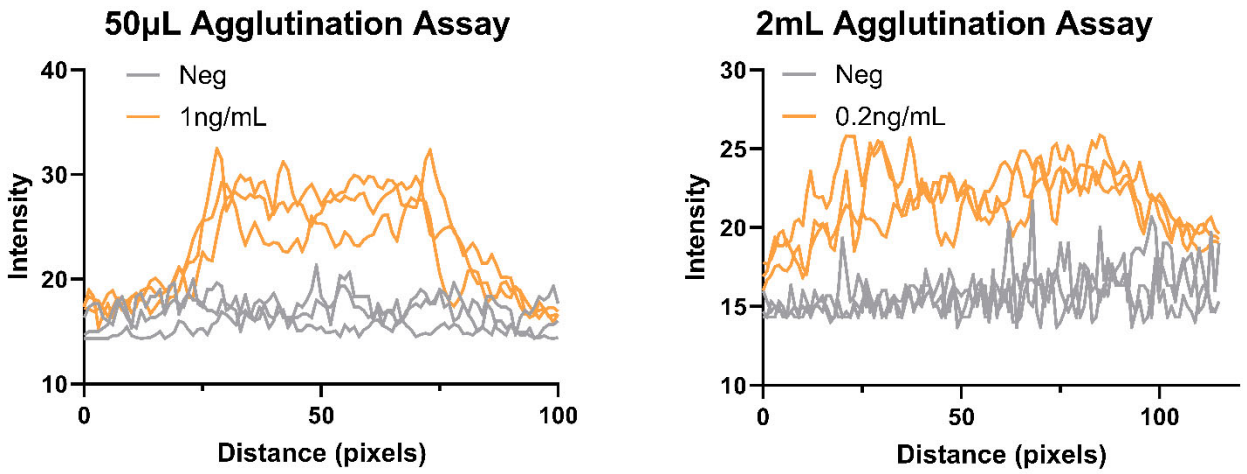

Figure 4.14. Line plots of the 50µL and 2mL agglutination assay results using ImageJ.

Only results of negative controls and highest antigen concentrations tested are plotted. For 50uL agglutination assays, a 100-pixel line through the center of the region of interest is drawn in ImageJ, and the intensity profile along the line without any background subtraction is plotted. For 2mL agglutination assays, the procedure is the same except a line of 115-pixel long is used to cover the whole area.

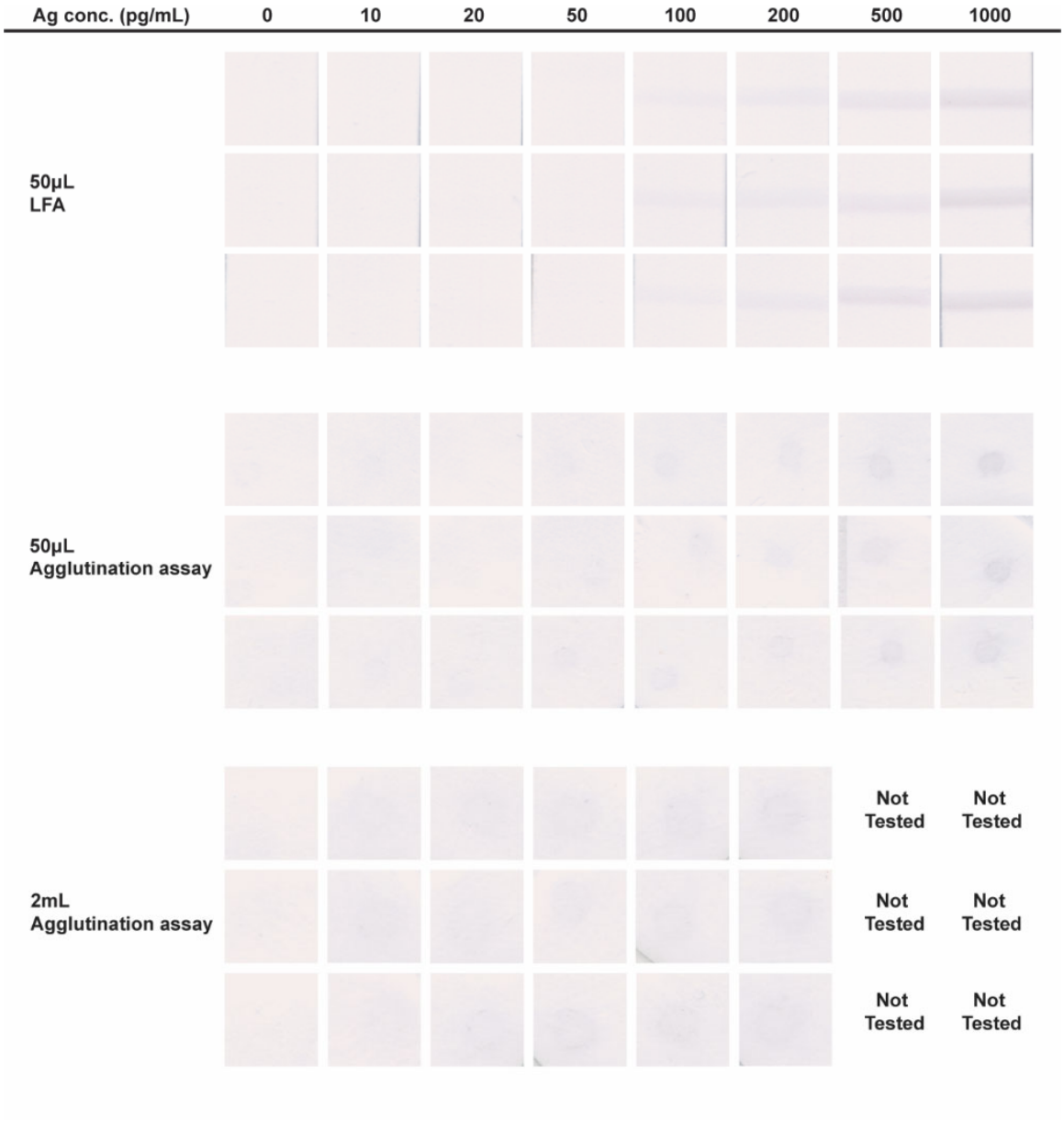

Figure 4.15. Scanned raw images of the signal regions for all three replicates in 50uL LFAs, 50uL agglutination assay, and 2mL agglutination assay.

No contrast added. N=3.

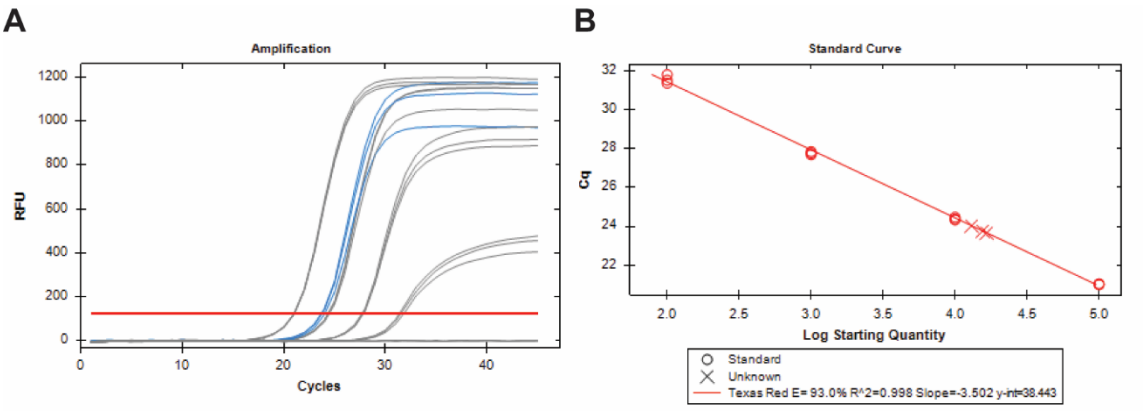

Figure 4.16. Quantification of the inactivated virus stock using rt-qPCR**.**

5uL of the inactivated virus stock was diluted to 140uL in PBS, followed by RNA extraction with QIAmp Viral RNA kits. 60uL eluted RNA was diluted 10-fold in water, and then 5uL was added to the InBios Smart Detect SARS-CoV-2 rRT-PCR kit for quantification. Synthetic SARS-CoV-2 RNA control from Twist Biosciences were used as the standards..

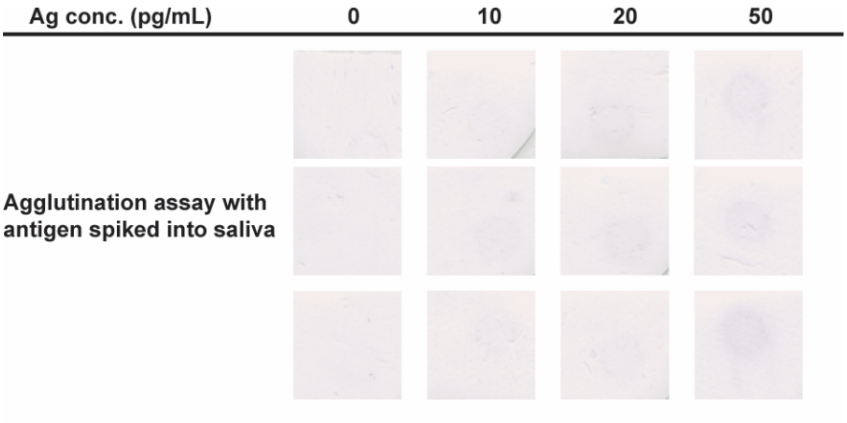

Figure 4.17. Scanned raw images of all replicates when testing the agglutination assay in saliva spiked with SARS-CoV-2 nucleocapsid antigen.
No contrast added. N=3.

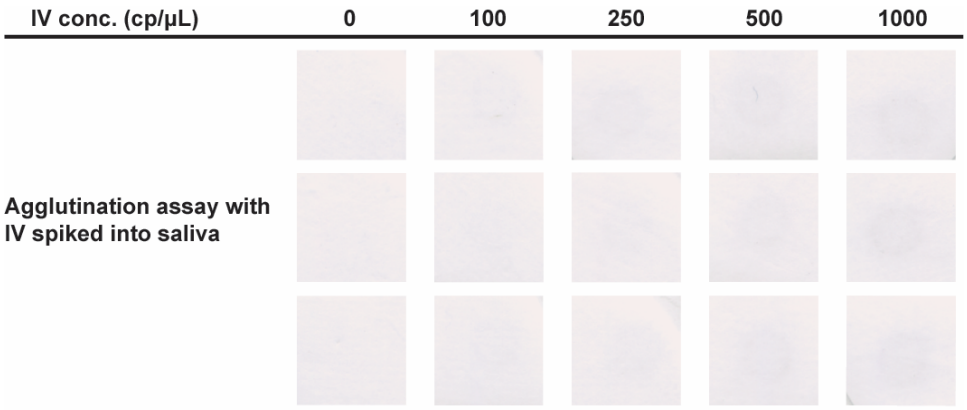

Figure 4.18. Scanned raw images of all replicates when testing the agglutination assay in saliva spiked with inactivated SARS-CoV-2.
No contrast added. N=3.

Chapter 5. Summary and Outlook

This chapter summarizes the thesis contributions and sketches potential directions for future work. Some thoughts in this chapter are not well developed but are included for future reference.

5.1 HIV Reverse Transcriptase Activity Assay

This section corresponds to the work described in Chapter 2.

5.1.1 **Summary of contributions**

In the context of sensitive point-of-care HIV tests, we have developed a sample-to-result workflow targeting the function of the reverse transcriptase encapsulated inside HIV virions, with a high sensitivity at 20 copies of recombinant HIV RT spiked into 25μL plasma. The workflow is simple to run and potentially suitable for low-resource settings, with antibody-coated magnetic beads for sample preparation, LAMP-based one-pot two-temperature HIV RT activity assay for amplification, and endpoint lateral flow assays for detection. In addition, we have developed a CRISPR-Cas-based HIV RT activity assay that only requires a single incubation temperature of 37°C. The quantitative readout of CRISPR-Cas detection enables the phenotypic characterization of HIV RT activity, with potential applications in therapeutic drug monitoring and HIV drug resistance testing. In addition, CRISPR-Cas detection is highly programmable and can be adapted to target other enzymes in other pathogens (e.g., DNA polymerase in hepatitis B virus that also has reverse transcription activity, RNA-dependent RNA polymerase in SARS-CoV-2 and hepatitis C virus). This approach could be used for pathogen detection, or in vitro studies of the enzymes and potentially drug development.

Developing point-of-care HIV tests is extremely challenging due to the demanding sensitivity requirement. The exploration towards the goal could trigger findings and tricks that may be helpful

to other applications in the field of molecular diagnostics. During the development of the one-pot LAMP-based HIV RT activity assay, we introduced the concept of dockers, short 3' blocked DNA oligos complementary to targeted primers, that could hybridize and sequester the matching primer at lower temperatures and release the primer at higher temperatures than the Tm. The concept of dockers could be applied in other multi-temperature reactions to minimize unwanted primer dimers at certain temperatures and avoid nonspecific amplifications. Additionally, we have validated an aptamer that could inhibit the activity of TFpol at 37°C, which is helpful in other applications using TFpol (e.g., avoid side reactions during reaction setup). In the sample-to-result workflow, we have shown that magnetic beads with captured HIV RT could be directly added to the assay without hurting assay performance, applicable in other bead-based workflows. The development of Cas-based HIV RT activity assay discovered several phenomena of Cas12a detection that may be interesting to the CRISPR-Cas community. Moreover, when adapting Cas12a for HIV integrase detection, we found that Cas12a could differentiate the disintegration substrate, where the whole target strand is included and only misses one phosphodiester bond at the disintegration site, from the disintegration product, where the disintegration site is linked by HIV IN, demonstrating the exceptional specificity of Cas12a detection (**Figure 2.7**). Since the substrate and product architecture are very similar to ligation, Cas12a could be used to detect ligation products in one pot (e.g., oligonucleotide ligation assay for detecting genetic mutations).

5.1.2 **Future assay development opportunities**

5.1.2.1 Sample preparation: Whole virus capture

The LAMP-based HIV RT activity assay demonstrated high sensitivity with recombinant HIV RT spiked into pooled HIV-negative plasma, but the assay with HIV-positive samples was not as sensitive as expected. One potential cause is the endogenous HIV antibody in HIV-positive plasma

that inhibits the capture of HIV RT or its cDNA generation activity. Sano K. *et al.* have found that 67% of HIV-seropositive individuals (33 of 49) produce an antibody that specifically targets the viral RT enzyme [95]. The current workflow lyses HIV viruses during the direct immunocapture step and exposes HIV RT to endogenous HIV antibodies. An alternative approach is to capture the whole virus through antibodies targeting viral surface antigen (e.g., gp40) or host cell markers (e.g., CD44), followed by virus lysis, to remove endogenous antibodies before releasing HIV RT. However, one risk with the whole virus capture approach is the potential heterogeneity of viral surface biomarkers which may affect the capture efficiency.

5.1.2.2 Sample preparation: Direct RT capture with aptamers

Various aptamers have been developed targeting HIV RT with strong binding affinities [146–148]. An alternative approach for sample preparation is direct HIV RT capture through aptamer-coated magnetic beads. Compared to antibody capture, using aptamers offers a few potential advantages. First, the captured HIV RT could be released from the aptamers by disrupting the secondary structures of aptamers (e.g., changing salt conditions) or strand displacement. Therefore, the potential inhibition of aptamers on HIV RT activity becomes irrelevant. Moreover, when integrating the workflow into a device, the ability to release the captured HIV RT adds more options to the device design. Second, since the inhibition of aptamers on HIV RT activity is irrelevant, multiple aptamers could be used simultaneously for HIV RT capture, potentially helping compete with endogenous HIV antibodies and improve robustness against mutated HIV RT. Lastly, aptamers have much lower costs compared to antibodies. However, the risk with aptamers is that they require certain buffer conditions to maintain the correct secondary structures, which limits the buffer options during sample preparation (e.g., HIV RT needs to be compatible with the buffer).

5.1.2.3 Increasing input sample volume to improve assay sensitivity

Since the HIV RT is captured and thereby concentrated before adding to the reaction, we could scale up the input sample volume to increase the number of HIV RT available for detection and improve assay sensitivity. It is reported that most (>85%) finger stick blood, when collected by trained personnel, could provide a volume over 150μL [149,150]. In addition, there are commercial blood collection devices that are user-friendly and able to collect over 500μL whole blood [104]. However, larger input sample volumes may pose the risk of false positives due to nonspecific capture of endogenous enzymes that also have reverse transcription activity.

5.2 Large-Volume RT-LAMP

This section corresponds to the work described in Chapter 3.

5.2.1 **Summary of contributions**

We have demonstrated that LAMP at large reaction volumes maintained the same performance as small volumes (~20μL). Nucleic acid amplification assays have typically been run at small volumes around 20μL, with the largest reaction volume reported in the literature at 100μL [110]. To our knowledge, this is the first time that LAMP is performed at volumes over 100μL. We found that LAMP at volumes up to 1mL and RT-LAMP at volumes up to 0.5mL (larger volumes were not tested in both cases) maintained the same amplification LoD as 20μL reactions. In addition, we demonstrated that the reagent cost, mostly from the proteins in the assay such as polymerases and RNase inhibitors, could be substantially reduced by using in-house or lower-cost reagents, making large-volume LAMP less impractical.

Isothermal amplification methods such as LAMP succeed from PCR where small volumes are necessary due to the need for rapid thermal cycling. However, isothermal amplification operating

at a single temperature removed the volume limit tied to thermal cycling. The large-volume LAMP approach provides a fresh perspective to the field of molecular diagnostics, demonstrating that reaction volumes of isothermal amplification assays (e.g., RPA, HDA, iSDA, etc.) could be expanded when necessary, such as accommodating more sample quantities including extracted DNA/RNA, providing a stronger signal readout, and diluting inhibitors in the sample.

In addition, our work echoed that sample dilution, a strategy often employed in reported extraction-free assays, could facilitate preserved assay LoD in the presence of crude samples. While the specific mechanisms by which different inhibitors affect nucleic acid amplification assays are not fully understood and likely vary case by case, dilution could be an effective strategy to mitigate the inhibitory effects of sample matrices, allowing the target nucleic acid amplification to outpace the inhibitory actions.

5.2.2 **Potential ways for further cost reduction**

As described in Chapter 3, the reagent cost for 500µL RT-LAMP is estimated to be $14.78, ~90% of which is from the RNase inhibitor and reverse transcriptase (RT). To further reduce the cost, both reagents could potentially be made in-house. Guo *et al.* developed a protocol for producing murine RNase inhibitors in *E. coli* with high solubility and thus high yield [117]. Oscorbin *et al.* demonstrated the in-house production of M-MuLV RT, the origin of most commercial RT, and its mutants including Superscript III and Superscript IV, which are the most popular RT [116]. Alekseenko *et al.* demonstrated the in-house production and application in a SARS-CoV-2 RT-LAMP assay of MashUp-RT, a reverse transcriptase developed by https://pipettejockey.com/ (a great and seemingly personal blog dedicated to reverse engineering methods and reagents for molecular biology) [57]. Work is also ongoing within our group to develop in-house reverse transcriptase.

In addition, we could potentially decrease the reverse transcriptase concentration in the assay to further reduce the cost. Since the assay demonstrated tolerance to GuSCN to some extent, GuSCN could be included in the assay, or mixed with the plasma sample at higher concentrations prior to being added to the assay and subsequently diluted, to further impede the activity of RNase in plasma. Since the reverse transcriptase acting on the RNA needed to outpace the RNase degrading the RNA, slowing down the RNase more may facilitate decreasing the reverse transcriptase concentration. Generally, the dilution strategy could be combined with simple and low-cost sample processing methods that could decrease the dilution factors or reagent concentrations required, to further bring down assay costs.

5.2.3 **Discussion: Do reaction volumes matter for nucleic acid amplification assays?**

Results in Chapter 3 showed that LAMP of reaction volumes up to 1mL maintained the same amplification LoD as typical 20μL reactions, suggesting that expanding reaction volumes does not affect assay LoD. However, most bulk reactions with microliter volumes could not achieve a LoD of 1 cp/rxn. In contrast, droplet digital LAMP, where each reaction operates at volumes from picoliters to nanoliters, demonstrates the ability to amplify a single copy of the target per reaction chamber for absolute quantification. This suggests that decreasing reaction volumes could improve assay LoD, which seems to disagree with the findings from large-volume LAMP. This section discusses how reaction volumes may affect the analytical performance of isothermal amplification assays. Answering this question not only helps guide the adoption of the large-volume-reaction approach but also offers insights on what may limit the sensitivity of a nucleic acid amplification assay when theoretically it should be able to detect a single copy of the target.

5.2.3.1 Competition between specific amplification and nonspecific reactions in the assay

The initiation of the specific target amplification relies on a series of events happening in the correct order: primers hybridizing with the target, reverse transcriptase or DNA polymerase binding the primer-target duplex, and the subsequent primer extension. Depending on the amplification machinery in different isothermal methods, the events may need to be repeated multiple times (e.g., both the forward and the reverse side), and additional events may be required (e.g., primers invading the double-stranded DNA in LAMP). While the assay designs should enable the execution of the events (e.g., primers are designed with melting temperatures well above reaction temperatures for target hybridization), the design criteria focus on equilibrium rather than kinetics (e.g., the melting temperatures of primers are derived from dissociation constants (K_d) at equilibrium of primer binding). Each event during the amplification initiation does not necessarily happen "right away" (e.g., the target sequence may first partially hybridize with a wrong primer and then dissociate as the partially hybridized duplex should not be stable at the reaction temperature, after which the target may hybridize with the right primer), which may lead to variance in the time that leads to successful amplification initiation. The variance may become more significant when the target copy number gets lower. Sun *et al.* monitored the single-molecule amplification in over 1000 wells in digital LAMP and found that the liftoff time among the wells ranges from 5 minutes to over 40 minutes [151]. The (potentially long) time for amplification initiation gives opportunities for nonspecific reactions in the assays.

Nonspecific reactions are unavoidable in nucleic acid amplification assays due to the large number of reagents. For example, the LAMP assay used in Chapter 3 includes ~0.8μM TFpol (DNA polymerase) and 0.6μM FIP and BIP (LAMP primers), which translates to 9.63e12 copies of TFpol and 7.22e12 copies of FIP and BIP in a 20μL reaction, compared to a few copies of targets. First,

the primers could form nonspecific dimers, even transiently, that could be subsequently extended. Second, the DNA polymerase or reverse transcriptase could have additional activities besides the specific templated synthesis, which may lead to unwanted products. For example, Bst polymerases are reported to have terminal transferase activity or template-independent synthesis, where the enzyme could add a few random bases to the 3' end of the substrate [111]. Lastly, the side products introduce new sequences into the system that could generate new rounds of nonspecific reactions. Unlike PCR where each cycle is gated by temperature controls, isothermal assays operate at constant temperatures and there are no stop signs for nonspecific reactions (i.e., nonspecific reactions are happening constantly in isothermal assays).

Therefore, there is competition between specific amplification and nonspecific reactions in nucleic acid amplification assays. When the nonspecific reactions can lead to exponential amplifications and thereby false positives, they compete for the amplification initiation "opportunities" with the specific amplification. In nucleic acid amplification assays, the earliest amplification initiation event, whether nonspecific or specific, is likely to dominate the subsequent reactions in the assay due to the exponential nature of the amplification. If the nonspecific exponential amplification happens to initiate first, then the specific amplification may not occur. Rolando J. C. *et al.* gradually decreased the target concentration in a LAMP reaction and used melting temperatures to differentiate nonspecific and specific amplifications [111]. They found that more false positives occurred at lower target concentrations (e.g., with 10cp/μL target, 1 out of 21 reactions showed false positives, while with 1cp/μL target, 18 out of 24 reactions showed false positives), which directly showed the competition between nonspecific and specific amplifications. When the nonspecific reactions could not lead to exponential amplification, they could still distract the machinery designed for specific amplification and therefore suppress the initiation. To name a few,

primer dimers could distract primers from binding the target (e.g., the Tm of primers is solely based on the equilibrium of primer-target binding, whereas the equilibrium is multi-state primer binding and should include other primer interactions). Primer dimers with extendable ends could distract the DNA polymerase from binding to the target. New products generated from the dimers could hybridize with the target without 3' templated ends (non-extendable). Although the probability of each nonspecific reaction is low in a well-designed assay, due to the large number of reagents, the incidence of nonspecific reactions could still be high to affect the initiation of the specific amplification.

5.2.3.2 Reaction volumes on assay LoD

When reaction volumes change but reagent concentrations stay the same, we hypothesize that the specific amplification may not be impacted since the target is essentially surrounded by the same environment. However, larger reaction volumes translate to higher numbers of reagents, which leads to increased competition from the nonspecific reactions on the specific amplification and may affect the assay LoD.

The competition from the nonspecific reactions may not increase linearly with the number of reagents. Therefore, the relationship between assay LoD and the reaction volume may not be linear and likely vary among assays (**Figure 5.1**). For example, it could be discrete (i.e., assay LoD may drop abruptly when reaction volumes increase to a tipping point). This could explain the discrepancy between maintained LoD when increasing reaction volumes from 20μL to 1mL (Chapter 3) and increased LoD from 1 cp/rxn in digital droplet assays (pL to nL volumes) to higher LoD in bulk reactions (μL volumes). Regardless, most nucleic acid amplification assays do not need to achieve a LoD of 1 cp/rxn, depending on the copy number of targets available in samples.

The reaction volume could still be expanded when helpful as long as the sensitivity meets the practical requirements.

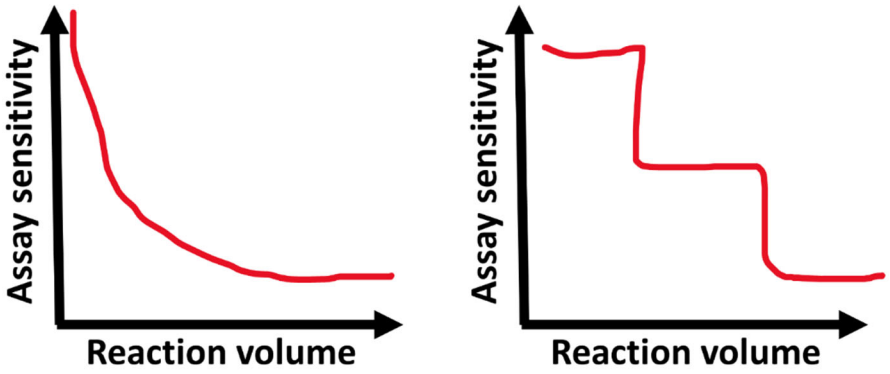

Figure 5.1. Guesses on relationships between the assay sensitivity and reaction volume. The relationship could be nonlinear (left) or discrete (right) and likely vary among assays.

5.2.3.3 Potential experiments for investigation

We hypothesize that the competition from nonspecific amplifications could be limiting the LoD of nucleic acid amplification assays. To investigate the hypothesis, since LAMP assays can amplify down to 1 cp/rxn at digital droplet volumes, we could gradually expand the reaction volume from nanoliters to microliters and observe how the assay LoD changes. When the LoD starts to increase (assay sensitivity starts to drop), the reaction could be sequenced or analyzed through gel electrophoresis to check if there are changes in side products. However, it may be difficult to manipulate droplet reactions. Alternatively, if there is an assay that demonstrates exceptional sensitivity (e.g., a single or a few copies per reaction) at bulk volumes (μL), we could keep expanding the reaction volume and track the LoD changes to find the tipping point. In summary, finding out at which point the reaction volume starts to affect assay LoD and fully scanning what has happened at that point could be a potential approach for investigation.

5.2.4 **Dilution-enabled extraction-free digital droplet assays**

We have shown that dilution can be effective in removing inhibition from sample matrices and maintaining the performance in extraction-free assays. The strategy of bypassing nucleic acid extraction and directly diluting samples in large-volume reactions is well suited for digital droplet assays where the total reaction is divided into nanoliter chambers and therefore the impact of reaction volumes on assay performance becomes irrelevant. For example, we found that 500μL RT-LAMP could dilute out the inhibition from 20μL plasma. Potentially, 20μL fingerstick plasma could be directly added to a 500μL RT-LAMP reaction, followed by standard digital LAMP workflow, for HIV viral load quantification. However, the increased total reaction volume requires a larger number of reaction chambers. If it becomes an issue in digital droplet platforms, the number of reaction chambers can be decreased (and the volume of each reaction chamber increases accordingly) as long as it meets the requirement of the quantification dynamic range. For example, for HIV viral load monitoring, exact quantification values may be less critical above 1000 cp/mL (unsuppressed) or below 50 cp/mL (undetectable), while a quantification range of 50-1000 cp/mL may be helpful for clinicians or regulatory purposes, translating to 1-20 copies of HIV RNA in 20μL fingerstick plasma (the 50-1000 cp/mL range is given as examples and may vary among different regions with different policies, but the point that exact viral load values become less critical when above and below certain thresholds should hold). Dividing the 500μL RT-LAMP into 20 reaction chambers may be adequate for quantifying 1-20 copies of HIV RNA targets. However, at a fixed total reaction volume required by sample dilution, decreasing the number of reaction chambers means increasing the volume of each reaction chamber, which may affect the 1 cp/rxn LoD in each chamber necessary for absolute quantification. Therefore, the experiment mentioned in section 5.2.3.3, determining the tipping point of reaction volumes where the LoD

starts to increase from 1 cp/rxn, could help set the volume requirement of each reaction chamber (and subsequently another limit for the number of reaction chambers). In summary, the large-volume approach suits digital droplet assays. The number of reaction chambers could be decreased as long as it meets the requirement of the quantification range, and the corresponding volume of each reaction chamber does not impact the 1 cp/rxn LoD.

5.3 Agglutination Assay

This section corresponds to the work described in Chapter 4.

We have developed a new agglutination system simply based on streptavidin-biotin interactions. The agglutination system relies on the multi-valency of streptavidin and multiple biotins per antibody. Through quantitative measurements, we have confirmed that an equal concentration ratio and higher valency of the agglutination components could facilitate agglutination. The SA-biotin-based agglutination is simple to build, as it only requires biotinylation of the antibody which is common in immunoassays. Unlike previously reported agglutination methods, the SA-biotin-based agglutination system is independent of target analyte concentrations and can thereby be applied in immunoassays to process large sample volumes and improve assay sensitivity. We have developed a COVID-19 agglutination assay that demonstrated enhanced sensitivity with increased input saliva sample volume. A similar strategy could be applied to other immunoassays when a larger sample volume is available.

The SA-biotin-based agglutination system has a few limitations. First, the agglutination process is irreversible due to the strong streptavidin-biotin interactions. Second, the number of biotins that can be conjugated to the antibody without affecting the antibody function is limited, thus affecting the valency of the biotin-Ab. Furthermore, some conjugated biotins may not be accessible due to steric hindrance. Future work could explore using DNA hybridization instead of streptavidin-

biotin interaction for agglutination. The DNA-hybridization-based agglutination could be used for nucleic acid capture or immunoassays when the DNA strands are conjugated to antibodies. The DNA-hybridization-based agglutination may offer a few advantages. First, the agglutination process is reversible, allowing the release of the captured product. Second, each DNA strand could have multiple hybridization regions for the other agglutination strand, increasing the binding valency. The distance between the hybridization regions could be controlled to minimize steric hindrance. Lastly, DNA hybridization allows the use of multiple agglutination pairs in one system. For example, strand A binds strand B, strand B binds strand C, and strand C binds strand A. It would be interesting to explore how the number of binding pairs and the concentration ratio of each pair would affect the agglutination process.

References

[1] World Health Organization, HIV and AIDS, (n.d.). https://www.who.int/news-room/fact-sheets/detail/hiv-aids (accessed October 11, 2023).

[2] L. Frescura, P. Godfrey-Faussett, A. Ali Feizzadeh, W. El-Sadr, O. Syarif, P.D. Ghys, S. Baptiste, M. Doherty, M. Dybul, J. Eaton, S. Eholie, J. Stover, S. Yotta, C. Fontaine, P. Ghys, J.A. Izazola, E. Lamontagne, I. Semini, Achieving the 95 95 95 targets for all: A pathway to ending AIDS, PLoS One. 17 (2022). https://doi.org/10.1371/journal.pone.0272405.

[3] B.S. Parekh, C.Y. Ou, P.N. Fonjungo, M.B. Kalou, E. Rottinghaus, A. Puren, H. Alexander, M.H. Cox, J.N. Nkengasong, Diagnosis of human immunodeficiency virus infection, Clin Microbiol Rev. 32 (2019). https://doi.org/10.1128/CMR.00064-18.

[4] World Health Organization, Consolidated guidelines on HIV testing services, 2019.

[5] P. Yager, G.J. Domingo, J. Gerdes, Point-of-care diagnostics for global health, Annu Rev Biomed Eng. 10 (2008) 107–144. https://doi.org/10.1146/annurev.bioeng.10.061807.160524.

[6] P. Patel, B. Bennett, T. Sullivan, M.M. Parker, J.D. Heffelfinger, P.S. Sullivan, Rapid HIV screening: missed opportunities for HIV diagnosis and prevention, Journal of Clinical Virology. 54 (2012) 42–47. https://doi.org/10.1016/j.jcv.2012.01.022.

[7] T.S. Alexander, Human immunodeficiency virus diagnostic testing: 30 years of evolution, Clinical and Vaccine Immunology. 23 (2016) 249–253. https://doi.org/10.1128/CVI.00053-16.

[8] I. v. Jani, B. Meggi, A. Vubil, N.E. Sitoe, N. Bhatt, O. Tobaiwa, J.I. Quevedo, O. Loquiha, J.D. Lehe, L. Vojnov, T.F. Peter, Evaluation of the whole-blood Alere Q NAT point-of-care RNA assay for HIV-1 viral load monitoring in a primary health care setting in Mozambique, J Clin Microbiol. 54 (2016) 2104–2108. https://doi.org/10.1128/JCM.00362-16.

[9] A. V. Ritchie, I. Ushiro-Lumb, D. Edemaga, H.A. Joshi, A. De Ruiter, E. Szumilin, I. Jendrulek, M. McGuire, N. Goel, P.I. Sharma, J.P. Allain, H.H. Lee, SAMBA HIV semiquantitative test, a new point-of-care viral-load-monitoring assay for resource-limited settings, J Clin Microbiol. 52 (2014) 3377–3383. https://doi.org/10.1128/JCM.00593-14.

[10] H.H. Lee, M.A. Dineva, Y.L. Chua, A. v. Ritchie, I. Ushiro-Lumb, C.A. Wisniewski, Simple amplification-based assay: a nucleic acid-based point-of-care platform for HIV-1 testing., J Infect Dis. 201 Suppl 1 (2010). https://doi.org/10.1086/650385.

[11] K. Steinmetzer, T. Seidel, A. Stallmach, E. Ermantraut, HIV load testing with small samples of whole blood, J Clin Microbiol. 48 (2010) 2786–2792. https://doi.org/10.1128/JCM.02276-09.

[12] S. Petralia, S. Conoci, PCR technologies for point of care testing: Progress and perspectives, ACS Sens. 2 (2017) 876–891. https://doi.org/10.1021/acssensors.7b00299.

[13] P.K. Drain, C. Rousseau, Point-of-care diagnostics: Extending the laboratory network to reach the last mile, Curr Opin HIV AIDS. 12 (2017) 175–181. https://doi.org/10.1097/COH.0000000000000351.

[14] J. Li, J. Macdonald, Advances in isothermal amplification: novel strategies inspired by biological processes, Biosens Bioelectron. 64 (2015) 196–211. https://doi.org/10.1016/J.BIOS.2014.08.069.

[15] N. Panpradist, E.C. Kline, R.G. Atkinson, M. Roller, Q. Wang, I.T. Hull, J.H. Kotnik, A.K. Oreskovic, C. Bennett, D. Leon, V. Lyon, S.D. Gilligan-Steinberg, P.D. Han, P.K. Drain, L.M. Starita, M.J. Thompson, B.R. Lutz, Harmony COVID-19: A ready-to-use kit, low-cost detector, and smartphone app for point-of-care SARS-CoV-2 RNA detection, Sci Adv. 7 (2021) 1281. https://www.science.org.

[16] C. Schrader, A. Schielke, L. Ellerbroek, R. Johne, PCR inhibitors - occurrence, properties and removal, J Appl Microbiol. 113 (2012) 1014–1026. https://doi.org/10.1111/j.1365-2672.2012.05384.x.

[17] N.B.Y. Tsui, E.K.O. Ng, Y.M. Dennis Lo, Stability of endogenous and added RNA in blood specimens, serum, and plasma, Clin Chem. 48 (2002) 1647–1653. https://academic.oup.com/clinchem/article/48/10/1647/5642225.

[18] Qiagen, QIAamp Viral RNA Mini Handbook, 2020.

[19] S.A. Byrnes, J.D. Bishop, L. Lafleur, J.R. Buser, B. Lutz, P. Yager, One-step purification and concentration of DNA in porous membranes for point-of-care applications, Lab Chip. 15 (2015) 2647–2659. https://doi.org/10.1039/c5lc00317b.

[20] J.F.C. Loo, H.C. Kwok, C.C.H. Leung, S.Y. Wu, I.L.G. Law, Y.K. Cheung, Y.Y. Cheung, M.L. Chin, P. Kwan, M. Hui, S.K. Kong, H.P. Ho, Sample-to-answer on molecular diagnosis of bacterial infection using integrated lab-on-a-disc, Biosens Bioelectron. 93 (2017) 212–219. https://doi.org/10.1016/j.bios.2016.09.001.

[21] K. Du, H. Cai, M. Park, T.A. Wall, M.A. Stott, K.J. Alfson, A. Griffiths, R. Carrion, J.L. Patterson, A.R. Hawkins, H. Schmidt, R.A. Mathies, Multiplexed efficient on-chip sample preparation and sensitive amplification-free detection of Ebola virus, Biosens Bioelectron. 91 (2017) 489–496. https://doi.org/10.1016/j.bios.2016.12.071.

[22] N. Li, Y. Lu, J. Cheng, Y. Xu, A self-contained and fully integrated fluidic cassette system for multiplex nucleic acid detection of bacteriuria, Lab Chip. 20 (2020) 384–393. https://doi.org/10.1039/c9lc00994a.

[23] M.N. Emaus, M. Varona, D.R. Eitzmann, S.-A. Hsieh, V.R. Zeger, J.L. Anderson, Nucleic acid extraction: Fundamentals of sample preparation methodologies, current advancements, and future endeavors, Trends in Analytical Chemistry. 130 (2020). https://doi.org/10.1016/j.trac.2020.115985.

[24] K.A. Curtis, D.L. Rudolph, S.M. Owen, Sequence-specific detection method for reverse transcription, loop-mediated isothermal amplification of HIV-1, J Med Virol. 81 (2009) 966–972. https://doi.org/10.1002/jmv.21490.

[25] G.L. Damhorst, C. Duarte-Guevara, W. Chen, T. Ghonge, B.T. Cunningham, R. Bashir, Smartphone-imaged HIV-1 reverse-transcription loop-mediated isothermal amplification (RT-LAMP) on a chip from whole blood, Engineering. 1 (2015) 324–335. https://doi.org/10.15302/J-ENG-2015072.

[26] R. Gurrala, Z. Lang, L. Shepherd, D. Davidson, E. Harrison, M. McClure, S. Kaye, C. Toumazou, G.S. Cooke, Novel pH sensing semiconductor for point-of-care detection of HIV-1 viremia, Sci Rep. 6 (2016). https://doi.org/10.1038/srep36000.

[27] H. Kong, W. Zhang, J. Yao, C. Li, R. Lu, Z. Guo, J. Li, C. Li, Y. Li, C. Zhang, L. Zhou, A RT-LAMP based hydrogen ion selective electrode sensing for effective detection HIV-1 RNA with high-sensitivity, Sens Actuators B Chem. 329 (2021). https://doi.org/10.1016/j.snb.2020.129118.

[28] K.A. Curtis, D. Morrison, D.L. Rudolph, A. Shankar, L.S.P. Bloomfield, W.M. Switzer, S.M. Owen, A multiplexed RT-LAMP assay for detection of group M HIV-1 in plasma or whole blood, J Virol Methods. 255 (2018) 91–97. https://doi.org/10.1016/j.jviromet.2018.02.012.

[29] W.-S. Hu, S.H. Hughes, HIV-1 reverse transcription, Cold Spring Harbor Perspective in Medicine. 2 (2012). https://doi.org/10.1101/cshperspect.a006882.

[30] S.P. Layne, M. 1 Merges, M. Dembo, J.L. Spouge, S.R. Conleyj, J.P. Moore, J.L. Raina, H. Renz, H.R. Gelderblom, P.L. Narat, Factors Underlying Spontaneous Inactivation and Susceptibility to Neutralization of Human lmmunodeficiency Virus, 1992.

[31] A.D. Hoffman, B. Banapour, J.A. Levy', Characterization of the AIDS-Associated Retrovirus Reverse Transcriptase and Optimal Conditions for Its Detection in Virions, 1985.

[32] M.H. Lee, K. Sano, F.E. Morales, D.T. Imagawa, Sensitive Reverse Transcriptase Assay To Detect and Quantitate Human Immunodeficiency Virus, 1987.

[33] M. Neumuller, Karlstrom AR., CF. Kallander, JS. Gronowitz, Improved assays for DNA-polymerizing enzymes by the use of enzymatically synthesized 5-[125I]iodo-2'-deoxyuridine triphosphate, illustrated by direct quantitation of anti-HIV reverse transcriptase antibody and by serum DNA polymerase analyses, Biotechnol Appl Biochem. 12 (1990) 34–56.

[34] K. Suzuki, B.P. Craddock, N. Okamoto, T. Kanoa, R.T. Steigbigel, Poly A-linked calorimetric microtiter plate assay for HIV reverse transcriptase, J Virol Methods. 44 (1993).

[35] J. Eberle, R. Seiblb, A new method for measuring reverse transcriptase activity by ELISA, J Virol Methods. 40 (1992) 341–356.

[36] A. Malmsten, X.-W. Shao, S. Sjödahl, E.-L. Fredriksson, I. Pettersson, T. Leitner, C.F.R. Källander, E. Sandström, J.S. Gronowitz, Improved HIV-1 viral load determination based on

reverse transcriptase activity recovered from human plasma, J Med Virol. 76 (2005) 291–296. https://doi.org/10.1002/jmv.20360.

[37] W. Heneine, S. Yamamoto, W.M. Switzer, T.J. Spira, T.M. Folks, Detection of reverse transcriptase by a highly sensitive assay in sera from persons infected with human immunodeficiency virus type 1, J Infect Dis. 171 (1995) 1210–1216.

[38] H. Pyra, J. Boni, J. Schupbach, Ultrasensitive retrovirus detection by a reverse transcriptase assay based on product enhancement, Proc. Natl. Acad. Sci. USA. 91 (1994) 1544–1548.

[39] P. Burgisser, P. Vernazza, M. Flepp, J. Boni, Z. Tomasik, U. Hummel, G. Pantaleo, J. Schupbach, Swiss HIV Cohort Study, Performance of five different assays for the quantification of viral load in persons infected with various subtypes of HIV-1, J Acquir Immune Defic Syndr (1988). 23 (2000) 138–144.

[40] J.G.G. Lerma, S. Yamamoto, M. Gomez-Cano, V. Soriano, T.A. Green, M.P. Busch, T.M. Folks, W. Heneine, Measurement of human immunodeficiency virus type 1 plasma virus load based on reverse transcriptase (RT) activity: evidence of variabilities in levels of virion-associated RT, J Infect Dis. 177 (1998) 1221–1229. https://academic.oup.com/jid/article/177/5/1221/803648 (accessed April 20, 2023).

[41] J.G.G. Lerma, V. Soriano, A. Mas, M.E. Quinones-Mateu, E.J. Arts, W. Heneine, Quantitation of human immunodeficiency virus type 1 group O load in plasma by measuring reverse transcriptase activity, J Clin Microbiol. 38 (2000) 402–405. http://jcm.asm.org/ (accessed May 6, 2021).

[42] G. Vázquez-Rosales, J.G.G. Lerma, S. Yamamoto, W.M. Switzer, D. Havlir, T.M. Folks, D.D. Richman, W. Heneine, Rapid screening of phenotypic resistance to nevirapine by direct analysis of HIV type 1 reverse transcriptase activity in plasma, AIDS Res Hum Retroviruses. 15 (1999) 1191–1200. www.liebertpub.com (accessed June 1, 2021).

[43] J.G.G. Lerma, R.F. Schinazi, A.S. Juodawlkis, V. Soriano, Y. Lin, K. Tatti, D. Rimland, T.M. Folks, W. Heneine, A rapid non-culture-based assay for clinical monitoring of phenotypic resistance of human immunodeficiency virus type 1 to lamivudine (3TC), Antimicrob Agents Chemother. 43 (1999) 264–270.

[44] F. Marino-Merlo, B. Macchi, D. Armenia, M.C. Bellocchi, F. Ceccherini-Silberstein, A. Mastino, S. Grelli, Focus on recently developed assays for detection of resistance/sensitivity to reverse transcriptase inhibitors, Appl Microbiol Biotechnol. (2018) 9925–9936. https://doi.org/10.1007/s00253-018-9390-x.

[45] D. Hoffmann, A.D. Garcia, P.R. Harrigan, I.C.D. Johnston, T. Nakasone, J.G. García-Lerma, W. Heneine, Measuring enzymatic HIV-1 susceptibility to two reverse transcriptase inhibitors as a rapid and simple approach to HIV-1 drug-resistance testing, PLoS One. 6 (2011). https://doi.org/10.1371/journal.pone.0022019.

[46] F.M. Walker, K. Hsieh, Advances in directly amplifying nucleic acids from complex samples, Biosensors (Basel). 9 (2019). https://doi.org/10.3390/bios9040117.

[47] A.T. Bender, B.P. Sullivan, L. Lillis, J.D. Posner, Enzymatic and chemical-based methods to inactivate endogenous blood ribonucleases for nucleic acid diagnostics, The Journal of Molecular Diagnostics. 22 (2020) 1030–1040. https://doi.org/10.1016/j.jmoldx.2020.04.211.

[48] S. Kemleu, D. Guelig, C.E. Moukoko, E. Essangui, S. Diesburg, A. Mouliom, B. Melingui, J. Manga, C. Donkeu, A. Epote, G. Texier, P. LaBarre, R. Burton, L. Ayong, A field-tailored reverse transcription loop- mediated isothermal assay for high sensitivity detection of Plasmodium falciparum infections, PLoS One. 11 (2016). https://doi.org/10.1371/journal.pone.0165506.

[49] L.L.M. Poon, B.W.Y. Wong, E.H.T. Ma, K.H. Chan, L.M.C. Chow, W. Abeyewickreme, N. Tangpukdee, K.Y. Yuen, Guan Yi, S. Looareesuwan, J.S.M. Peiris, H.G. Huang, Sensitive and inexpensive molecular test for Falciparum Malaria: Detecting Plasmodium falciparum DNA directly from heat-treated blood by loop-mediated isothermal amplification, Clin Chem. 52 (2006). https://doi.org/10.1373/clinchem.2005.057893.

[50] Y. Mori, K. Nagamine, N. Tomita, T. Notomi, Detection of loop-mediated isothermal amplification reaction by turbidity derived from magnesium pyrophosphate formation, Biochem Biophys Res Commun. 289 (2001) 150–154. https://doi.org/10.1006/bbrc.2001.5921.

[51] M. Sidstedt, J. Hedman, E.L. Romsos, L. Waitara, L. Wadsö, C.R. Steffen, P.M. Vallone, P. Rådström, Inhibition mechanisms of hemoglobin, immunoglobulin G, and whole blood in digital and real-time PCR, Anal Bioanal Chem. 410 (2018) 2569–2583. https://doi.org/10.1007/s00216-018-0931-z.

[52] N.A. Tanner, Y. Zhang, T.C. Evans, Visual detection of isothermal nucleic acid amplification using pH-sensitive dyes, Biotechniques. 58 (2015) 59–68. https://doi.org/10.2144/000114253.

[53] B.R. Bista, C. Ishwad, R.M. Wadowsky, P. Manna, P.S. Randhawa, G. Gupta, M. Adhikari, R. Tyagi, G. Gasper, A. Vats, Development of a loop-mediated isothermal amplification assay for rapid detection of BK Virus, J Clin Microbiol. 45 (2007) 1581–1587. https://doi.org/10.1128/JCM.01024-06.

[54] A. Priye, S.W. Bird, Y.K. Light, C.S. Ball, O.A. Negrete, R.J. Meagher, A smartphone-based diagnostic platform for rapid detection of Zika, chikungunya, and dengue viruses, Sci Rep. 7 (2017). https://doi.org/10.1038/srep44778.

[55] B.A. Rabe, C. Cepko, SARS-CoV-2 detection using isothermal amplification and a rapid, inexpensive protocol for sample inactivation and purification, P.N.A.S. 117 (2020) 24450–24458. https://doi.org/10.1073/pnas.2011221117/-/DCSupplemental.

[56] E.C. Kline, N. Panpradist, I.T. Hull, Q. Wang, A.K. Oreskovic, P.D. Han, L.M. Starita, B.R. Lutz, Multiplex target-redundant RT-LAMP for robust detection of SARS-CoV-2 using

fluorescent universal displacement probes, Microbiol Spectr. 10 (2022). https://doi.org/10.1128/spectrum.01583-21.

[57] A. Alekseenko, D. Barrett, Y. Pareja-Sanchez, R.J. Howard, E. Strandback, H. Ampah-Korsah, U. Rovšnik, S. Zuniga-Veliz, A. Klenov, J. Malloo, S. Ye, X. Liu, B. Reinius, S.J. Elsässer, T. Nyman, G. Sandh, X. Yin, V. Pelechano, Direct detection of SARS-CoV-2 using non-commercial RT-LAMP reagents on heat-inactivated samples, Sci Rep. 11 (2021) 1820. https://doi.org/10.1038/s41598-020-80352-8.

[58] World Health Organization, WHO Coronavirus (COVID-19) Dashboard, (n.d.).

[59] M. Fisher, C. Sang-Hun, How South Korea flattened the curve, The New York Times. (2020).

[60] G.C. Mak, P.K. Cheng, S.S. Lau, K.K. Wong, C.S. Lau, E.T. Lam, R.C. Chan, D.N. Tsang, Evaluation of rapid antigen test for detection of SARS-CoV-2 virus, Journal of Clinical Virology. 129 (2020). https://doi.org/10.1016/j.jcv.2020.104500.

[61] V.M. Corman, V.C. Haage, T. Bleicker, M.L. Schmidt, B. Mühlemann, M. Zuchowski, W.K. Jo, P. Tscheak, E. Möncke-Buchner, M.A. Müller, A. Krumbholz, J.F. Drexler, C. Drosten, Comparison of seven commercial SARS-CoV-2 rapid point-of-care antigen tests: a single-centre laboratory evaluation study, Lancet Microbe. 2 (2021) e311–e319. https://doi.org/10.1016/S2666-5247(21)00056-2.

[62] B.D. Grant, C.E. Anderson, J.R. Williford, L.F. Alonzo, V.A. Glukhova, D.S. Boyle, B.H. Weigl, K.P. Nichols, SARS-CoV - 2 Coronavirus Nucleocapsid Antigen-Detecting Half-Strip Lateral Flow Assay Toward the Development of Point of Care Tests Using Commercially Available Reagents, Anal Chem. 92 (2020) 11305–11309. https://doi.org/10.1021/acs.analchem.0c01975.

[63] A.J. Jamal, M. Mozafarihashjin, E. Coomes, J. Powis, A.X. Li, A. Paterson, S. Anceva-Sami, S. Barati, G. Crowl, A. Faheem, L. Farooqi, S. Khan, K. Prost, S. Poutanen, M. Taylor, L. Yip, X.Z. Zhong, A.J. Mcgeer, S. Mubareka, Sensitivity of Nasopharyngeal Swabs and Saliva for the Detection of Severe Acute Respiratory Syndrome Coronavirus 2, Clinical Infectious Diseases. 72 (2021) 1064–1066. https://doi.org/10.1093/cid/ciaa848.

[64] S.Y. Chen, A.Y. Wu, R. Lunde, J.J. Lai, Osmotic Processor for Enabling Sensitive and Rapid Biomarker Detection via Lateral Flow Assays, Front Bioeng Biotechnol. 10 (2022). https://doi.org/10.3389/fbioe.2022.884271.

[65] C. Kim, Y.K. Yoo, S. il Han, J. Lee, D. Lee, K. Lee, K.S. Hwang, K.H. Lee, S. Chung, J.H. Lee, Battery operated preconcentration-assisted lateral flow assay, Lab Chip. 17 (2017) 2451–2458. https://doi.org/10.1039/c7lc00036g.

[66] R.Y.T. Chiu, A. v. Thach, C.M. Wu, B.M. Wu, D.T. Kamei, An Aqueous Two-Phase System for the Concentration and Extraction of Proteins from the Interface for Detection Using

the Lateral-Flow Immunoassay, PLoS One. 10 (2015). https://doi.org/10.1371/journal.pone.0142654.

[67] B.Y. Moghadam, K.T. Connelly, J.D. Posner, Two Orders of Magnitude Improvement in Detection Limit of Lateral Flow Assays Using Isotachophoresis, Anal Chem. 87 (2015) 1009–1017. https://doi.org/10.1021/ac504552r.

[68] A.L. Golden, C.F. Battrell, S. Pennell, A.S. Hoffman, J.J. Lai, P.S. Stayton, Simple Fluidic System for Purifying and Concentrating Diagnostic Biomarkers Using Stimuli-Responsive Antibody Conjugates and Membranes, Bioconjug Chem. 21 (2010) 1820–1826. https://doi.org/10.1021/bc100169y.

[69] S.H. Tan, O. Allicock, M. Armstrong-Hough, A.L. Wyllie, Saliva as a gold-standard sample for SARS-CoV-2 detection, Lancet Respir Med. 9 (2021) 562–564. https://doi.org/10.1016/S2213-2600(21)00178-8.

[70] L.A. Olopoenia, A.L. King, Widal Agglutination Test - 100 years later: still plagued by controversy, Postgrad Med J. 76 (2000) 80–84. https://doi.org/10.1136/pmj.76.892.80.

[71] A. Mujahid, F.L. Dickert, Blood Group Typing: From Classical Strategies to the Application of Synthetic Antibodies Generated by Molecular Imprinting, Sensors. 16 (2016). https://doi.org/10.3390/s16010051.

[72] A.J. Eisfeld, G. Neumann, Y. Kawaoka, Influenza A virus isolation, culture and identification, Nature Protocol. 9 (2014) 2663–2681. https://doi.org/10.1038/nprot.2014.180.

[73] V. Kesarwani, J.A. Walker, E.C. Henderson, G. Huynh, H. McLiesh, M. Graham, M. Wieringa, M.M.B. Holl, G. Garnier, S.R. Corrie, Column Agglutination Assay Using Polystyrene Microbeads for Rapid Detection of Antibodies against SARS-CoV-2, ACS Appl Mater Interfaces. 14 (2022) 2501–2509. https://doi.org/10.1021/acsami.1c17859.

[74] R.W. Ellis, M.A. Sobanski, Diagnostic particle agglutination using ultrasound: a new technology to rejuvenate old microbiological methods, J Med Microbiol. 49 (2000) 853–859.

[75] C.J.G. Cruz, R. Kil, S. Wong, L.C. Dacquay, D. Mirano-Bascos, P.T. Rivera, D.R. McMillen, Malarial Antibody Detection with an Engineered Yeast Agglutination Assay, ACS Synth Biol. 11 (2022) 2938–2946. https://doi.org/10.1021/acssynbio.2c00160.

[76] N. Kylilis, P. Riangrungroj, H.-E. Lai, V. Salema, L.A. Fernández, G.-B. V. Stan, P.S. Freemont, K.M. Polizzi, Whole-Cell Biosensor with Tunable Limit of Detection Enables Low-Cost Agglutination Assays for Medical Diagnostic Applications, ACS Sens. 4 (2019) 370–378. https://doi.org/10.1021/acssensors.8b01163.

[77] X.-W. Shao, A. Malmsten, J. Lennerstrand, A. Sönnerborg D, T. Unge, S.J. Gronowitz, C.F.R. Källander, Use of HIV-1 reverse transcriptase recovered from human plasma for phenotypic drug susceptibility testing, AIDS. 17 (2003) 1463–1471. https://doi.org/10.1097/01.aids.0000072670.21517.0d.

[78] S.P. Layne, M.J. Merges, M. Dembo, J.L. Spouge, S.R. Conley, J.P. Moore, J.L. Raina, H. Renz, H.R. Gelderblom, P.L. Nara, Factors underlying spontaneous inactivation and susceptibility to neutralization of human immunodeficiency virus, Virology. 189 (1992) 695–714.

[79] T. Notomi, H. Okayama, H. Masubuchi, T. Yonekawa, K. Watanabe, N. Amino, T. Hase, Loop-mediated isothermal amplification of DNA, Nucleic Acids Res. 28 (2000) 63.

[80] C. Myhrvold, C.A. Freije, J.S. Gootenberg, O.O. Abudayyeh, H.C. Metsky, A.F. Durbin, M.J. Kellner, A.L. Tan, L.M. Paul, L.A. Parham, K.F. Garcia, K.G. Barnes, B. Chak, A. Mondini, M.L. Nogueira, S. Isern, S.F. Michael, I. Lorenzana, N.L. Yozwiak, B.L. MacInnis, I. Bosch, L. Gehrke, F. Zhang, P.C. Sabeti, Field-deployable viral diagnostics using CRISPR-Cas13, Science (1979). 360 (2018) 444–448. https://www.science.org.

[81] J.S. Chen, E. Ma, L.B. Harrington, M. Da Costa, X. Tian, J.M. Palefsky, J.A. Doudna, CRISPR-Cas12a target binding unleashes indiscriminate single-stranded DNase activity, Science (1979). 360 (2018) 436–439.

[82] O.O. Abudayyeh, J.S. Gootenberg, CRISPR diagnostics, Science (1979). 372 (2021) 914–915.

[83] M.M. Kaminski, O.O. Abudayyeh, J.S. Gootenberg, F. Zhang, J.J. Collins, CRISPR-based diagnostics, Nat Biomed Eng. 5 (2021) 643–656. https://doi.org/10.1038/s41551-021-00760-7.

[84] S. Yamamoto, T.M. Folks, W. Heneine, Highly sensitive qualitative and quantitative detection of reverse transcriptase activity: optimization, validation, and comparative analysis with other detection systems, J Virol Methods. 61 (1996) 135–143. https://doi.org/10.1016/0166-0934(96)02078-2.

[85] M.D. Jones, N.S. Foulkes, Reverse transcription of mRNA by Thermus aquaticus DNA polymerase, Nucleic Acids Res. 17 (1989) 8387–8388.

[86] G. Divita, U. Immendorfer, M. Gautel, K. Rittinger, T. Restle, R.S. Goody, Kinetics of interaction of HIV reverse transcriptase with primer/template, Biochemistry. 32 (1993) 7966–7971. https://pubs.acs.org/sharingguidelines (accessed January 30, 2020).

[87] C. Shi, X. Shen, S. Niu, C. Ma, Innate reverse transcriptase activity of DNA polymerase for isothermal RNA direct detection, J Am Chem Soc. 137 (2015) 13804–13806. https://doi.org/10.1021/jacs.5b08144.

[88] C. Dang, S.D. Jayasena, Oligonucleotide inhibitors of Taq DNA polymerase facilitate detection of low copy number targets by PCR, J Mol Biol. 264 (1996) 268–278. https://doi.org/10.1006/JMBI.1996.0640.

[89] Y. Lin, S.D. Jayasena, Inhibition of multiple thermostable DNA polymerases by a heterodimeric aptamer, J Mol Biol. 271 (1997) 100–111. https://doi.org/10.1006/JMBI.1997.1165.

[90] T.L. Dangerfield, I. Paik, S. Bhadra, K.A. Johnson, A.D. Ellington, Kinetics of elementary steps in loop-mediated isothermal amplification (LAMP) show that strand invasion during

initiation is rate-limiting, Nucleic Acids Res. 51 (2023) 488–499. https://doi.org/10.1093/nar/gkac1221.

[91] A. Chang, J.M. Ostrove, R.E. Bird, Development of an improved product enhanced reverse transcriptase assay, J Virol Methods. 65 (1997) 45–54. https://doi.org/10.1016/S0166-0934(96)02168-4.

[92] Y. Chen, N. Cheng, Y. Xu, K. Huang, Y. Luo, W. Xu, Point-of-care and visual detection of P. aeruginosa and its toxin genes by multiple LAMP and lateral flow nucleic acid biosensor, Biosens Bioelectron. 81 (2016) 317–323. https://doi.org/10.1016/j.bios.2016.03.006.

[93] P. Mikel, P. Vasickova, R. Tesarik, H. Malenovska, P. Kulich, T. Vesely, P. Kralik, Preparation of MS2 phage-like particles and their use as potential process control viruses for detection and quantification of enteric RNA viruses in different matrices, Front Microbiol. 7 (2016). https://doi.org/10.3389/fmicb.2016.01911.

[94] N. Panpradist, Q. Wang, P.S. Ruth, J.H. Kotnik, A.K. Oreskovic, A. Miller, S.W.A. Stewart, J. Vrana, P.D. Han, I.A. Beck, L.M. Starita, L.M. Frenkel, B.R. Lutz, Simpler and faster Covid-19 testing: strategies to streamline SARS-CoV-2 molecular assays, EBioMedicine. 64 (2021). https://doi.org/10.1016/j.ebiom.2021.103236.

[95] K. Sano, M.H. Lee, F. Morales, P. Nishanian, J. Fahey, R. Detels, D.T. Imagawa, Antibody that inhibits human immunodeficiency virus reverse transcriptase and association with inability to isolate virus, J Clin Microbiol. 25 (1987) 2415–2417. http://jcm.asm.org/ (accessed February 18, 2020).

[96] J.C. Phan, B.J. Nehilla, S. Srinivasan, R.W. Coombs, K.A. Woodrow, J.J. Lai, Human immunodeficiency virus (HIV) separation and enrichment via the combination of antiviral lectin recognition and a thermoresponsive reagent system, Pharm Res. 33 (2016) 2411–2420. https://doi.org/10.1007/S11095-016-1980-7/METRICS.

[97] L.T. Nguyen, B.M. Smith, P.K. Jain, Enhancement of trans-cleavage activity of Cas12a with engineered crRNA enables amplified nucleic acid detection, Nat Commun. 11 (2020). https://doi.org/10.1038/s41467-020-18615-1.

[98] P. Fozouni, S. Son, M. Díaz de León Derby, G.J. Knott, C.N. Gray, M. V. D'Ambrosio, C. Zhao, N.A. Switz, G.R. Kumar, S.I. Stephens, D. Boehm, C.L. Tsou, J. Shu, A. Bhuiya, M. Armstrong, A.R. Harris, P.Y. Chen, J.M. Osterloh, A. Meyer-Franke, B. Joehnk, K. Walcott, A. Sil, C. Langelier, K.S. Pollard, E.D. Crawford, A.S. Puschnik, M. Phelps, A. Kistler, J.L. DeRisi, J.A. Doudna, D.A. Fletcher, M. Ott, Amplification-free detection of SARS-CoV-2 with CRISPR-Cas13a and mobile phone microscopy, Cell. 184 (2021) 323–333. https://doi.org/10.1016/j.cell.2020.12.001.

[99] Y. Liu, L. Zhan, Z. Qin, J. Sackrison, J.C. Bischof, Ultrasensitive and highly specific lateral flow assays for point-of-care diagnosis, ACS Nano. 15 (2021) 3593–3611. https://doi.org/10.1021/acsnano.0c10035.

[100] J.S. Gootenberg, O.O. Abudayyeh, M.J. Kellner, J. Joung, J.J. Collins, F. Zhang, Multiplexed and portable nucleic acid detection platform with Cas13, Cas12a, and Csm6, Science (1979). 360 (2018) 439–444. http://science.sciencemag.org/ (accessed June 7, 2021).

[101] A.O. Olanrewaju, B.P. Sullivan, A.H. Gim, C.A. Craig, D. Sevenler, A.T. Bender, P.K. Drain, J.D. Posner, REverSe TRanscrIptase chain termination (RESTRICT) for selective measurement of nucleotide analogs used in HIV care and prevention, Bioeng Transl Med. 8 (2023). https://doi.org/10.1002/btm2.10369.

[102] C.A.B. Boucher, N. Cammack, P. Schipper, R. Schuurman, P. Rouse, M.A. Wainberg, J.M. Cameron, High-Level resistance to (-) enantiomeric 2'-deoxy-3'-thiacytidine in vitro is due to one amino acid substitution in the catalytic site of human immunodeficiency virus type 1 reverse transcriptase, Antimicrob Agents Chemother. 37 (1993) 2231–2234. https://journals.asm.org/journal/aac.

[103] J. Deval, K.L. White, M.D. Miller, N.T. Parkin, J. Courcambeck, P. Halfon, B. Selmi, J. Boretto, B. Canard, Mechanistic basis for reduced viral and enzymatic fitness of HIV-1 reverse transcriptase containing both K65R and M184V Mutations, J Biol Chem. 279 (2004) 509–516. https://doi.org/10.1074/jbc.M308806200.

[104] C.A. Cannon, M.S. Ramchandani, M.R. Golden, Feasibility of a novel self-collection method for blood samples and its acceptability for future home-based PrEP monitoring, BMC Infect Dis. 22 (2022). https://doi.org/10.1186/s12879-022-07432-0.

[105] R. Craigie, F.D. Bushman, HIV DNA integration, Cold Spring Harb Perspect Med. 2 (2012).

[106] R. Craigie, The molecular biology of HIV integrase, Future Virol. 7 (2012) 679–686. https://doi.org/10.2217/fvl.12.56.

[107] T.L. Diamond, F.D. Bushman, Role of metal ions in catalysis by HIV integrase analyzed using a quantitative PCR disintegration assay, Nucleic Acids Res. 34 (2006) 6116–6125. https://doi.org/10.1093/nar/gkl862.

[108] S.A. Chow, K.A. Vincent, V. Ellison, P.O. Brown, Reversal of integration and DNA splicing mediated by integrase of human immunodeficiency virus, Science (1979). 255 (1992) 723–726.

[109] T.J. Moehling, G. Choi, L.C. Dugan, M. Salit, R.J. Meagher, LAMP diagnostics at the point-of-care: Emerging trends and perspectives for the developer community, Expert Rev Mol Diagn. 21 (2021) 43–61. https://doi.org/10.1080/14737159.2021.1873769.

[110] K.A. Curtis, D.L. Rudolph, S.M. Owen, Rapid detection of HIV-1 by reverse-transcription, loop-mediated isothermal amplification (RT-LAMP), J Virol Methods. 151 (2008) 264–270. https://doi.org/10.1016/J.JVIROMET.2008.04.011.

[111] J.C. Rolando, E. Jue, J.T. Barlow, R.F. Ismagilov, Real-time kinetics and high-resolution melt curves in single-molecule digital LAMP to differentiate and study specific and non-specific amplification, Nucleic Acids Res. 48 (2021). https://doi.org/10.1093/NAR/GKAA099.

[112] J. Qian, S.A. Boswell, C. Chidley, Z. Lu, M.E. Pettit, B.L. Gaudio, J.M. Fajnzylber, R.T. Ingram, R.H. Ward, J.Z. Li, M. Springer, An enhanced isothermal amplification assay for viral detection, Nat Commun. 11 (2020). https://doi.org/10.1038/s41467-020-19258-y.

[113] B. Sun, F. Shen, S.E. McCalla, J.E. Kreutz, M.A. Karymov, R.F. Ismagilov, Mechanistic evaluation of the pros and cons of digital RT-LAMP for HIV-1 viral load quantification on a microfluidic device and improved efficiency via a two-step digital protocol, Anal Chem. 85 (2013) 1540–1546. https://doi.org/10.1021/ac3037206.

[114] J. Schupbach, J. Boni, Quantitative and sensitive detection of immune-complexed and free HIV antigen after boiling of serum, J Virol Methods. 43 (1992) 247–256.

[115] A.T. Bender, B.P. Sullivan, J.Y. Zhang, D.C. Juergens, L. Lillis, D.S. Boyle, J.D. Posner, HIV detection from human serum with paper-based isotachophoretic RNA extraction and reverse transcription recombinase polymerase amplification, Analyst. 146 (2021) 2851–2861. https://doi.org/10.1039/d0an02483j.

[116] I.P. Oscorbin, L.M. Novikova, M.L. Filipenko, Comparison of reverse transcriptase (RT) activities of various M-MuLV RTs for RT-LAMP assays, Biology (Basel). 11 (2022) 1809. https://doi.org/10.3390/biology11121809.

[117] W. Guo, L. Cao, Z. Jia, G. Wu, T. Li, F. Lu, Z. Lu, High level soluble production of functional ribonuclease inhibitor in Escherichia coli by fusing it to soluble partners, Protein Expr Purif. 77 (2011) 185–192. https://doi.org/10.1016/j.pep.2011.01.015.

[118] R. Boom, C.J.A. Sol, R. Heijtink, P.M.E. Wertheim-Van Dillen, J. van der Noordaa, Rapid purification of Hepatitis B virus DNA from serum, J Clin Microbiol. 29 (1991) 1804–1811. https://journals.asm.org/journal/jcm.

[119] W.A. Al-Soud, P. Rådström, Purification and characterization of PCR-inhibitory components in blood cells, J Clin Microbiol. 39 (2001) 485–493. https://doi.org/10.1128/JCM.39.2.485-493.2001.

[120] M. Nash, J.N. Waitumbi, A. Hoffman, P. Yager, P.S. Stayton, Multiplexed enrichment and detection of Malarial biomarkers using a stimuli-responsive iron oxide and gold nanoparticle reagent system, ACS Nano. 6 (2012) 6776–6785. https://pubs-acs-org.offcampus.lib.washington.edu/doi/pdf/10.1021/nn3015008 (accessed June 3, 2019).

[121] B.J. Nehilla, J.J. Hill, S. Srinivasan, Y.-C. Chen, T.H. Schulte, P.S. Stayton, J.J. Lai, A Stimuli-Responsive, Binary Reagent System for Rapid Isolation of Protein Biomarkers, Anal Chem. 88 (2016) 10404–10410. https://doi.org/10.1021/acs.analchem.6b01961.

[122] Y.-C. Wang, J. Han, Pre-binding dynamic range and sensitivity enhancement for immuno-sensors using nanofluidic preconcentrator, Lab Chip. 8 (2008) 392–394. https://doi.org/10.1039/b717220f.

[123] J.L. Ortega-Vinuesa, D. Bastos-González, A review of factors affecting the performances of latex agglutination tests, J. Biomater. Sci. Polymer Edn. 12 (2001) 379–408.

[124] M. Nagura-Ikeda, K. Imai, S. Tabata, K. Miyoshi, N. Murahara, T. Mizuno, M. Horiuchi, K. Kato, Y. Imoto, S. Mimura, T. Ito, K. Tamura, Y. Kato, Clinical Evaluation of Self-Collected Saliva by Quantitative Reverse Transcription-PCR (RT-qPCR), Direct RT-qPCR, Reverse Transcription–Loop-Mediated Isothermal Amplification, and a Rapid Antigen Test To Diagnose COVID-19, J Clin Microbiol. 58 (2020). https://doi.org/10.1128/JCM.01438-20.

[125] M. Hagbom, N. Carmona-Vicente, S. Sharma, H. Olsson, M. Jämtberg, Å. Nilsdotter-Augustinsson, J. Sjöwall, J. Nordgren, Evaluation of SARS-CoV-2 rapid antigen diagnostic tests for saliva samples, Heliyon. 8 (2022). https://doi.org/10.1016/j.heliyon.2022.e08998.

[126] E.T. Kisak, M.T. Kennedy, D. Trommeshauser, J.A. Zasadzinski, Self-limiting aggregation by controlled ligand-receptor stoichiometry, Langmuir. 16 (2000) 2825–2831. https://doi.org/10.1021/la990787a.

[127] F. Family, D.P. Landau, eds., Kinetics of Aggregation and Gelation, 1984.

[128] R.J. Goldberg, Theory of Antibody-Antigen Reactions A Theory of Antibody-Antigen Reactions. II. Theory for Reactions of Multivalent Antigen with Multivalent Antibody1, (1953). https://doi.org/10.1021/ja01109a025.

[129] J.A. Spiers, Goldberg's Theory of Antigen-Antibody Reactions in Vitro, Immunology. (1958) 89–102.

[130] B.D. Grant, C.E. Anderson, L.F. Alonzo, S.H. Garing, J.R. Williford, T.A. Baughman, R. Rivera, V.A. Glukhova, D.S. Boyle, P.K. Dewan, B.H. Weigl, K.P. Nichols, A SARS-CoV-2 coronavirus nucleocapsid protein antigen-detecting lateral flow assay, PLoS One. 16 (2021). https://doi.org/10.1371/journal.pone.0258819.

[131] D.W. Bradbury, J.T. Trinh, M.J. Ryan, C.M. Cantu, J. Lu, F.D. Nicklen, Y. Du, R. Sun, B.M. Wu, D.T. Kamei, On-demand nanozyme signal enhancement at the push of a button for the improved detection of SARS-CoV-2 nucleocapsid protein in serum, Analyst. 146 (2021) 7383–7490. https://doi.org/10.1039/d1an01350e.

[132] M. Chabi, B. Vu, K. Brosamer, M. Smith, D. Chavan, J.C. Conrad, R.C. Willson, K. Kourentzi, Smartphone-read phage lateral flow assay for point-of-care detection of infection, Analyst. (2023). https://doi.org/10.1039/d2an01499h.

[133] J. Moreno-Contreras, M.A. Espinoza, C. Sandoval-Jaime, M.A. Cantú-Cuevas, H. Barón-Olivares, O.D. Ortiz-Orozco, A. V. Muñoz-Rangel, M. Hernández-De La Cruz, C.M. Eroza-Osorio, C.F. Arias, S. López, Saliva Sampling and Its Direct Lysis, an Excellent Option To

Increase the Number of SARS-CoV-2 Diagnostic Tests in Settings with Supply Shortages, J Clin Microbiol. 58 (2020). https://doi.org/10.1128/JCM.01659-20.

[134] K. Cassinari, E. Alessandri-Gradt, P. Chambon, F. Charbonnier, S. Gracias, L. Beaussire, K. Alexandre, N. Sarafan-Vasseur, C. Houdayer, M. Etienne, F. Caron, J.C. Plantier, T. Frebourg, Assessment of Multiplex Digital Droplet RT-PCR as a Diagnostic Tool for SARS-CoV-2 Detection in Nasopharyngeal Swabs and Saliva Samples, Clin Chem. 67 (2021) 736–741. https://doi.org/10.1093/clinchem/hvaa323.

[135] D.A. Armbruster, T. Pry, Limit of Blank, Limit of Detection and Limit of Quantitation, Clin Biochem Rev. 29 (2008).

[136] G.H. Carpenter, The secretion, components, and properties of saliva, Annu Rev Food Sci Technol. 4 (2013) 267–276. https://doi.org/10.1146/ANNUREV-FOOD-030212-182700.

[137] S.P. Humphrey, R.T. Williamson, A review of saliva: normal composition, flow and function., J Prosthet Dent. 85 (2001).

[138] A.L. Sheffner, The Reduction in Vitro In Viscosity of Mucoprotein Solutions by a New Mucolytic Agent, N-Acetyl-L-Cysteine, Ann N Y Acad Sci. 106 (1963) 298–310. https://doi.org/10.1111/J.1749-6632.1963.TB16647.X.

[139] N.R. Pollock, T.J. Savage, H. Wardell, R.A. Lee, A. Mathew, M. Stengelin, G.B. Sigal, Correlation of SARS-CoV-2 Nucleocapsid Antigen and RNA Concentrations in Nasopharyngeal Samples from Children and Adults Using an Ultrasensitive and Quantitative Antigen Assay, J Clin Microbiol. 59 (2021). https://doi.org/10.1128/JCM.03077-20.

[140] World Health Organization, Target product profiles for priority diagnostics to support response to the COVID-19 pandemic, (2020). https://www.who.int/publications/m/item/covid-19-target-product-profiles-for-priority-diagnostics-to-support-response-to-the-covid-19-pandemic-v.0.1 (accessed December 6, 2022).

[141] D. Shan, J.M. Johnson, S.C. Fernandes, H. Suib, S. Hwang, D. Wuelfing, M. Mendes, M. Holdridge, E.M. Burke, K. Beauregard, Y. Zhang, M. Cleary, S. Xu, X. Yao, P.P. Patel, T. Plavina, D.H. Wilson, L. Chang, K.M. Kaiser, J. Nattermann, S. v. Schmidt, E. Latz, K. Hrusovsky, D. Mattoon, A.J. Ball, N-protein presents early in blood, dried blood and saliva during asymptomatic and symptomatic SARS-CoV-2 infection, Nat Commun. 12 (2021). https://doi.org/10.1038/s41467-021-22072-9.

[142] K.K.W. To, O.T.Y. Tsang, W.S. Leung, A.R. Tam, T.C. Wu, D.C. Lung, C.C.Y. Yip, J.P. Cai, J.M.C. Chan, T.S.H. Chik, D.P.L. Lau, C.Y.C. Choi, L.L. Chen, W.M. Chan, K.H. Chan, J.D. Ip, A.C.K. Ng, R.W.S. Poon, C.T. Luo, V.C.C. Cheng, J.F.W. Chan, I.F.N. Hung, Z. Chen, H. Chen, K.Y. Yuen, Temporal profiles of viral load in posterior oropharyngeal saliva samples and serum antibody responses during infection by SARS-CoV-2: an observational cohort study, Lancet Infect Dis. 20 (2020) 565–574. https://doi.org/10.1016/S1473-3099(20)30196-1.

[143] J.L. Davidson, J. Wang, M.K. Maruthamuthu, A. Dextre, A. Pascual-Garrigos, S. Mohan, S.V.S. Putikam, F.O.I. Osman, D. McChesney, J. Seville, M.S. Verma, A paper-based colorimetric molecular test for SARS-CoV-2 in saliva, Biosens Bioelectron X. 9 (2021). https://doi.org/10.1016/J.BIOSX.2021.100076.

[144] S.W. Song, R. Gupta, J. Niharika, X. Qian, Y. Gu, V.V. Lee, Y. Sapanel, D.M. Allen, J. Eu, L. Wong, P.A. Macary, D. Ho, A. Blasiak, SHEAR Saliva Collection Device Augments Sample Properties for Improved Analytical Performance, MedRxiv. (2022). https://doi.org/10.1101/2022.07.07.22277204.

[145] Z. Noroozi, H. Kido, R. Peytavi, R. Nakajima-Sasaki, A. Jasinskas, M. Micic, P.L. Felgner, M.J. Madou, A Multiplexed Immunoassay System Based Upon Reciprocating Centrifugal Microfluidics, Review of Scientific Instruments. 82 (2011). https://doi.org/10.1063/1.3597578.

[146] S. Ratanabunyong, N. Aeksiri, S. Yanaka, M. Yagi-Utsumi, K. Kato, K. Choowongkomon, S. Hannongbua, Characterization of New DNA Aptamers for Anti-HIV-1 Reverse Transcriptase, ChemBioChem. 22 (2021) 915–923. https://doi.org/10.1002/cbic.202000633.

[147] I.A. Ferreira-Bravo, C. Cozens, P. Holliger, J.J. DeStefano, Selection of 2′-deoxy-2′-fluoroarabinonucleotide (FANA) aptamers that bind HIV-1 reverse transcriptase with picomolar affinity, Nucleic Acids Res. 43 (2015) 9587–9599. https://doi.org/10.1093/nar/gkv1057.

[148] J.J. DeStefano, I. Alves Ferreira-Bravo, A highly sensitive aptamer-based HIV reverse transcriptase detection assay, J Virol Methods. 257 (2018) 22–28. https://doi.org/10.1016/j.jviromet.2018.04.005.

[149] T.J. Maiers, N. Gous, M. Nduna, S.M. McFall, D.M. Kelso, M.J. Fisher, K.M. Palamountain, L.E. Scott, W.S. Stevens, M. BCh, An investigation of fingerstick blood collection for point-of-care HIV-1 viral load monitoring in South Africa, 105 (2015). https://doi.org/10.7196/SAMJ.7799.

[150] C.G. Sutcliffe, K.M. Palamountain, S. Maunga, K.M. Searle, P.E. Thuma, W.J. Moss, M.J. Fisher, The feasibility of fingerstick blood collection for point-of-care HIV-1 viral load monitoring in rural Zambia, Glob Health Innov. 1 (2018). https://doi.org/10.15641/ghi.v1i2.585.

[151] B. Sun, J. Rodriguez-Manzano, D.A. Selck, E. Khorosheva, M.A. Karymov, R.F. Ismagilov, Measuring fate and rate of single-molecule competition of amplification and restriction digestion, and its use for rapid genotyping tested with hepatitis C viral RNA, Angewandte Chemie - International Edition. 53 (2014) 8088–8092. https://doi.org/10.1002/anie.201403035.